Chemistry–A European Journal

Supporting Information

Multi-functional, Low Symmetry Pd_2L_4 Nanocage Libraries**

James E. M. Lewis*[a]

General Experimental

Synthesis: Unless otherwise stated, all reagents, including anhydrous solvents, were purchased from commercial sources and used without further purification. $CDCl_3$ and NEt_3 were stored over 4 Å molecular sieves prior to use. All reactions were carried out under air using reagent grade solvents unless otherwise stated. Reactions carried out under an atmosphere of N_2 used degassed solvents. Analytical TLC was performed on pre-coated silica gel plates (0.25 mm thick, 60F254, Merck, Germany) and observed under UV light. EDTA solution refers to a 0.1 M solution of EDTA-Na_2 in 3% $NH_{3(aq)}$.

Analysis: NMR spectra were recorded on Bruker AV400 or AV500 instrument, at a constant temperature of 300 K. Chemical shifts are reported in parts per million from low to high field and referenced to residual solvent. Standard abbreviations indicating multiplicity were used as follows: m = multiplet, quint = quintet, q = quartet, t = triplet, d = doublet, s = singlet, app. = apparent, br. = broad. Signal assignment was carried out using 2D NMR methods (HSQC, HMBC, COSY, NOESY) where necessary. In the case of some signals absolute assignment was not possible. Here indicative either/or assignments (e.g. H_A/H_B for H_A or H_B) are provided. All melting points were determined using a hot stage apparatus and are uncorrected. Mass spectrometry was carried out by the Imperial College London, Department of Chemistry Mass Spectroscopy Service using Waters LCT Premier for HR-ESI-MS.

Synthetic Procedures

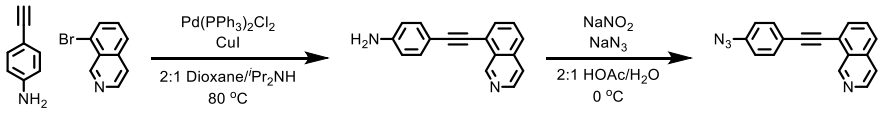

General CuAAC Procedure

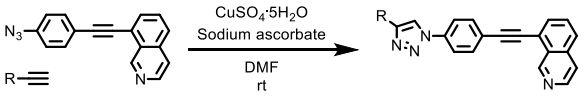

1 (67.6 mg, 0.25 mmol, 1.0 eq), $CuSO_4 \cdot 5H_2O$ (31.2 mg, 0.125 mmol, 0.5 eq.), sodium ascorbate (49.5 mg, 0.25 mmol, 1.0 eq) and alkyne were stirred at rt in DMF (5 mL) for 16 h. EtOAc (40 mL) was added and washed with EDTA solution (10 mL), brine (4 × 10 mL), dried ($MgSO_4$), and the solvent removed *in vacuo* to give the crude product which was purified by column chromatography on silica gel.

Synthesis of S1

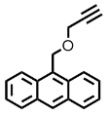

9-Hydroxymethylanthracene (0.417 g, 2 mmol, 1 eq.) was added as a solid to NaH (60% dispersion in mineral oil, 0.200 g, 5 mmol, 2.5 eq.) in DMF (4 mL) at 0 °C under N_2. Propargyl bromide (80 wt. % in toluene, 0.33 mL, 3 mmol, 1.5 eq.) was subsequently added via syringe and the reaction stirred, allowing to warm to rt, for 19 h. H_2O (50 mL) was added and the resultant precipitate isolated by filtration on paper, washed copiously with H_2O, dissolved in CH_2Cl_2, dried ($MgSO_4$) and the solvent removed *in vacuo*. Purification by column chromatography on silica (1:1 pentane/CH_2Cl_2) gave the product as a yellow solid (0.429 g, 87%). Spectra were consistent with those previously reported.[1] ^{1}H NMR (400 MHz, $CDCl_3$) δ: 8.49 (s, 1H), 8.45 (dd, *J* = 8.9, 1.0 Hz, 2H), 8.02 (app. dt, *J* = 8.4, 0.7 Hz, 2H), 7.57 (ddd, *J* = 8.9, 6.5, 1.4 Hz, 2H), 7.49 (ddd, *J* = 8.5, 6.5, 1.1 Hz, 2H), 5.62 (s, 2H), 4.33 (d, *J* = 2.4 Hz, 2H), 2.63 (t, *J* = 2.4 Hz, 1H). ^{13}C NMR (101 MHz, $CDCl_3$) δ: 131.5, 131.3, 129.1, 128.9, 127.9, 126.5, 125.1, 124.3, 80.3, 75.1, 63.7, 57.6.

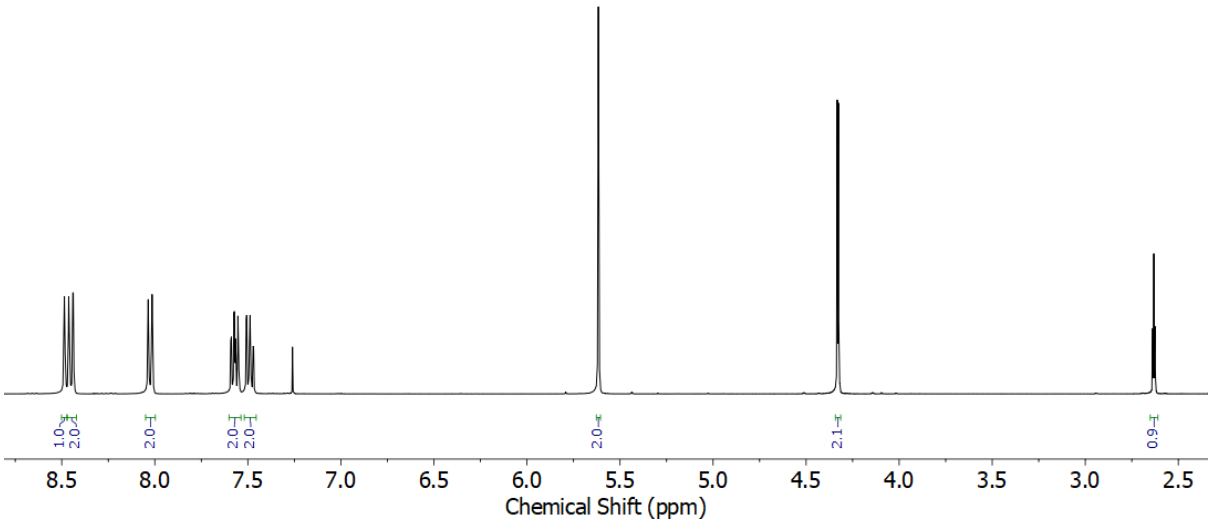

Figure S1 ^{1}H NMR ($CDCl_3$, 400 MHz) of **S1**.

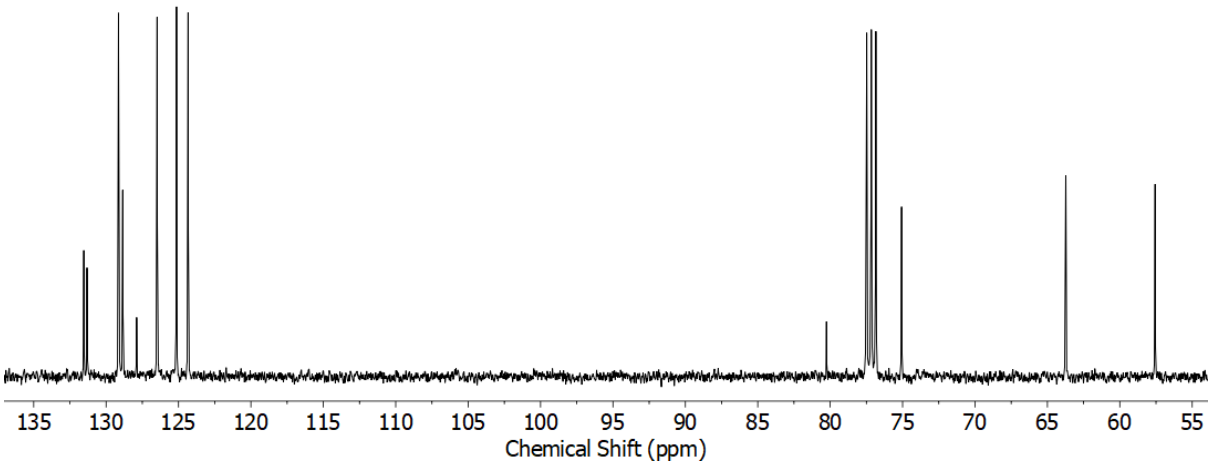

Figure S2 ^{13}C NMR ($CDCl_3$, 101 MHz) of **S1**.

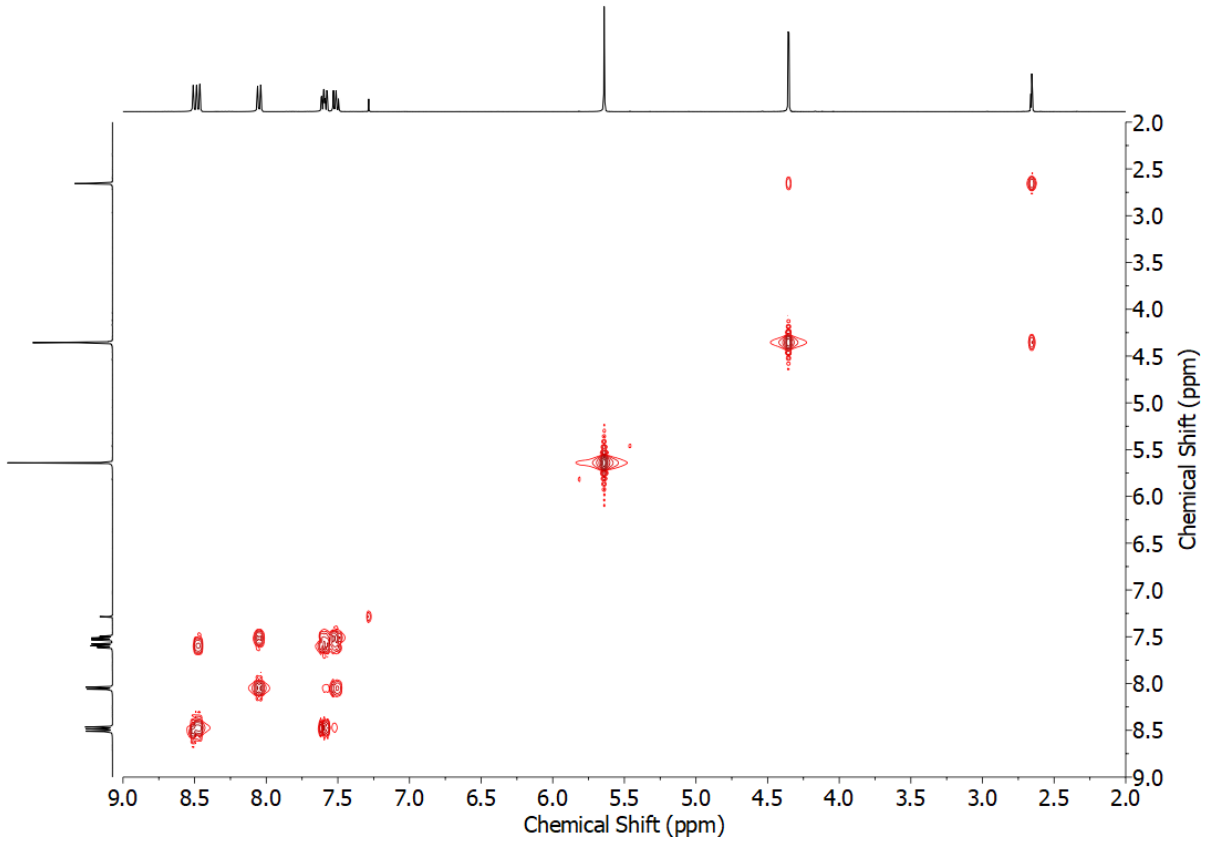

Figure S3 COSY NMR ($CDCl_3$) of **S1**.

Synthesis of S2

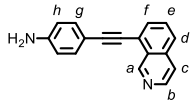

8-Bromoisoquinoline (0.626 g, 3.0 mmol, 1.0 eq.), 4-ethynylaniline (0.387 g, 3.3 mmol, 1.1 eq.), $Pd(PPh_3)_2Cl_2$ (0.053 g, 0.075 mmol, 2.5 mol%) and CuI (0.029 g, 0.150 mmol, 5 mol%) were stirred at 80 °C in 2:1 dioxane/$^{i}Pr_2NH$ (18 mL) under N_2 in a sealed vial for 16 h. After the solvent was removed *in vacuo*, the residue was dissolved in CH_2Cl_2 (50 mL) and washed with EDTA solution (20 mL). The aqueous phase was extracted with CH_2Cl_2 and the combined organic phases dried ($MgSO_4$) and the solvent removed *in vacuo*. After purification by column chromatography on silica (acetone/CH_2Cl_2 step gradient 0:100 ⟶ 5:95 ⟶ 10:90 ⟶ 15:85) the product was obtained as a bright yellow solid (0.659 g, 90%). R_f = 0.30 (1:9 acetone/CH_2Cl_2). M.p. 169-171 °C. ^{1}H NMR (400 MHz, $CDCl_3$) δ: 9.82 (s, 1H, H_a), 8.58 (d, *J* = 5.7 Hz, 1H, H_b), 7.77-7.74 (m, 2H, H_f, H_d/H_e), 7.66-7.62 (m, 2H, H_c, H_d/H_e), 7.46 (d, *J* = 8.6 Hz, 2H, H_g), 6.69 (d, *J* = 8.6 Hz, 2H, H_h), 3.90 (br. s, 2H, H_{NH}). ^{13}C NMR (101 MHz, $CDCl_3$) δ: 151.6, 147.4, 143.8, 136.0, 133.4, 130.9, 130.0, 128.1, 126.3, 122.6, 120.6, 115.0, 112.1, 97.1, 83.9. HR-ESI-MS m/z = 245.1067 $[M+H]^+$ calc. 245.1073.

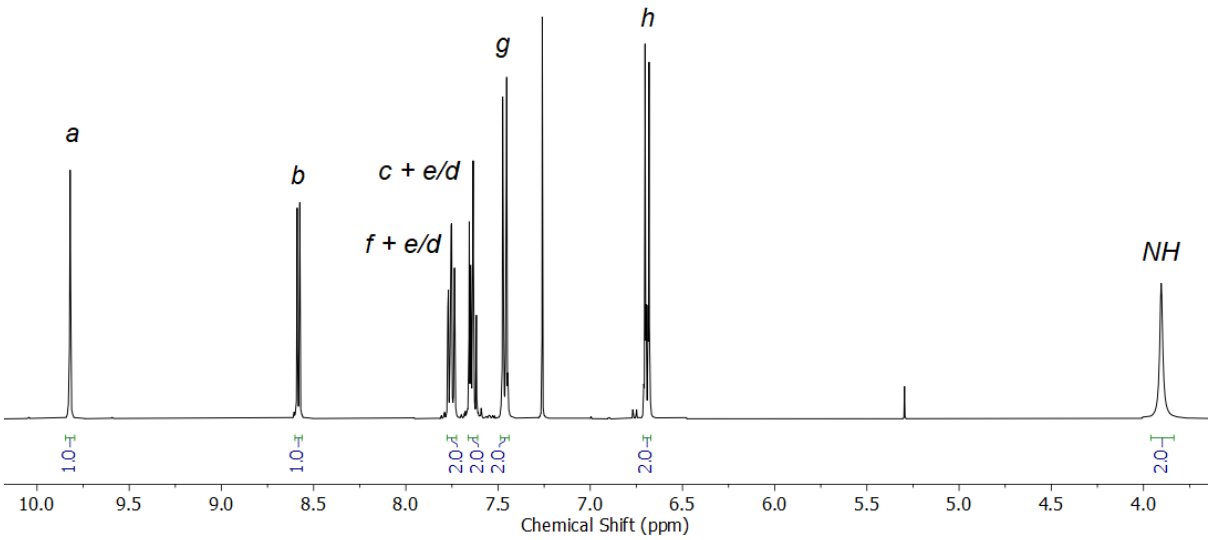

Figure S4 ^{1}H NMR ($CDCl_3$, 400 MHz) of **S2**.

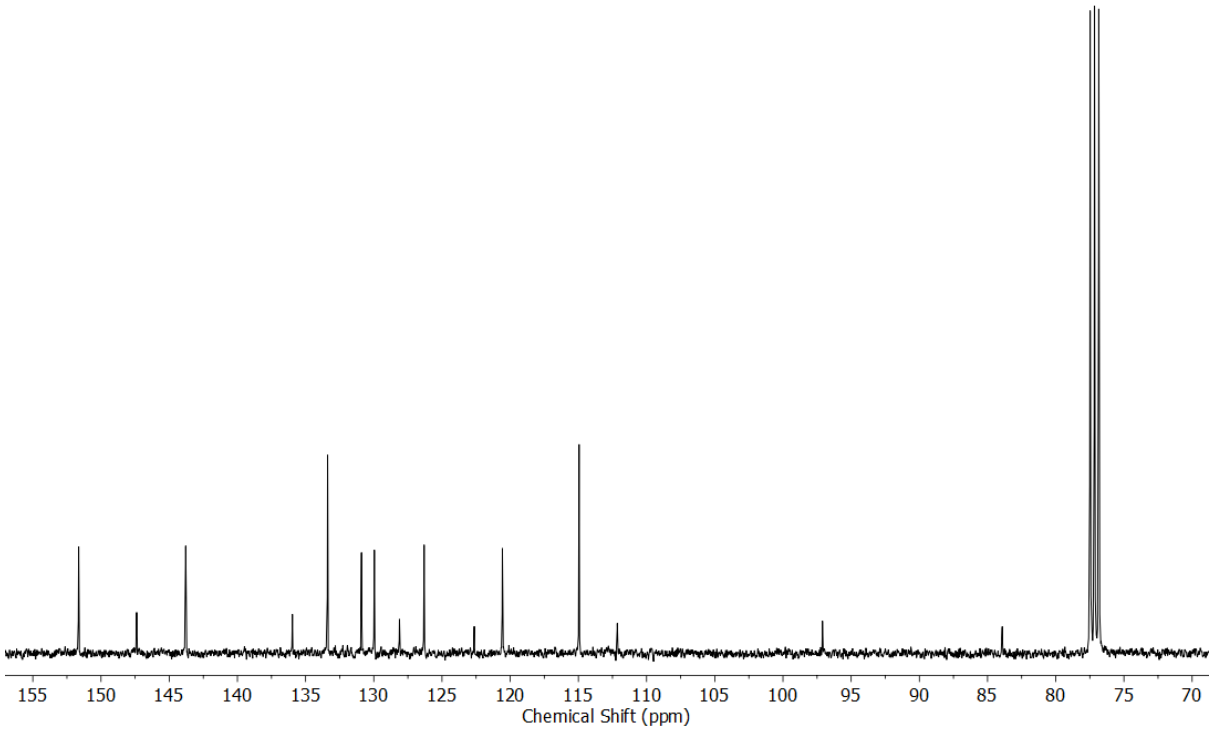

Figure S5 ^{13}C NMR ($CDCl_3$, 101 MHz) of **S2**.

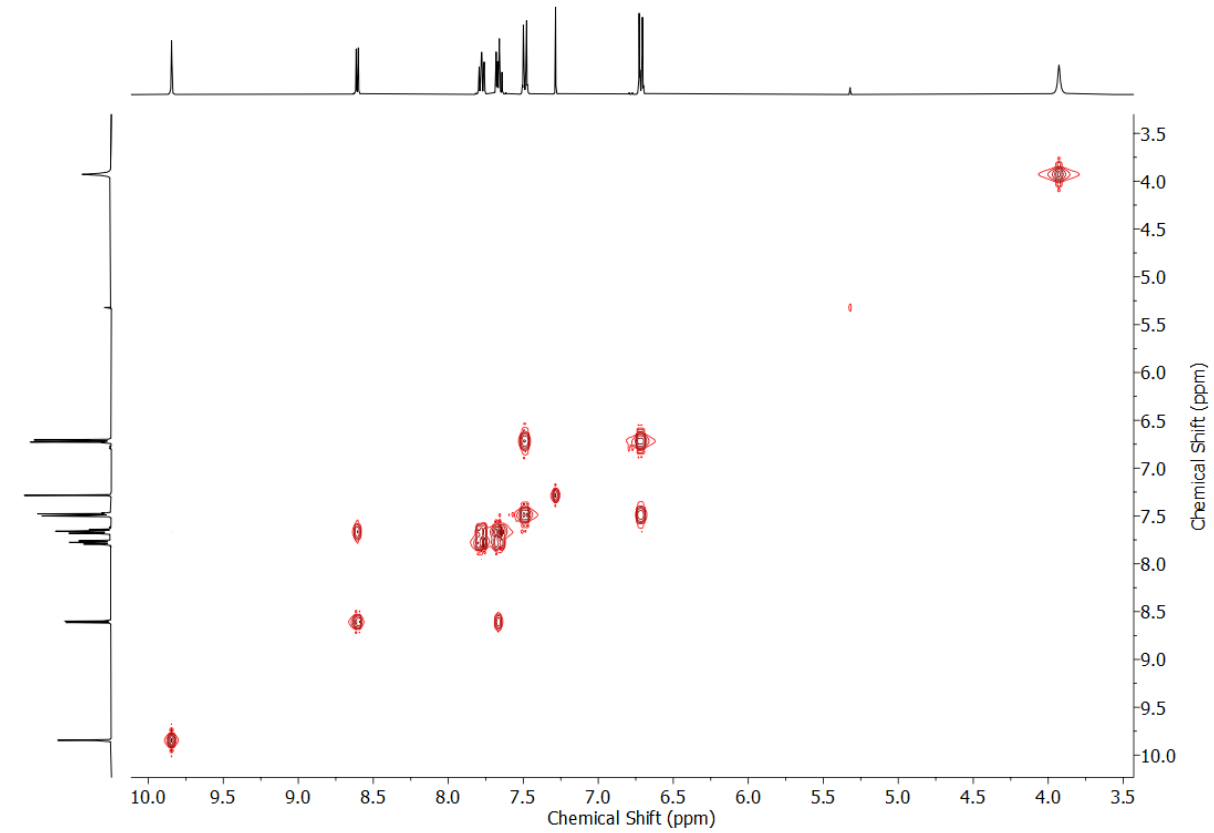

Figure S6 COSY NMR ($CDCl_3$) of **S2**.

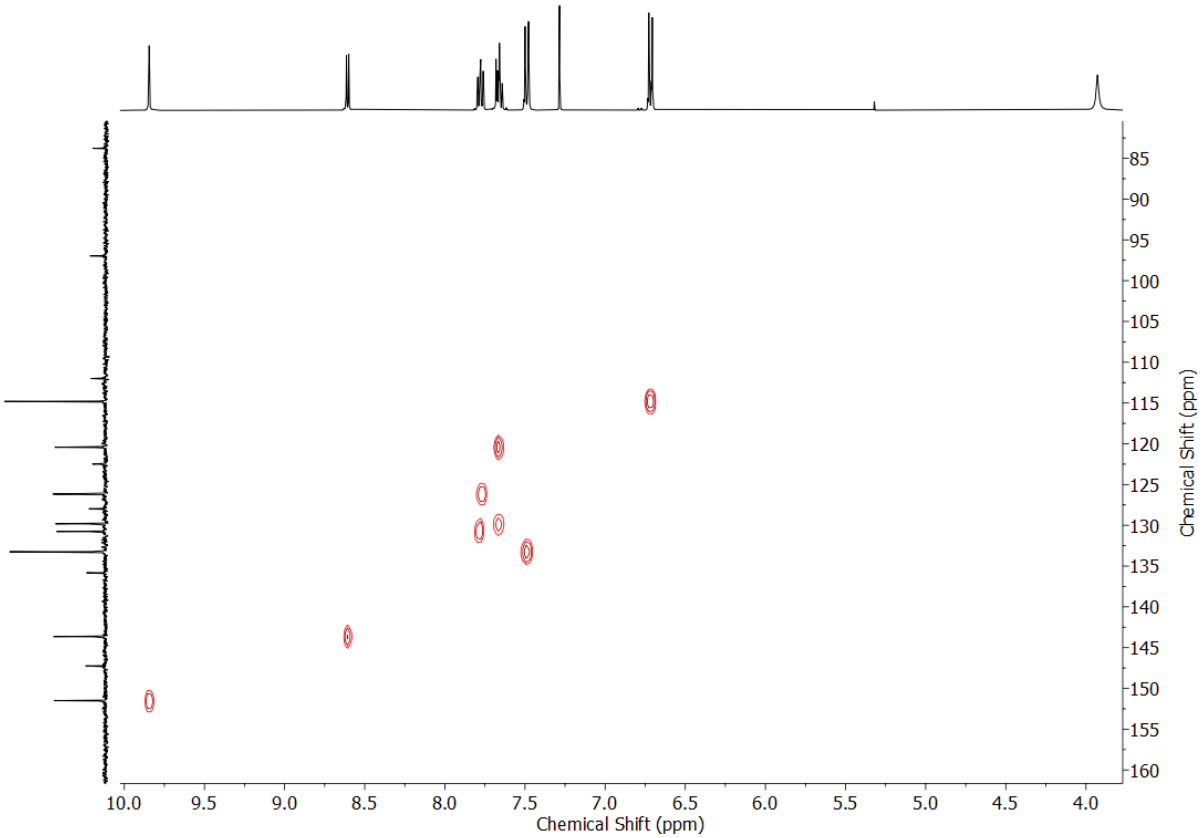

Figure S7 HSQC NMR ($CDCl_3$) of **S2**.

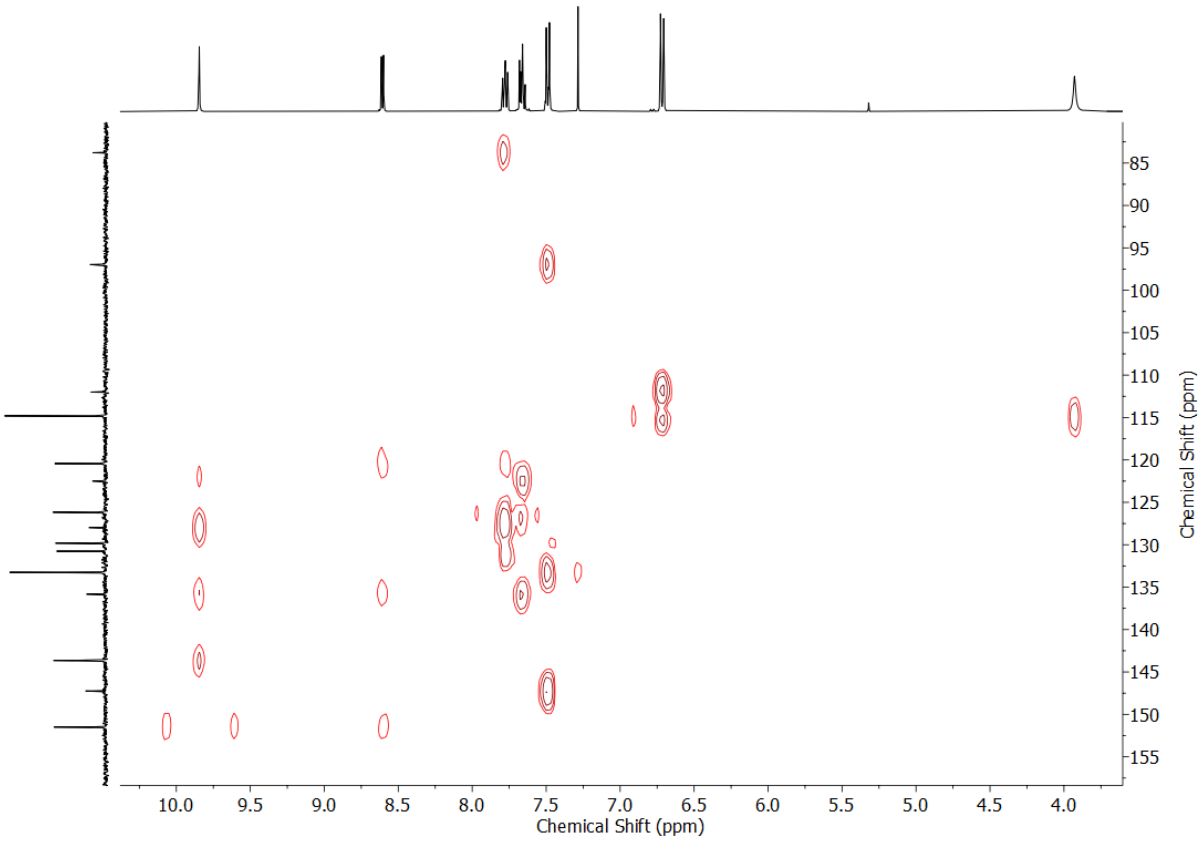

Figure S8 HMBC NMR ($CDCl_3$) of **S2**.

Synthesis of 1

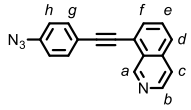

To a stirring solution of **S2** (0.392 g, 1.60 mmol, 1.0 eq.) in 2:1 AcOH/H_2O (6 mL) at 0 °C was added $NaNO_2$ (0.155 g, 2.25 mmol, 1.4 eq.). After 2 h, NaN_3 (0.312 g, 4.8 mmol, 3.0 eq.) was added portionwise and the reaction allowed to warm to rt. After 30 min, sat. aq. $NaHCO_3$ (80 mL) was added carefully and the aqueous phase extracted with CH_2Cl_2 (4 × 25 mL). The combined organic extracts were dried ($MgSO_4$) and the solvent removed *in vacuo* to give the product as a dark orange solid (0.412 g, 95%). M.p. 92-94 °C. ^{1}H NMR (400 MHz, $CDCl_3$) δ: 9.80 (s, 1H, H_a), 8.61 (d, *J* = 5.7 Hz, 1H, H_b), 7.81-7.79 (m, 2H, H_f, H_d/H_e), 7.68-7.65 (m, 2H, H_c, H_d/H_e), 7.64 (d, *J* = 8.6 Hz, 2H, H_g), 7.07 (d, *J* = 8.7 Hz, 2H, H_h). ^{13}C NMR (101 MHz, $CDCl_3$) δ: 151.4, 147.0, 144.0, 140.8, 136.0, 133.4, 131.5, 129.9, 128.1, 127.2, 121.7, 120.6, 119.4, 95.3, 86.1. HR-ESI-MS m/z = 243.0921 $[M+H-N_2]^+$ calc. 243.0917; 271.0984 $[M+H]^+$ calc. 271.0978.

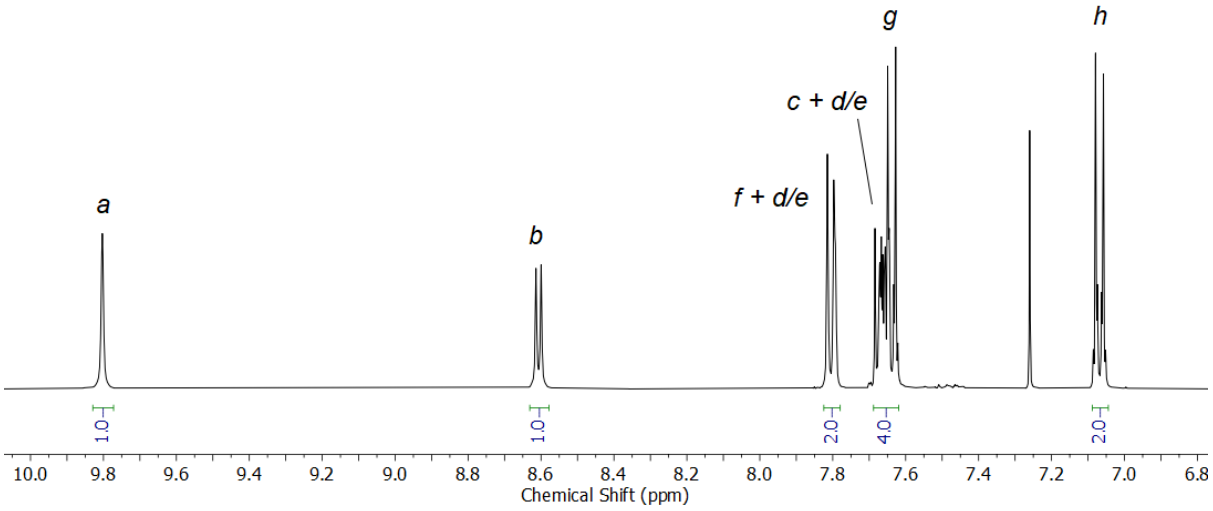

Figure S9 ^{1}H NMR ($CDCl_3$, 400 MHz) of **1**.

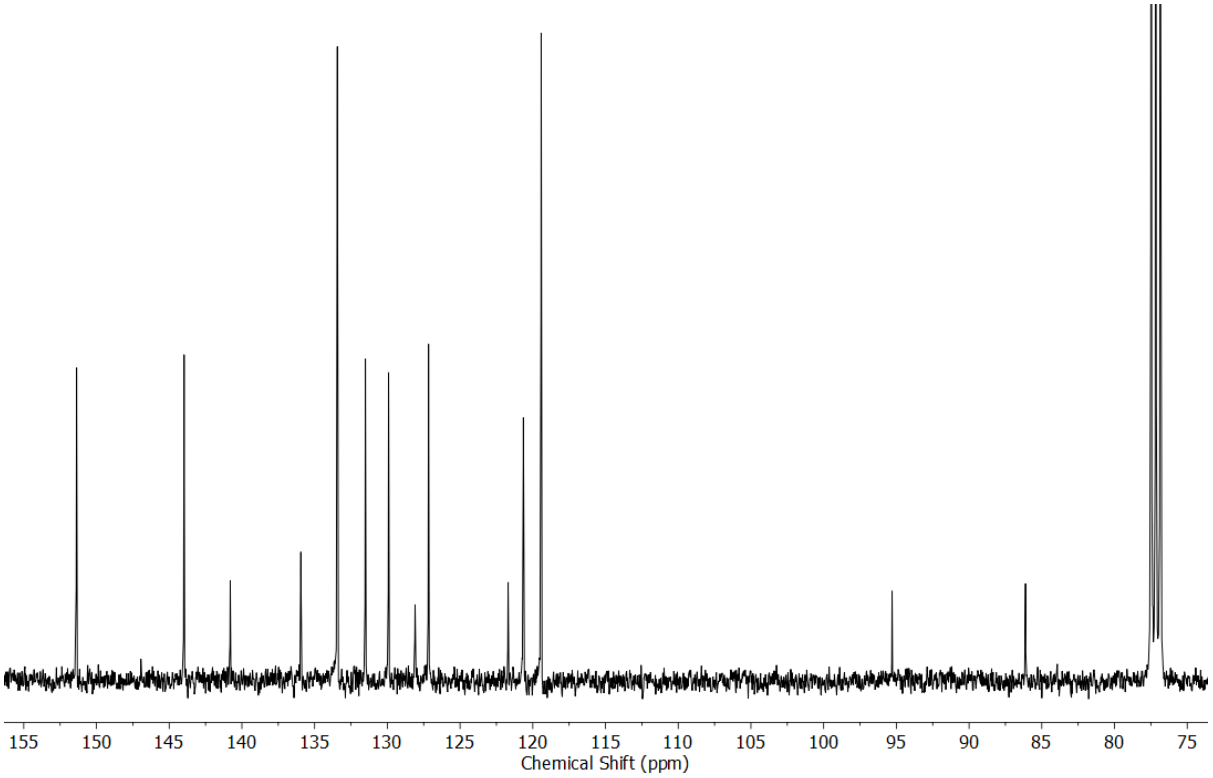

Figure S10 ^{13}C NMR ($CDCl_3$, 101 MHz) of **1**.

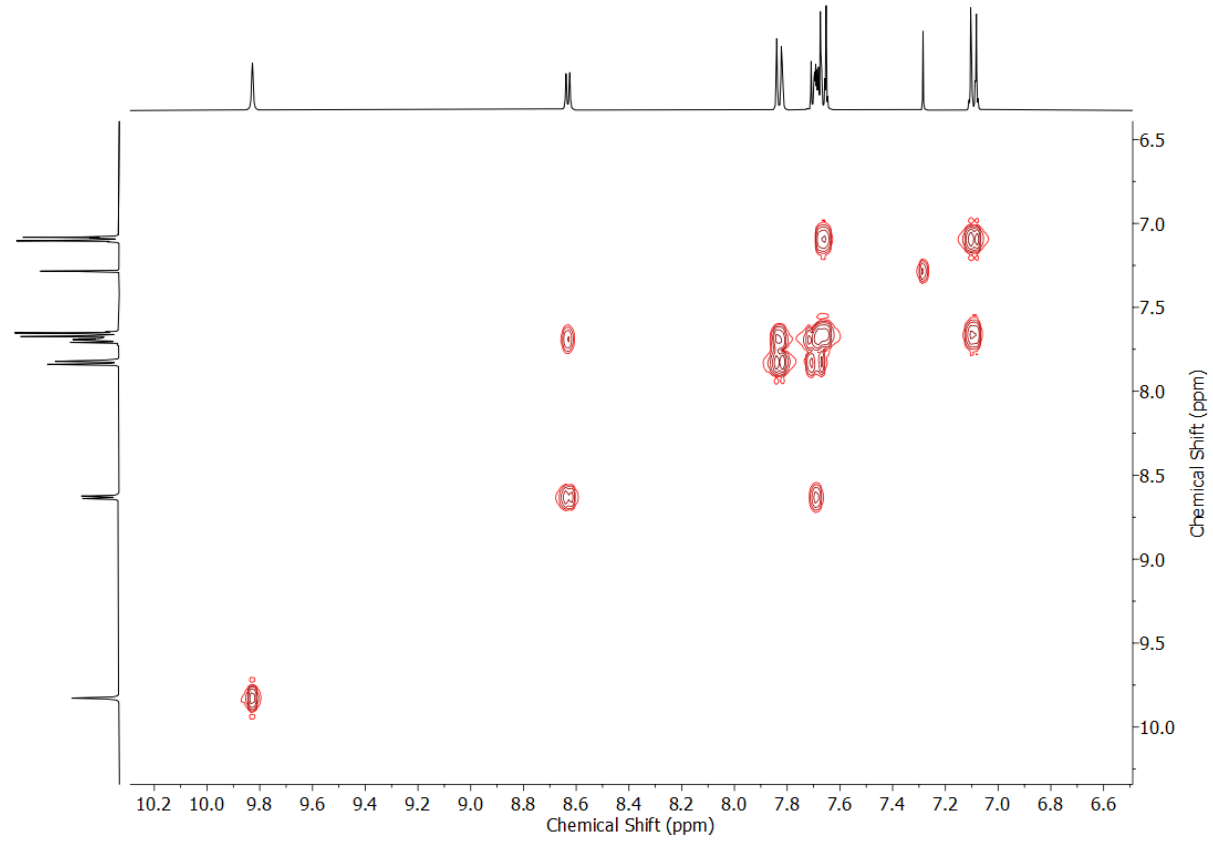

Figure S11 COSY NMR ($CDCl_3$) of **1**.

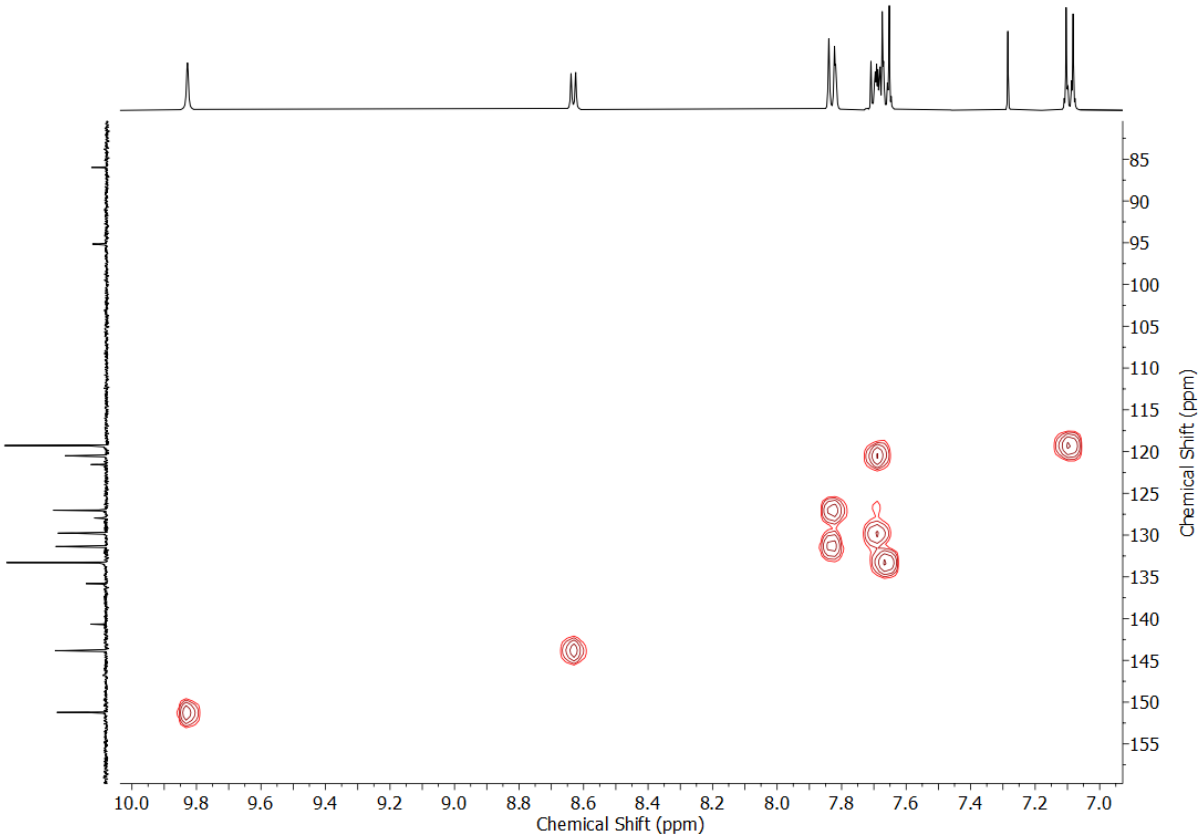

Figure S12 HSQC NMR ($CDCl_3$) of **1**.

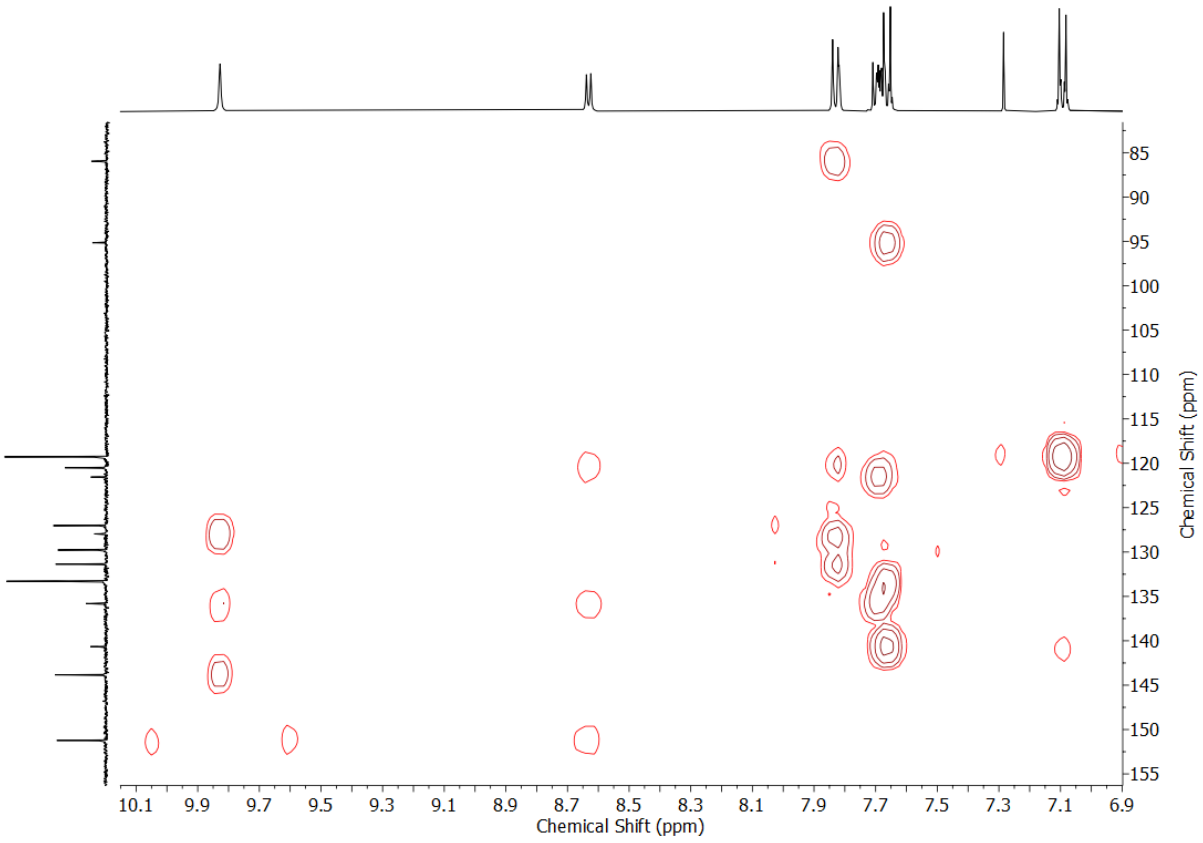

Figure S13 HMBC NMR ($CDCl_3$) of **1**.

Synthesis of L^{Bu}

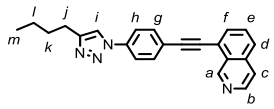

Prepared according to the general procedure with hex-1-yne (86 µL, 0.75 mmol, 3.0 eq.). Purification by column chromatography (acetone/CH_2Cl_2 step gradient 0:100 ⟶ 5:95 ⟶ 10:90) gave the product as a light yellow solid (78.6 mg, 89%). R_f = 0.29 (1:9 acetone/CH_2Cl_2). M.p. 132-134 °C. ^{1}H NMR (400 MHz, $CDCl_3$) δ: 9.82 (s, 1H, H_a), 8.62 (d, J = 5.7 Hz, 1H, H_b), 7.86-7.77 (m, 7H, H_f, H_g, H_h, H_i, H_d/H_e), 7.71-7.67 (m, 2H, H_c, H_d/H_e), 2.82 (t, J = 7.7 Hz, 2H, H_j), 1.73 (app. p, J = 7.5 Hz, 2H, H_k), 1.45 (m, 2H, H_l), 0.97 (t, J = 7.4 Hz, 3H, H_m). ^{13}C NMR (101 MHz, $CDCl_3$) δ: 151.3, 149.6, 144.0, 137.2, 136.0, 133.3, 131.8, 129.9, 128.1, 127.5, 123.0, 121.3, 120.7, 120.3, 118.7, 94.6, 87.3, 31.6, 25.5, 22.5, 14.0. HR-ESI-MS m/z = 353.1763 $[M+H]^+$ calc. 353.1761.

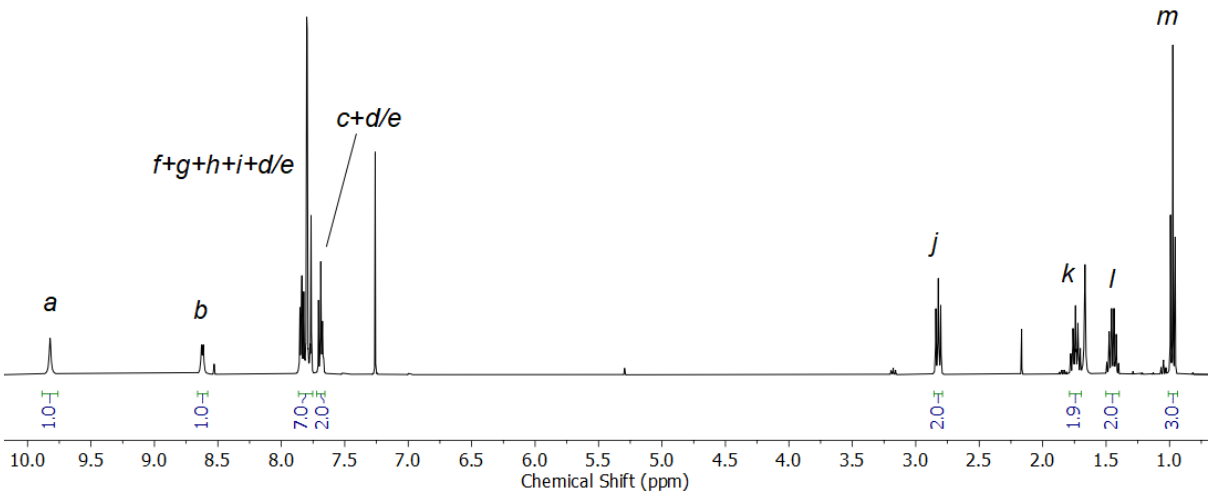

Figure S14 ^{1}H NMR ($CDCl_3$, 400 MHz) of L^{Bu}.

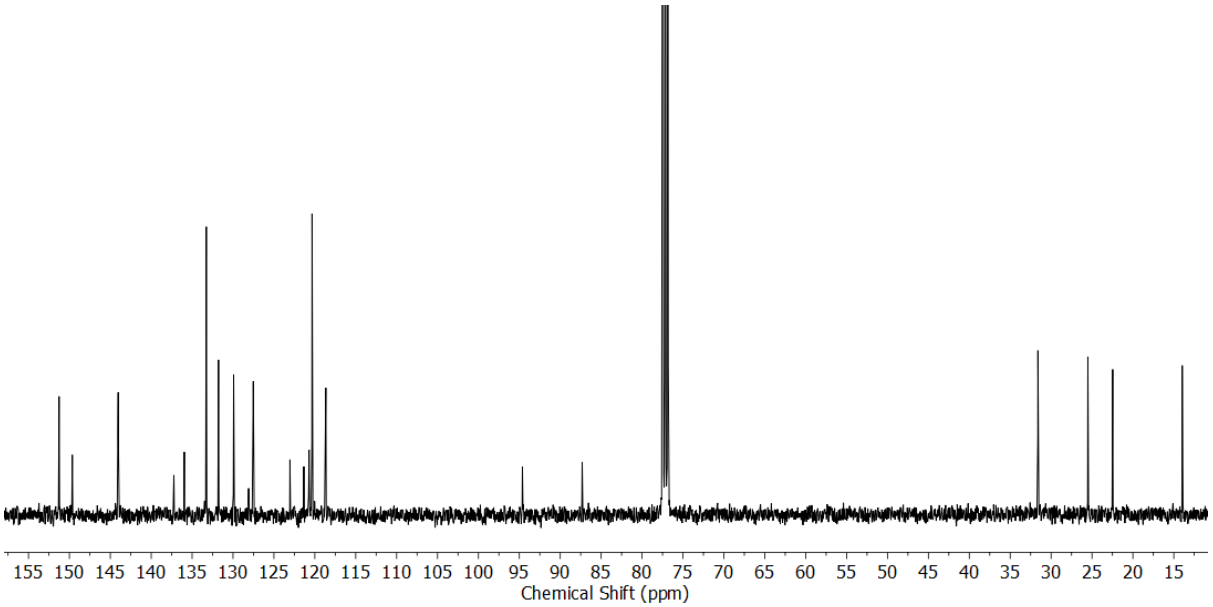

Figure S15 ^{13}C NMR ($CDCl_3$, 101 MHz) of L^{Bu}.

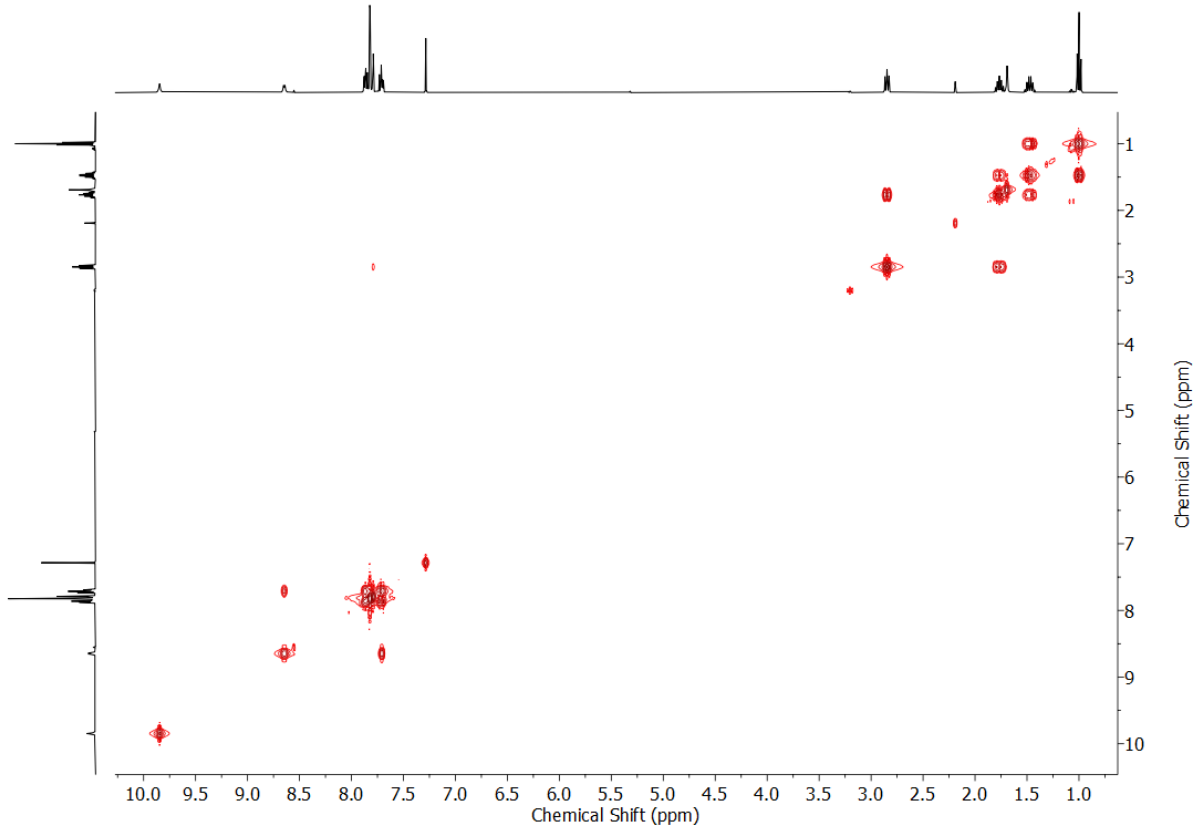

Figure S16 COSY NMR ($CDCl_3$) of $\mathbf{L^{Bu}}$.

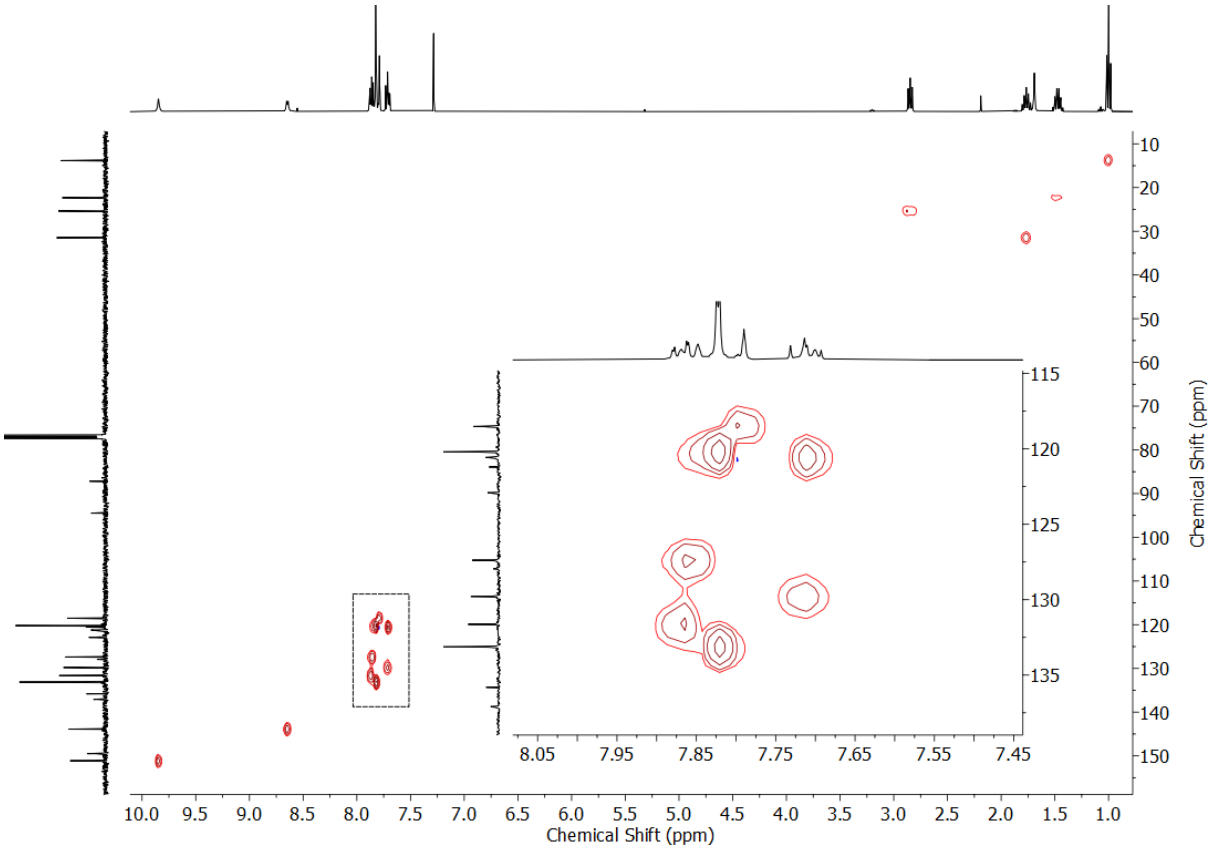

Figure S17 HSQC NMR ($CDCl_3$) of $\mathbf{L^{Bu}}$.

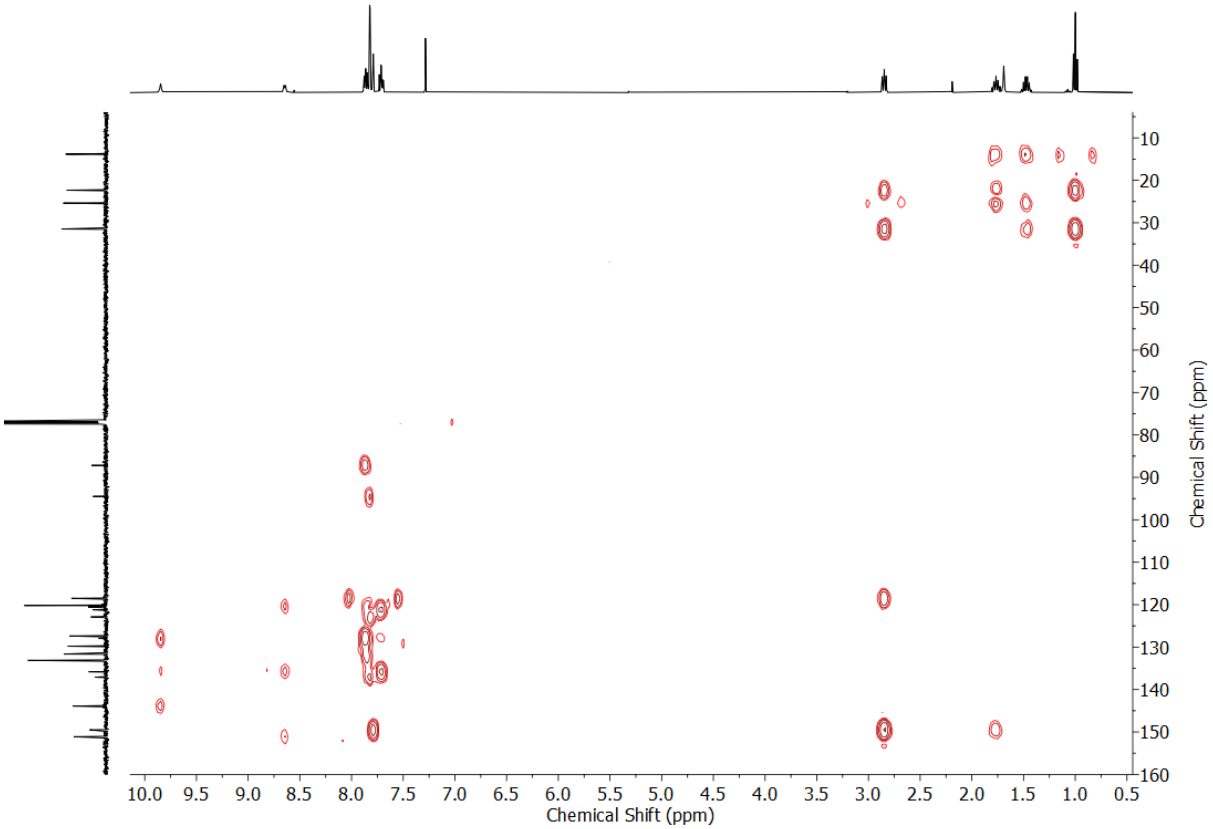

Figure S18 HMBC NMR ($CDCl_3$) of $\mathbf{L^{Bu}}$.

Synthesis of L^{Bn}

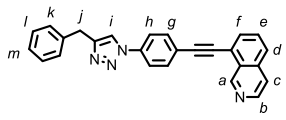

Prepared according to the general procedure with 3-phenyl-1-propyne (93 µL, 0.75 mmol, 3.0 eq.). Purification by column chromatography ($EtOAc/CH_2Cl_2$ step gradient 0:100 ⟶ 10:90 ⟶ 20:80 ⟶ 30:70) gave the product as a light beige solid (77.1 mg, 80%). R_f = 0.43 (1:3 $EtOAc/CH_2Cl_2$). M.p. 158-160 °C. ^{1}H NMR (400 MHz, $CDCl_3$) δ: 9.72 (s, 1H, H_a), 8.62 (d, J = 5.7 Hz, 1H, H_b), 7.85-7.82 (m, 2H, H_f, 1 of $H_d/H_e/H_k/H_l/H_m$), 7.77 (s, 4H, H_g, H_h), 7.70-7.67 (m, 2H, H_c, 1 of $H_d/H_e/H_k/H_l/H_m$), 7.64 (s, 1H, H_j), 7.37-7.32 (m, 4H, 4 of $H_d/H_e/H_k/H_l/H_m$), 7.29-7.25 (m, 2H, 2 of $H_d/H_e/H_k/H_l/H_m$), 4.19 (s, 2H, H_j). ^{13}C NMR (101 MHz, $CDCl_3$) δ: 151.3, 149.0, 144.1, 138.8, 137.1, 136.0, 133.3, 131.8, 129.9, 129.0, 128.9, 128.1, 127.6, 126.9, 123.2, 121.3, 120.7, 120.4, 119.5, 94.6, 87.4, 32.5. HR-ESI-MS m/z = 387.1608 $[M+H]^+$ calc. 387.1604.

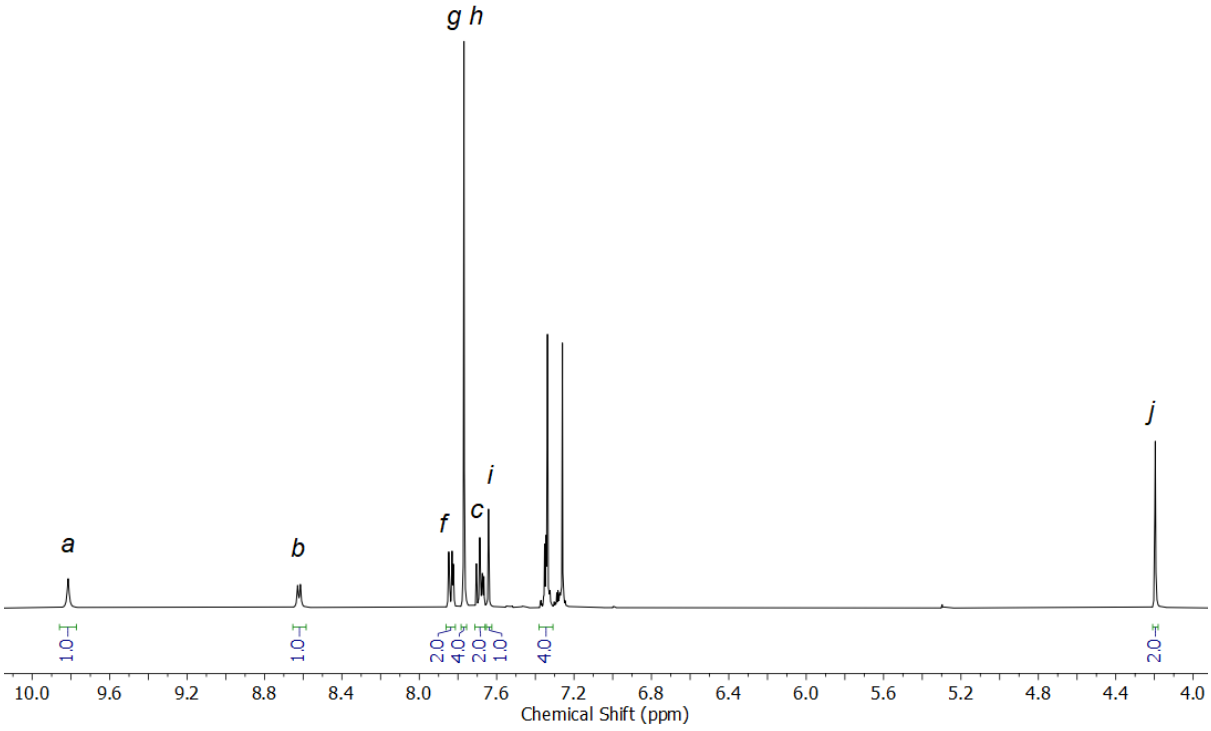

Figure S19 ^{1}H NMR ($CDCl_3$, 400 MHz) of L^{Bn}.

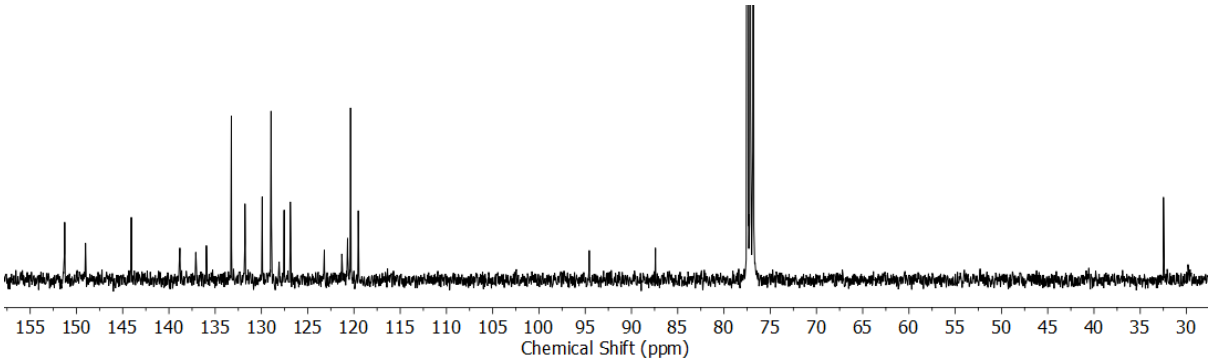

Figure S20 ^{13}C NMR ($CDCl_3$, 101 MHz) of L^{Bn}.

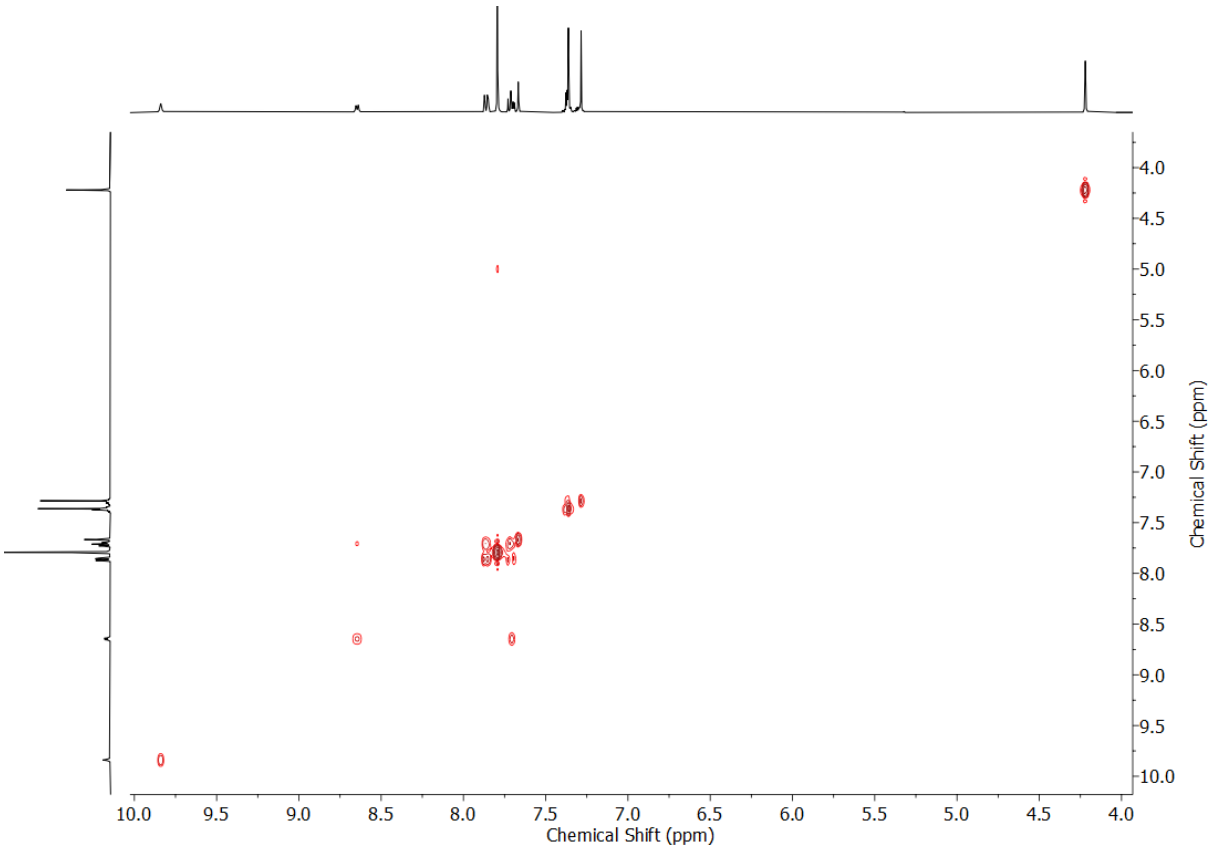

Figure S21 COSY NMR ($CDCl_3$) of $\mathbf{L^{Bn}}$.

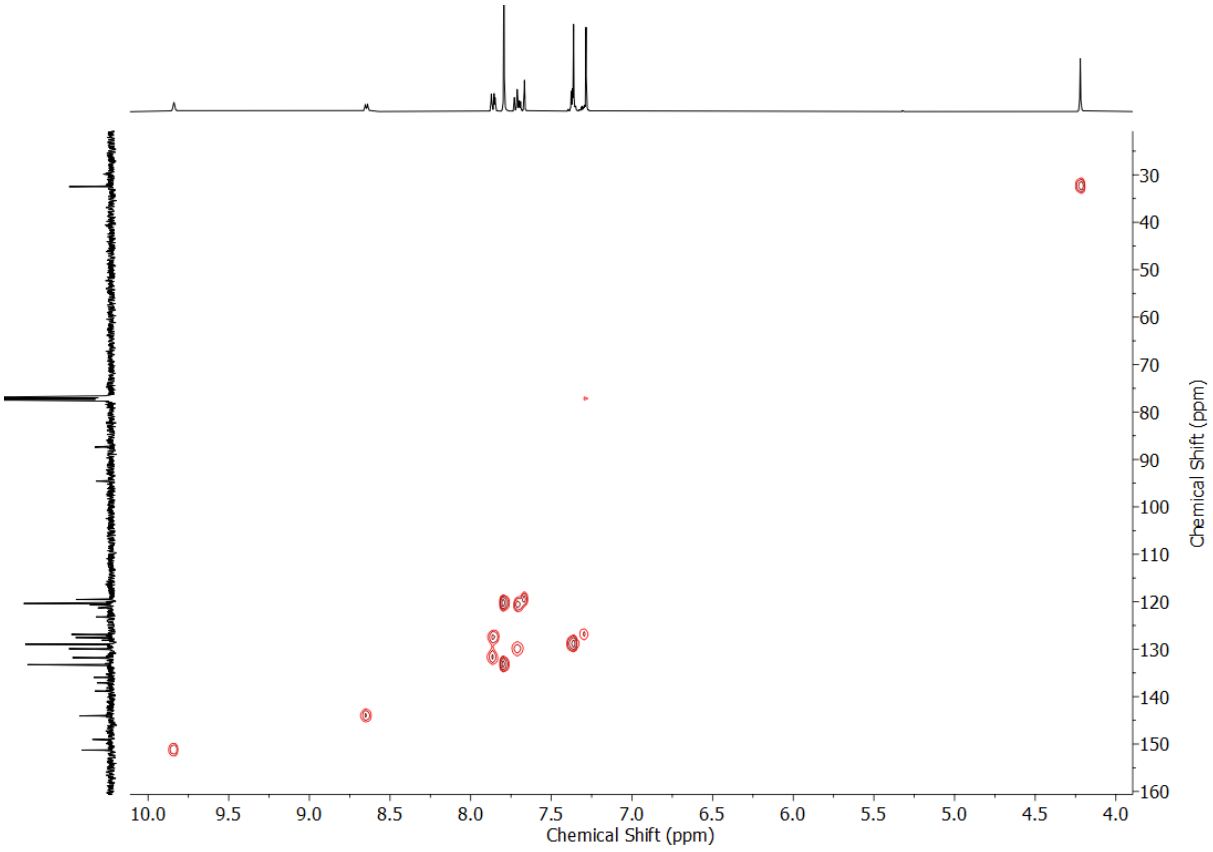

Figure S22 HSQC NMR ($CDCl_3$) of $\mathbf{L^{Bn}}$.

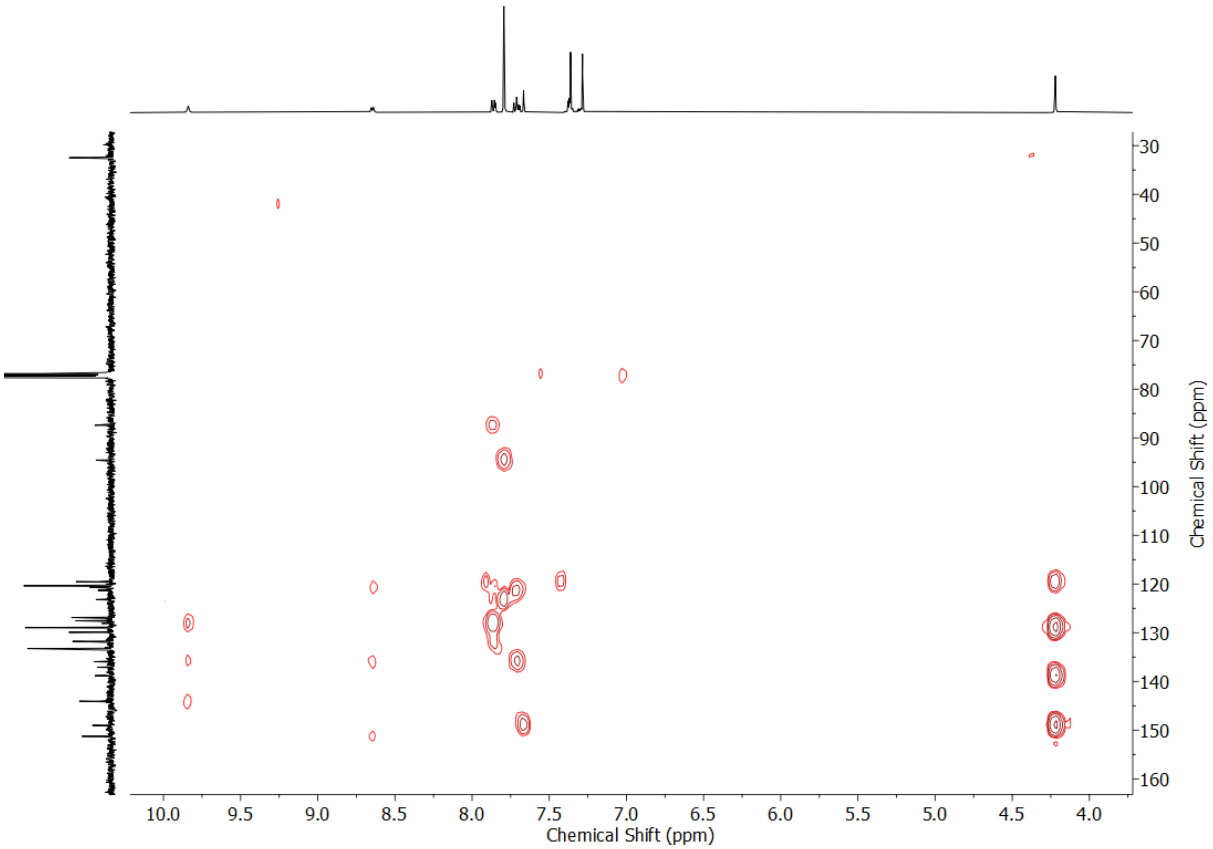

Figure S23 HMBC NMR ($CDCl_3$) of $\mathbf{L^{Bn}}$.

Synthesis of L^{OH}

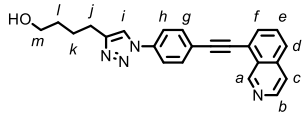

Prepared according to the general procedure with 5-hexyn-1-ol (83 µL, 0.75 mmol, 3.0 eq.). Purification by column chromatography ($MeOH/CH_2Cl_2$ step gradient 0:100 ⟶ 2:98 ⟶ 3:97 ⟶ 4:96 ⟶ 5:95) gave the product as a light beige solid (60.1 mg, 65%). R_f = 0.26 (1:19 $MeOH/CH_2Cl_2$). M.p. 192-194 °C. ^{1}H NMR (400 MHz, $CDCl_3$) δ: 9.79 (s, 1H, H_a), 8.62 (d, *J* = 5.7 Hz, 1H, H_b), 7.87-7.83 (m, 2H, H_f, 1 of H_d/H_e), 7.80 (app. s, 5H, H_g, H_h, H_i), 7.72-7.68 (m, 2H, H_c, 1 of H_d/H_e), 3.73 (t, *J* = 6.4 Hz, 2H, H_m), 2.87 (m, 2H, H_j), 1.91-1.83 (m, 2H, H_k), 1.75-1.67 (m, 2H, H_l). ^{13}C NMR (101 MHz, $CDCl_3$) δ: 151.1, 149.2, 143.8, 137.1, 136.0, 133.3, 131.8, 130.0, 127.5, 123.1, 121.4, 120.9, 120.8, 120.4, 118.8, 94.6, 87.3, 62.7, 32.3, 25.7, 25.5. HR-ESI-MS m/z = 369.1719 $[M+H]^+$ calc. 369.1710.

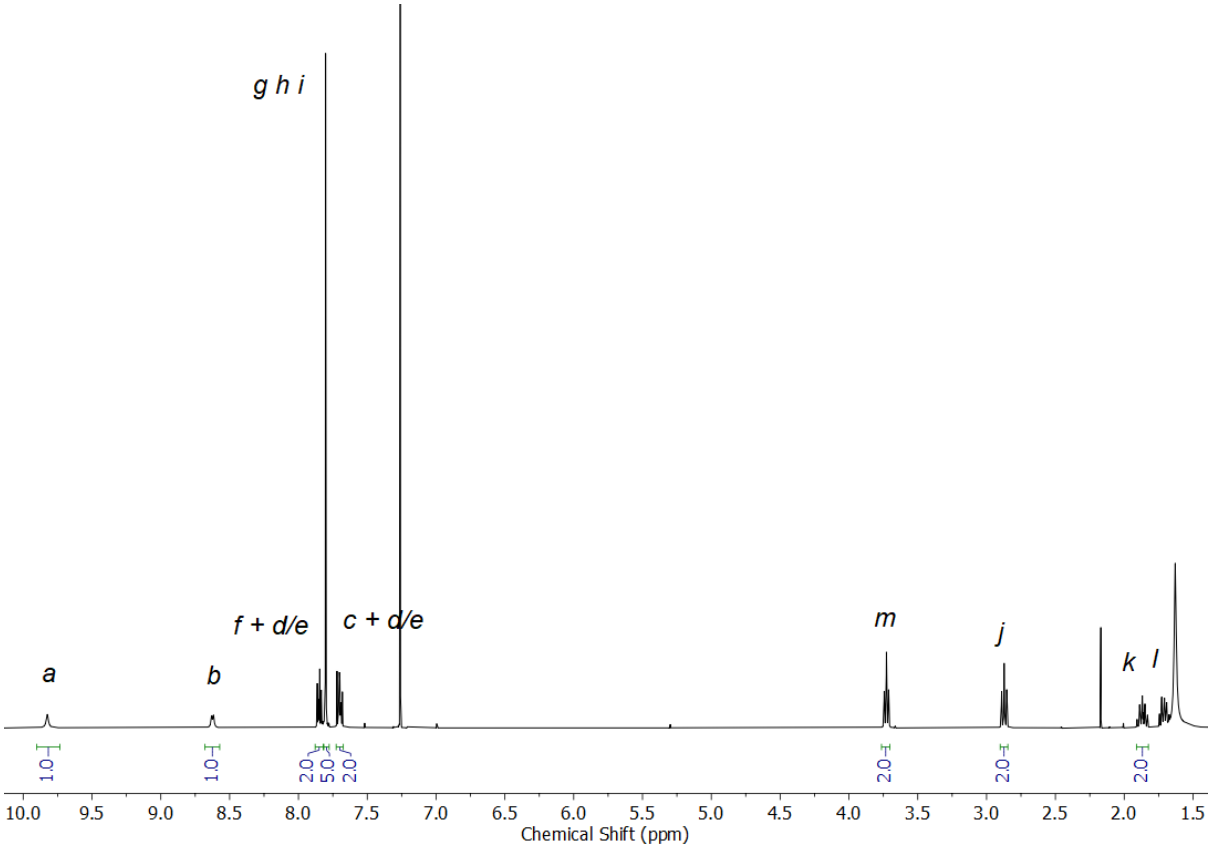

Figure S24 ^{1}H NMR ($CDCl_3$, 400 MHz) of L^{OH}.

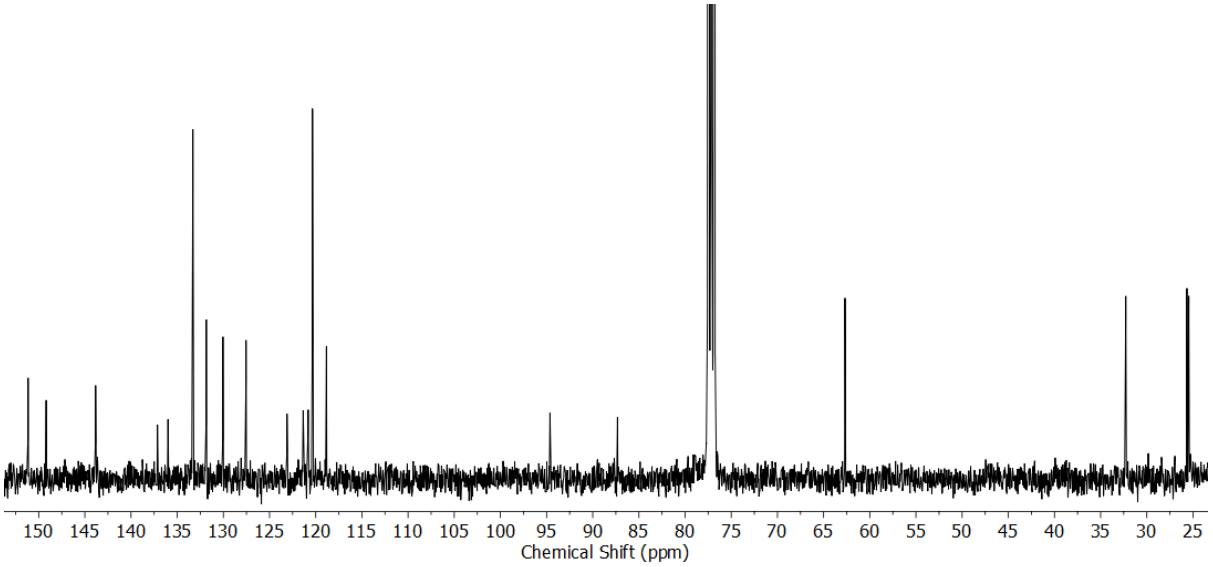

Figure S25 ^{13}C NMR ($CDCl_3$, 101 MHz) of $\mathbf{L^{OH}}$.

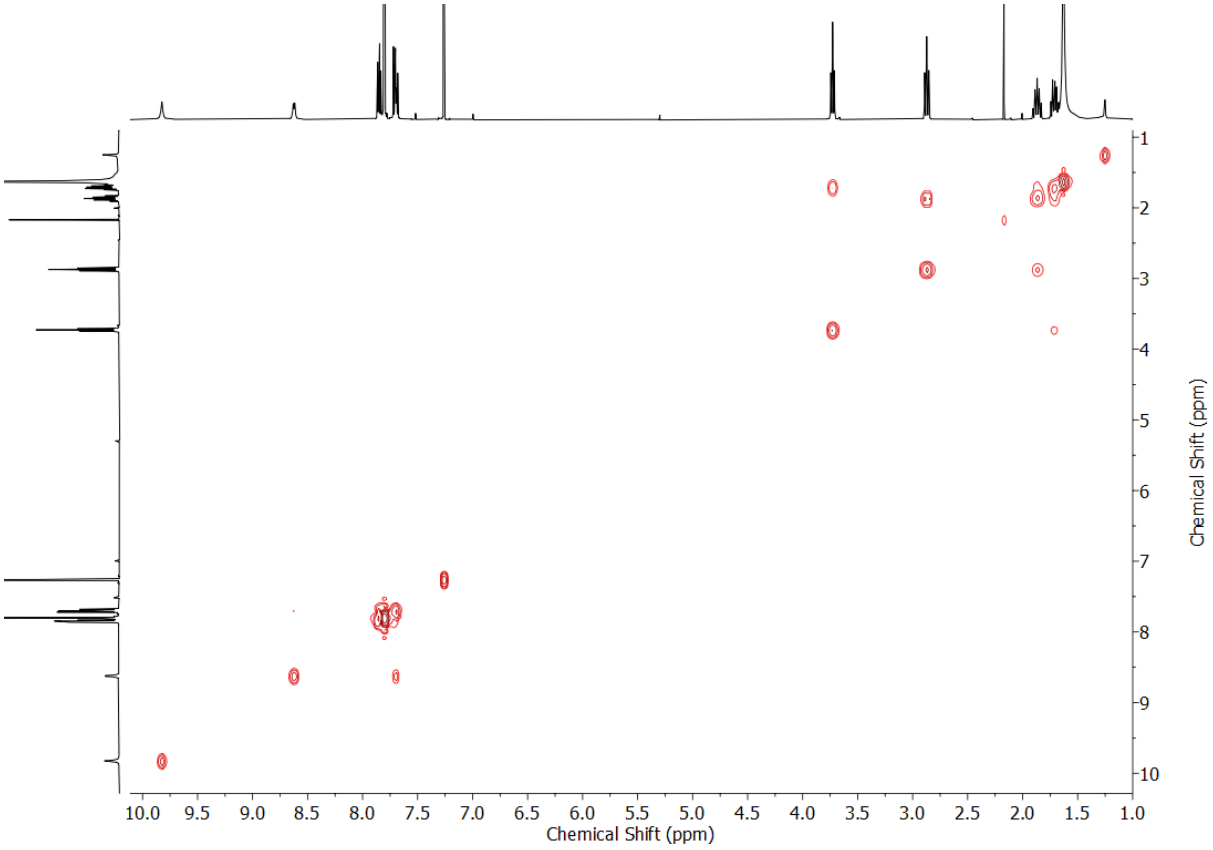

Figure S26 COSY NMR ($CDCl_3$) of $\mathbf{L^{OH}}$.

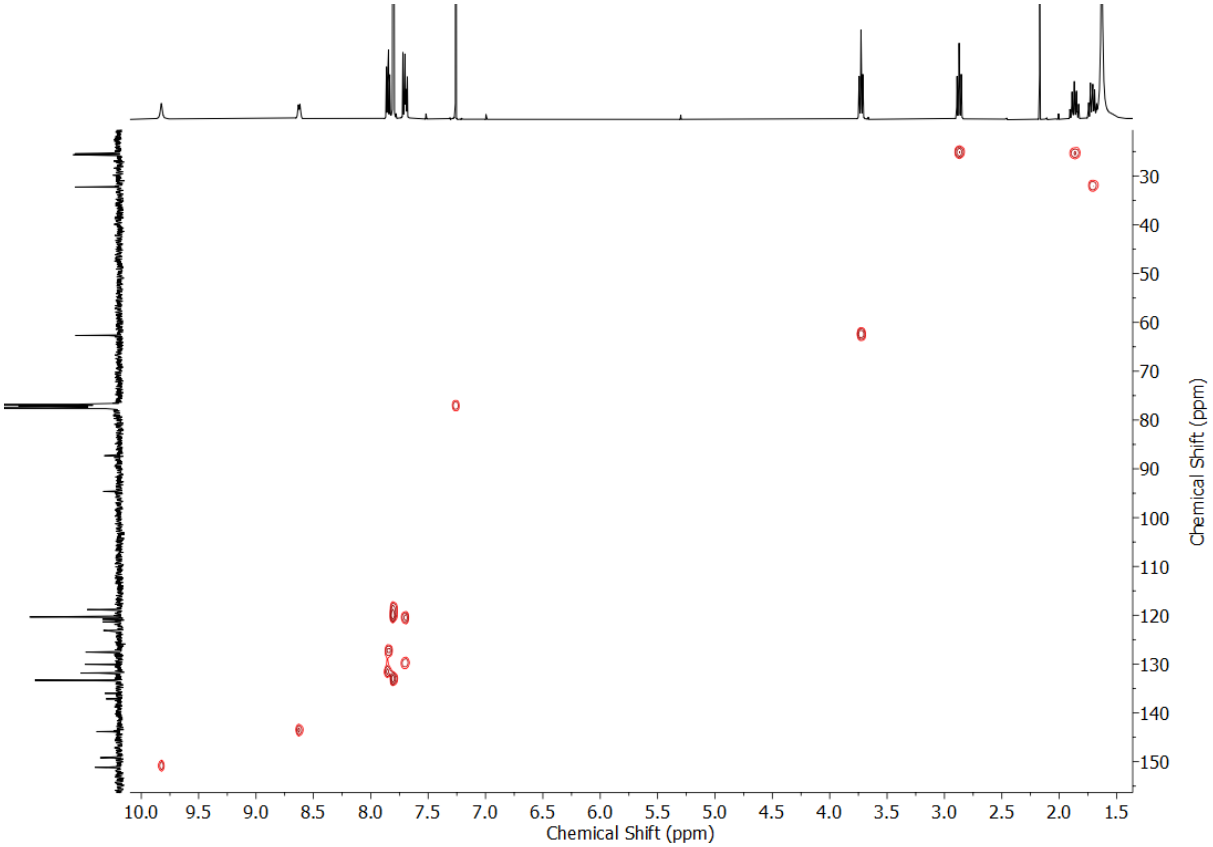

Figure S27 HSQC NMR ($CDCl_3$) of $\mathbf{L^{OH}}$.

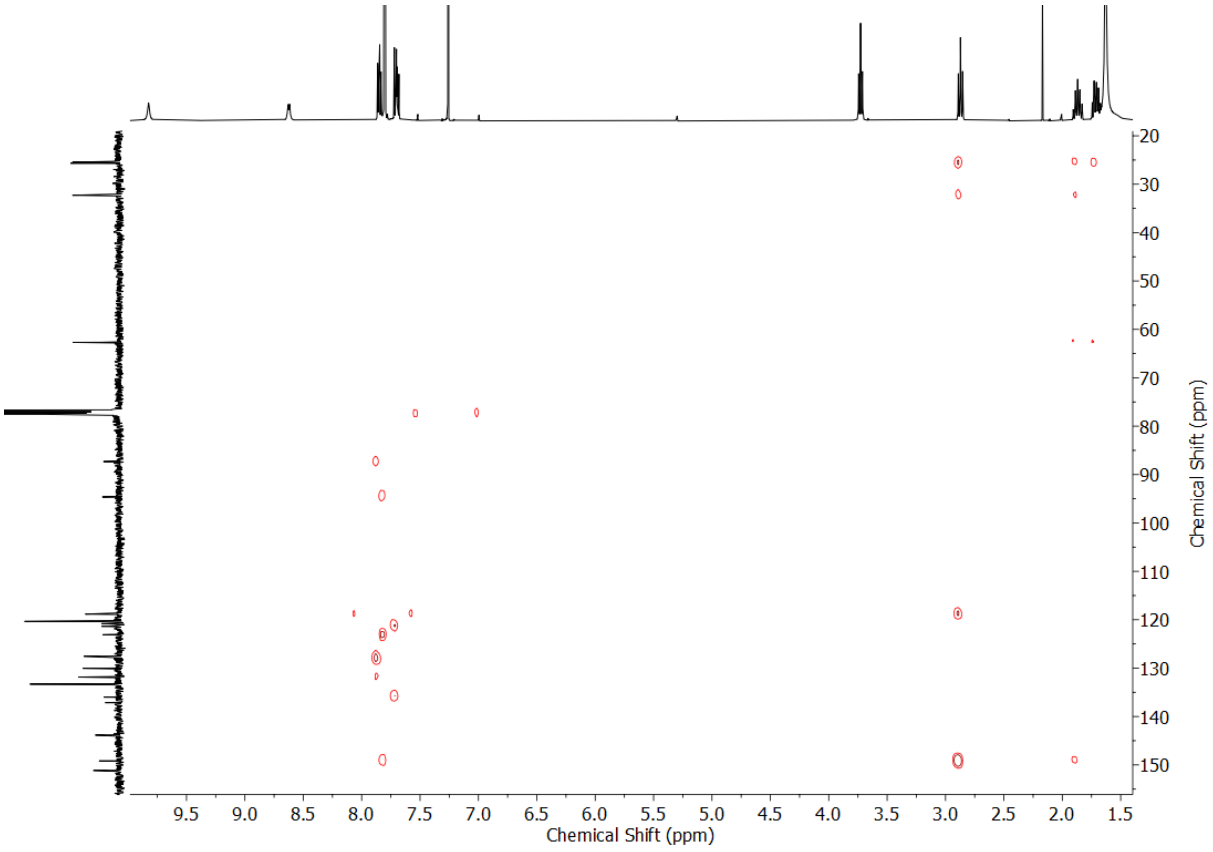

Figure S28 HBMC NMR ($CDCl_3$) of $\mathbf{L^{OH}}$.

Synthesis of L^{Phth}

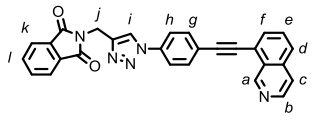

Prepared according to the general procedure with N-propargylphthalimide (57.9 mg, 0.313 mmol, 1.25 eq.). Purification by column chromatography (acetone/CH_2Cl_2 step gradient 0:100 ⟶ 15:85 in 5% increments) gave the product as a light yellow solid (113 mg, 99%). R_f = 0.30 (1:9 acetone/CH_2Cl_2). M.p. 219-221 °C. ^{1}H NMR (400 MHz, $CDCl_3$) δ: 9.83 (s, 1H, H_a), 8.61 (d, *J* = 5.9 Hz, 1H, H_b), 8.10 (s, 1H, H_i), 7.92-7.87 (m, 4H, H_d/H_e, H_f, H_k/H_l), 7.81-7.78 (m, 6H, H_c, H_d/H_e, H_g, H_h), 7.75-7.73 (dd, *J* = 5.5, 3.0 Hz, 2H, H_k/H_l), 5.11 (s, 2H, H_j). ^{13}C NMR (101 MHz, $CDCl_3$) δ: 167.8, 149.8, 143.9, 141.4, 137.0, 136.6, 134.4, 133.4, 132.5, 132.2, 131.3, 127.9, 127.6, 123.7, 123.1, 122.0, 121.8, 121.1, 120.6, 95.3, 86.9, 33.2. HR-ESI-MS m/z = 456.1463 $[M+H]^+$ calc. 456.1461.

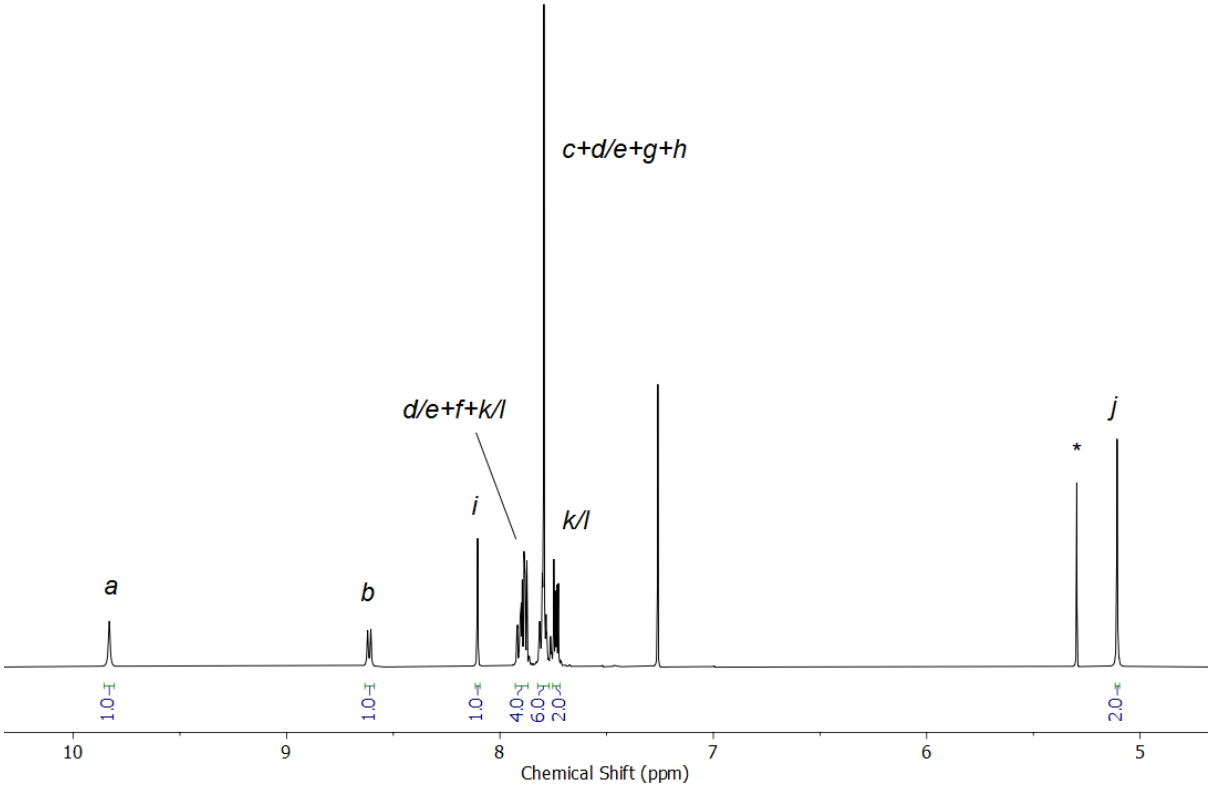

Figure S29 ^{1}H NMR ($CDCl_3$, 400 MHz) of L^{Phth}.

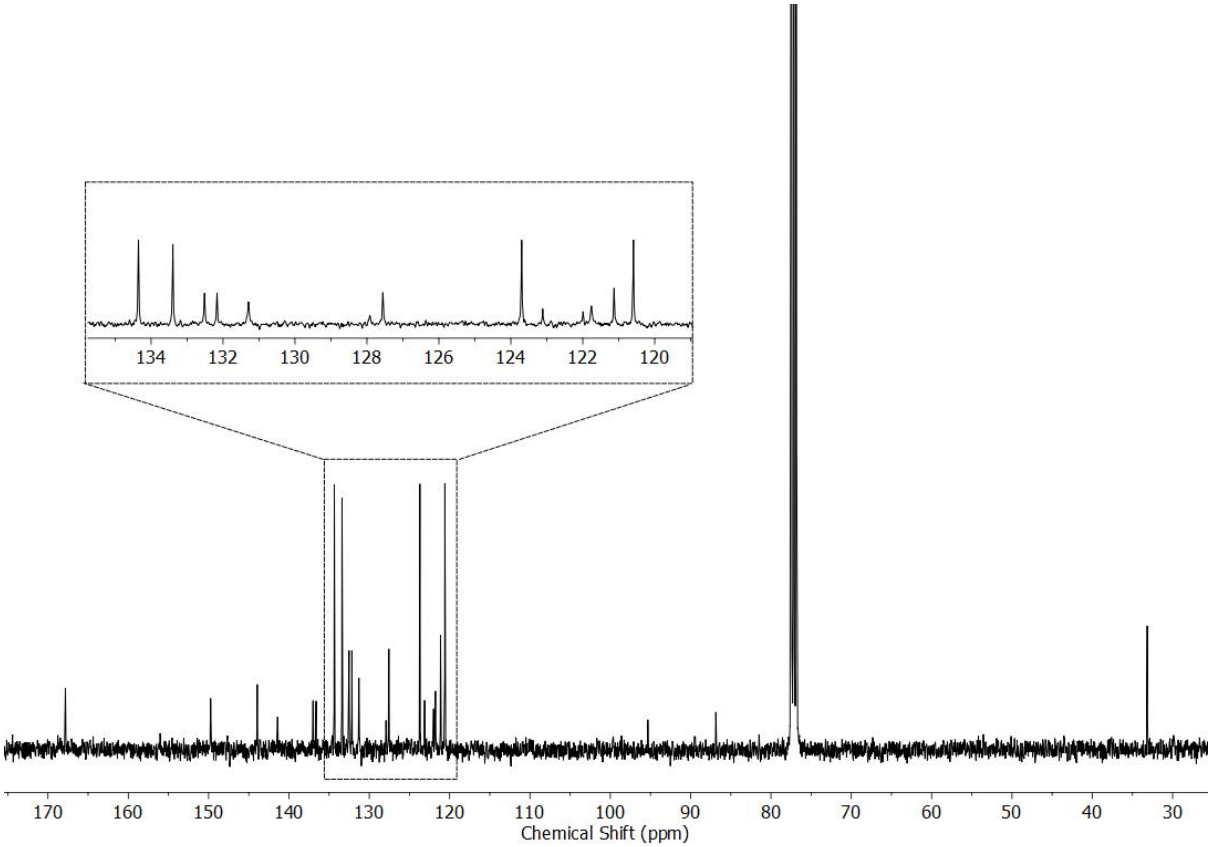

Figure S30 ^{13}C NMR ($CDCl_3$, 101 MHz) of $\mathbf{L^{Phth}}$.

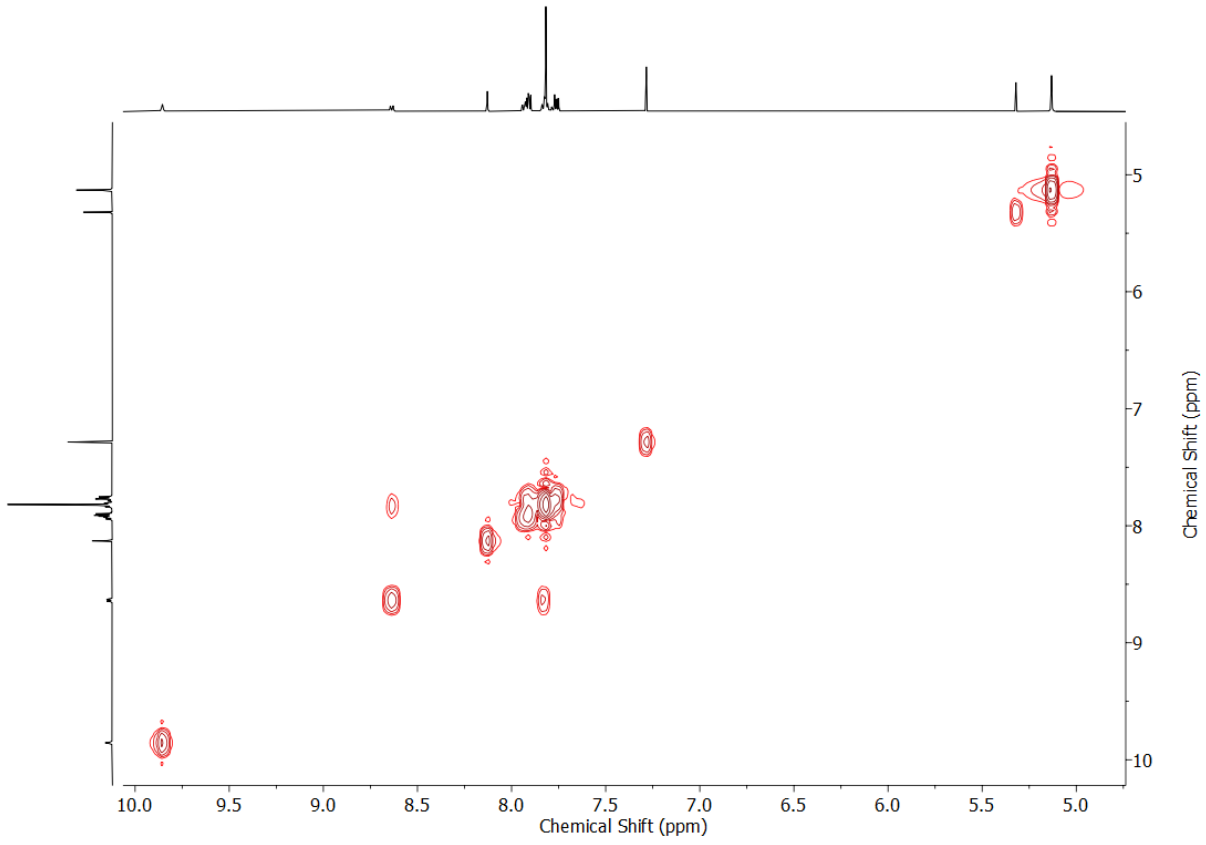

Figure S31 COSY NMR ($CDCl_3$) of $\mathbf{L^{Phth}}$.

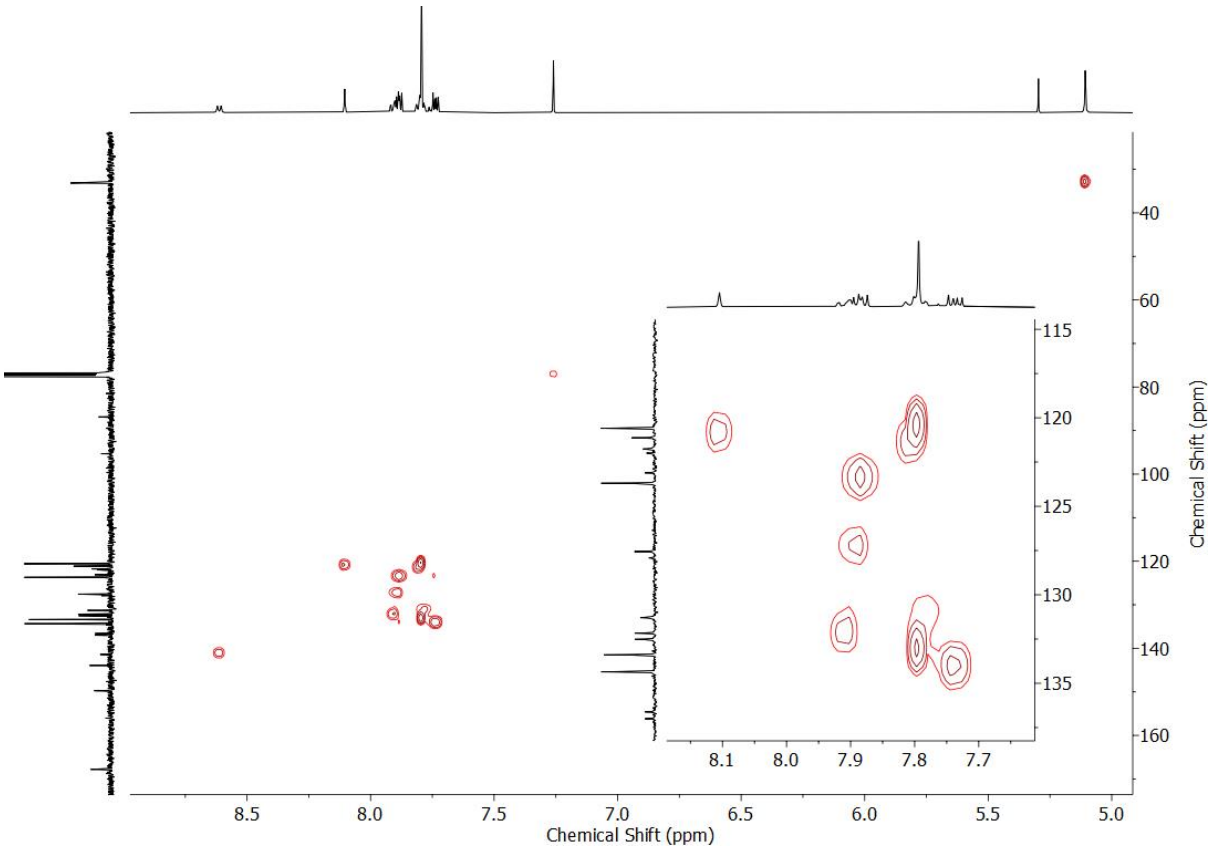

Figure S32 HSQC NMR ($CDCl_3$) of $\mathbf{L^{Phth}}$.

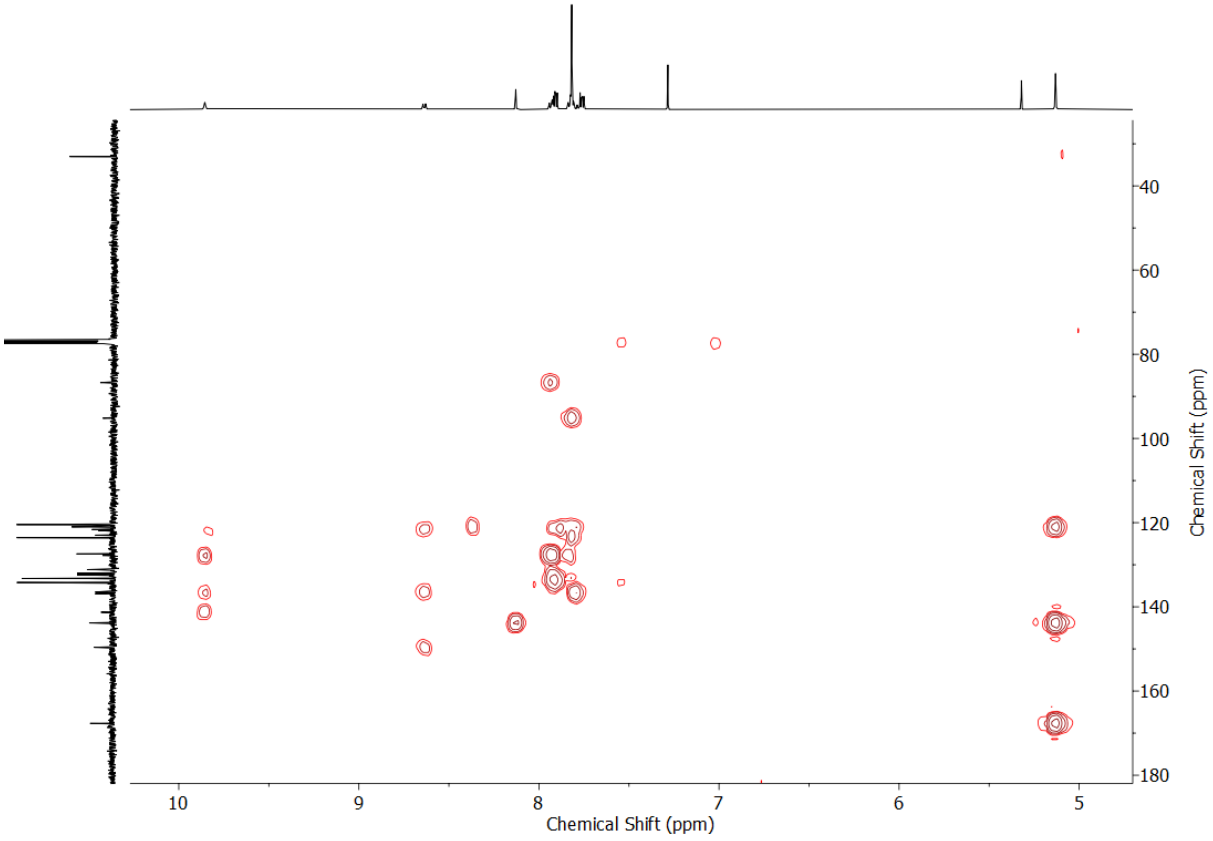

Figure S33 HMBC NMR ($CDCl_3$) of $\mathbf{L^{Phth}}$.

Synthesis of L^{Ene}

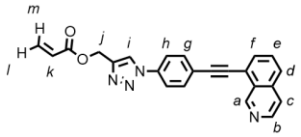

Prepared according to the general procedure with propargyl acrylate (83 µL, 0.75 mmol, 3 eq.). Purification by column chromatography (acetone/CH_2Cl_2 step gradient 0:100 ⟶ 15:85 in 5% increments) gave the product as a light yellow solid (79.4 mg, 83%). R_f = 0.34 (1:9 acetone/CH_2Cl_2). M.p. 145-147 °C. ^{1}H NMR (500 MHz, $CDCl_3$) δ: 9.88 (br. s, 1H, H_a), 8.66 (br. s, 1H, H_b), 8.14 (s, 1H, H_i), 7.89 (m, 2H, H_d/H_e, H_f), 7.87-7.74 (m, 6H, H_c, H_d/H_e, H_g, H_h), 6.48 (dd, *J* = 17.4, 1.3 Hz, 1H, H_m), 6.17 (dd, *J* = 17.3, 10.5 Hz, 1H, H_k), 5.89 (dd, *J* = 10.5, 1.4 Hz, 1H, H_l), 5.41 (s, 2H, H_j). ^{13}C NMR (126 MHz, $CDCl_3$) δ: 166.2, 150.3, 144.0, 142.4, 136.9, 136.3, 133.4, 132.3, 131.9, 130.7, 128.0, 127.6, 123.4, 122.1, 121.7, 120.6, 94.9, 87.2, 57.7 (2 × 4° C signals missing). HR-ESI-MS m/z = 381.1356 $[M+H]^+$ calc. 381.1352.

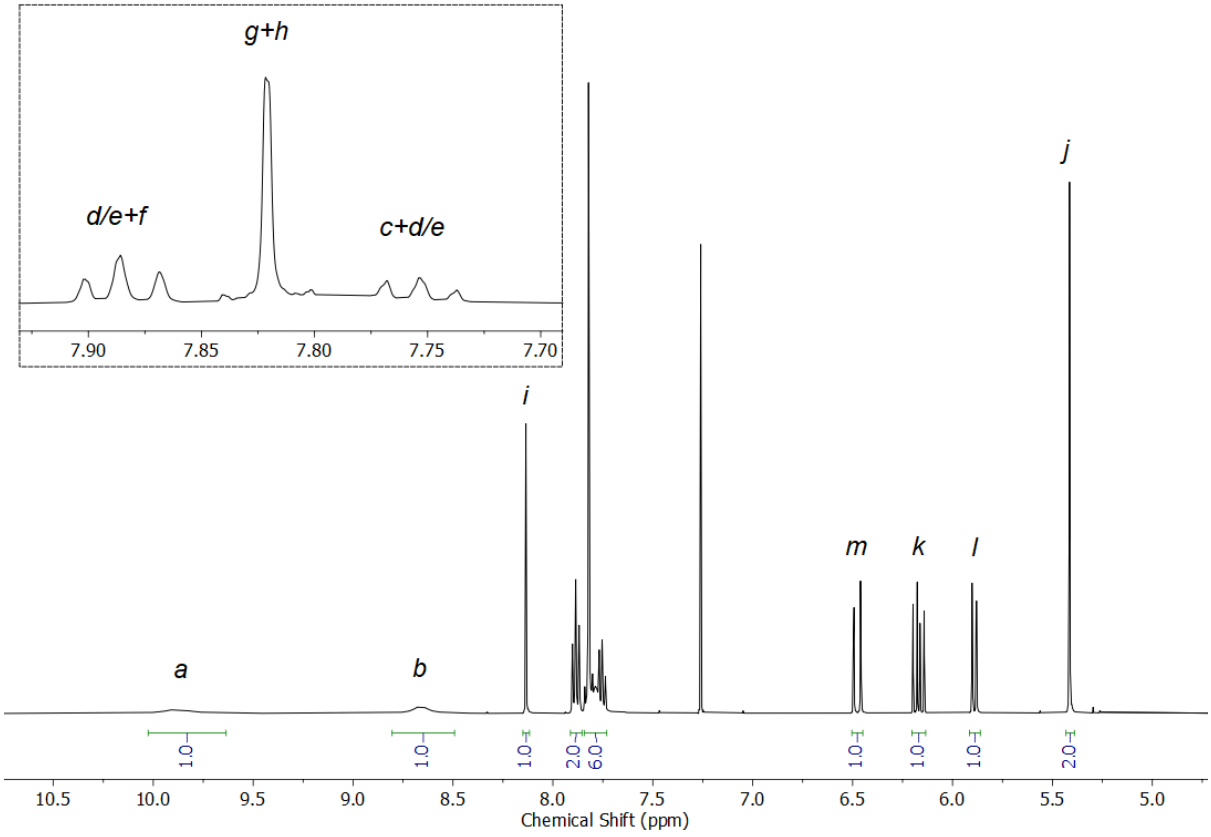

Figure S34 ^{1}H NMR ($CDCl_3$, 500 MHz) of L^{Ene}.

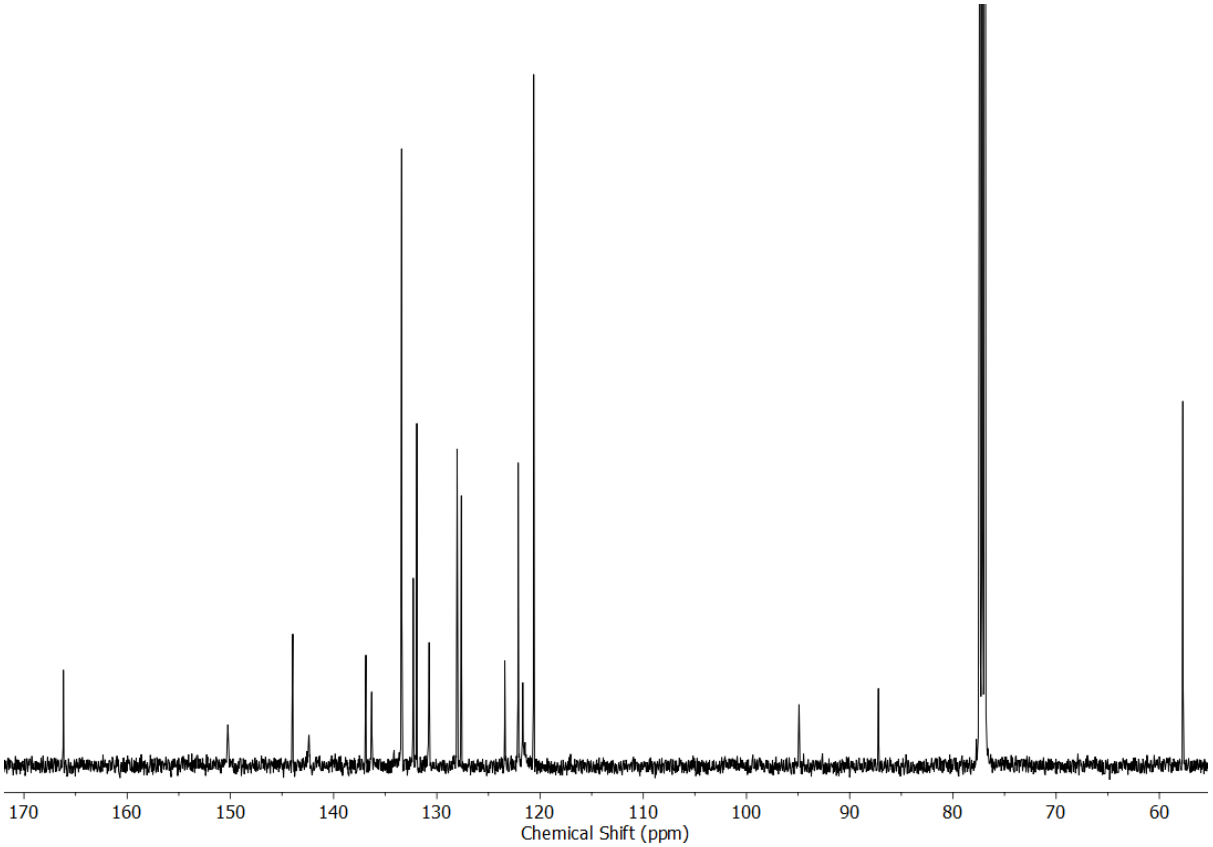

Figure S35 ^{13}C NMR ($CDCl_3$, 126 MHz) of $\mathbf{L^{Ene}}$.

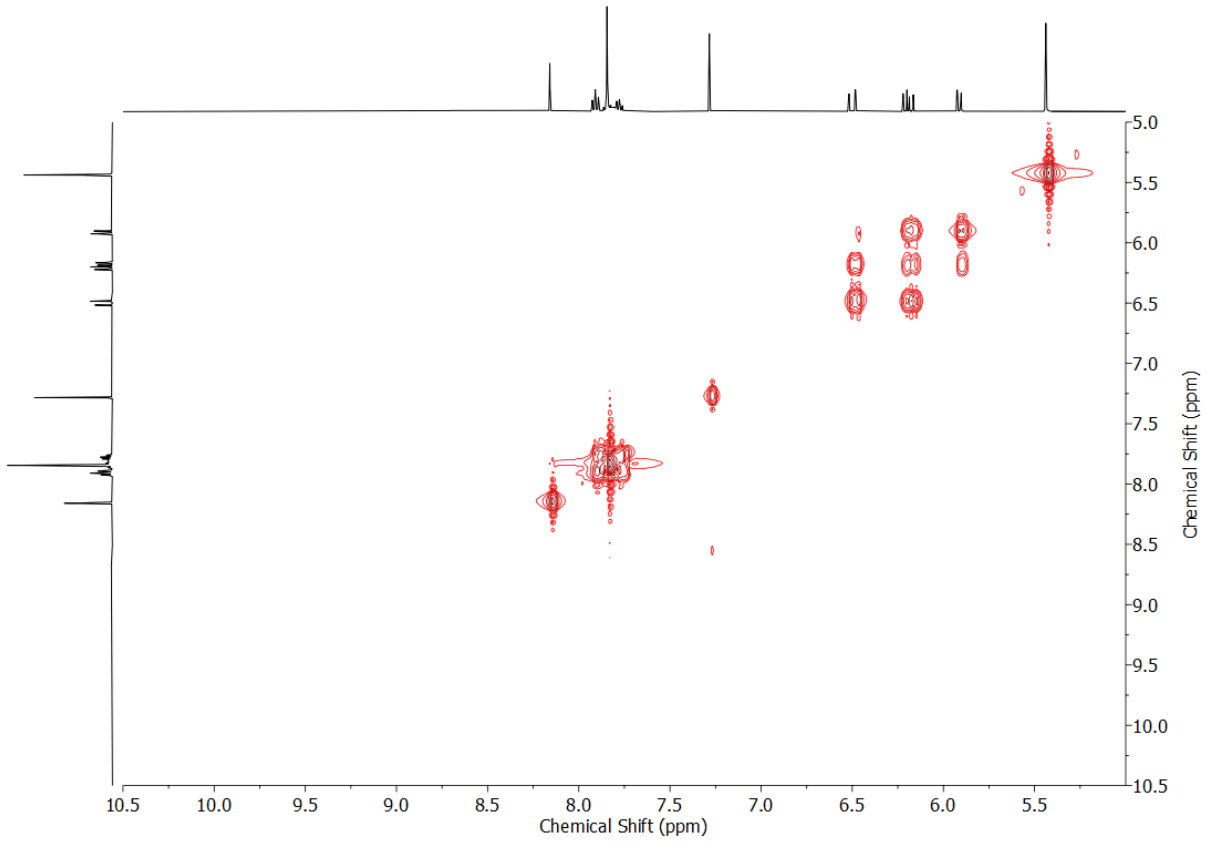

Figure S36 COSY NMR ($CDCl_3$) of $\mathbf{L^{Ene}}$.

Synthesis of L^{Anth}

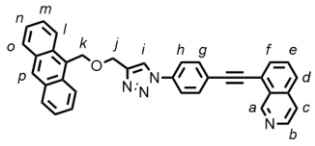

Prepared according to the general procedure with **S1** (77.0 mg, 0.313 mmol, 1.25 eq.). Purification by column chromatography (1:9 acetone/CH_2Cl_2) gave the product as a yellow solid (110 mg, 85%). R_f = 0.44 (1:9 acetone/CH_2Cl_2). ^{1}H NMR (400 MHz, $CDCl_3$) δ: 9.82 (s, 1H, H_a), 8.61 (d, *J* = 5.8 Hz, 1H, H_b), 8.48 (s, 1H, H_p), 8.38 (dd, *J* = 8.9, 1.0 Hz, 2H, H_o/H_l), 8.02 (m, 2H, H_o/H_l), 7.92 (s, 1H, H_i), 7.89-7.86 (m, 2H, H_d/H_e, H_f), 7.80-7.73 (m, 6H, H_c, H_d/H_e, H_g, H_h), 7.55 (ddd, *J* = 8.8, 6.5, 1.4 Hz, 2H, H_m/H_n), 7.48 (ddd, *J* = 7.8, 6.5, 1.1 Hz, 2H, H_m/H_n), 5.67 (s, 2H, H_k), 4.96 (d, *J* = 0.7 Hz, 2H, H_j). ^{13}C NMR (101 MHz, $CDCl_3$) δ: 150.2, 146.8, 142.2, 137.0, 136.4, 133.4, 132.3, 131.6, 131.2, 130.8, 129.2, 128.8, 128.3, 128.0, 127.5, 126.5, 125.2, 124.4, 123.1, 121.8, 121.4, 120.7, 120.5, 95.1, 87.0, 65.0, 64.1. HR-ESI-MS m/z = 517.2024 $[M+H]^+$ calc. 517.2028.

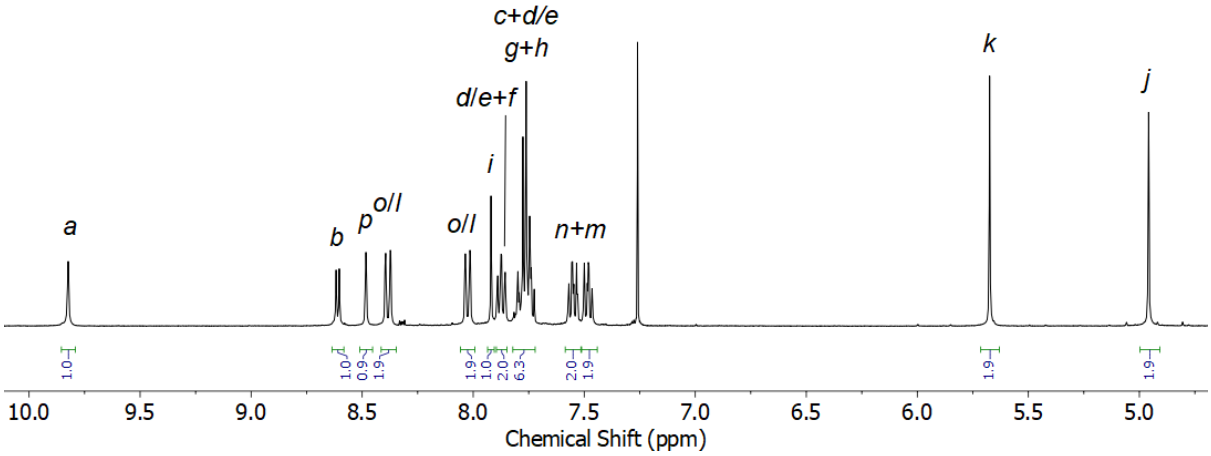

Figure S37 ^{1}H NMR ($CDCl_3$, 400 MHz) of L^{Anth}.

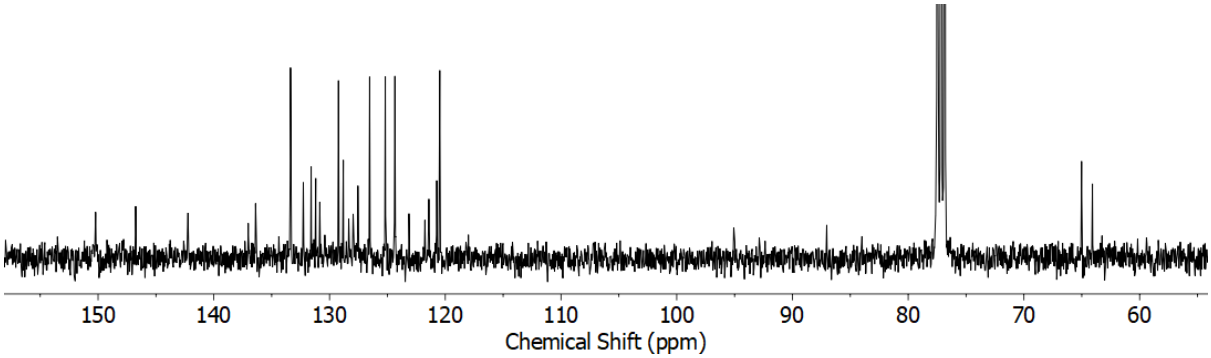

Figure S38 ^{13}C NMR ($CDCl_3$, 101 MHz) of L^{Anth}.

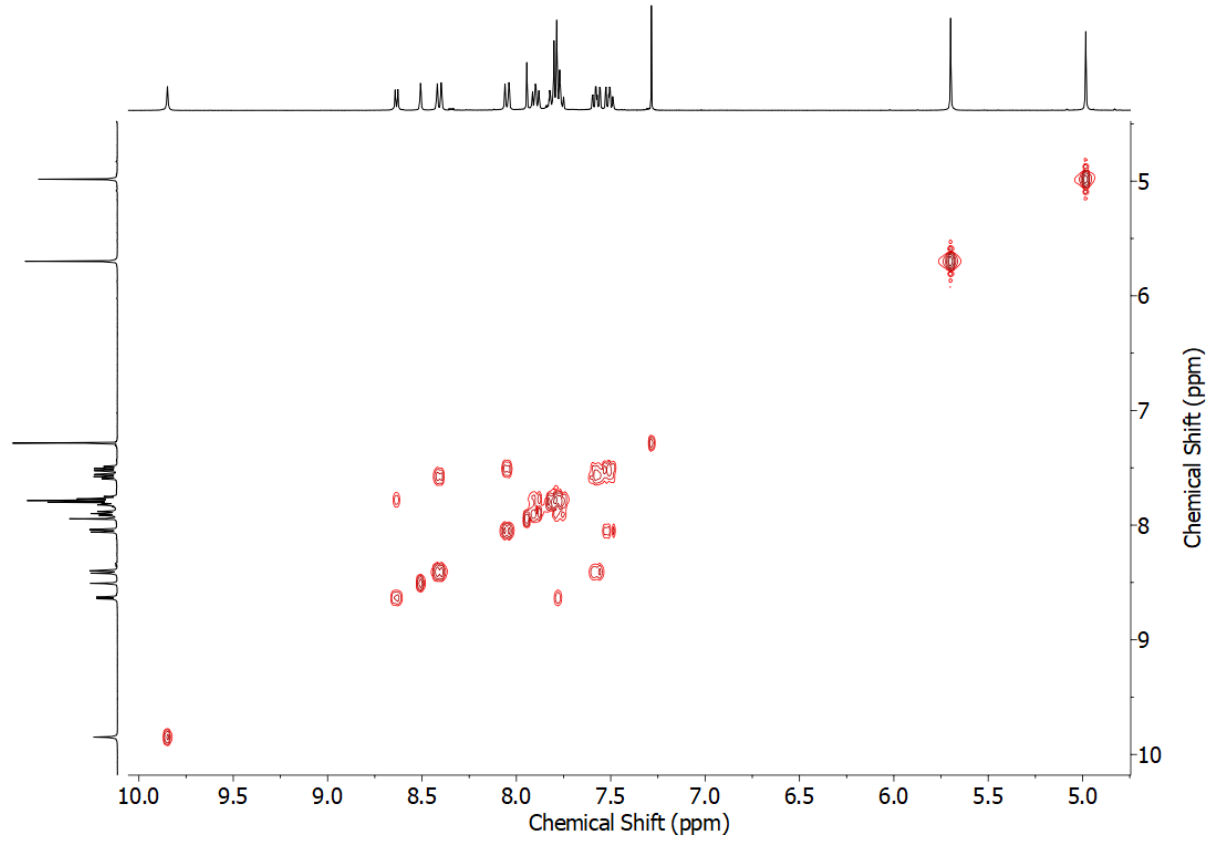

Figure S39 COSY NMR ($CDCl_3$) of $\mathbf{L^{Anth}}$.

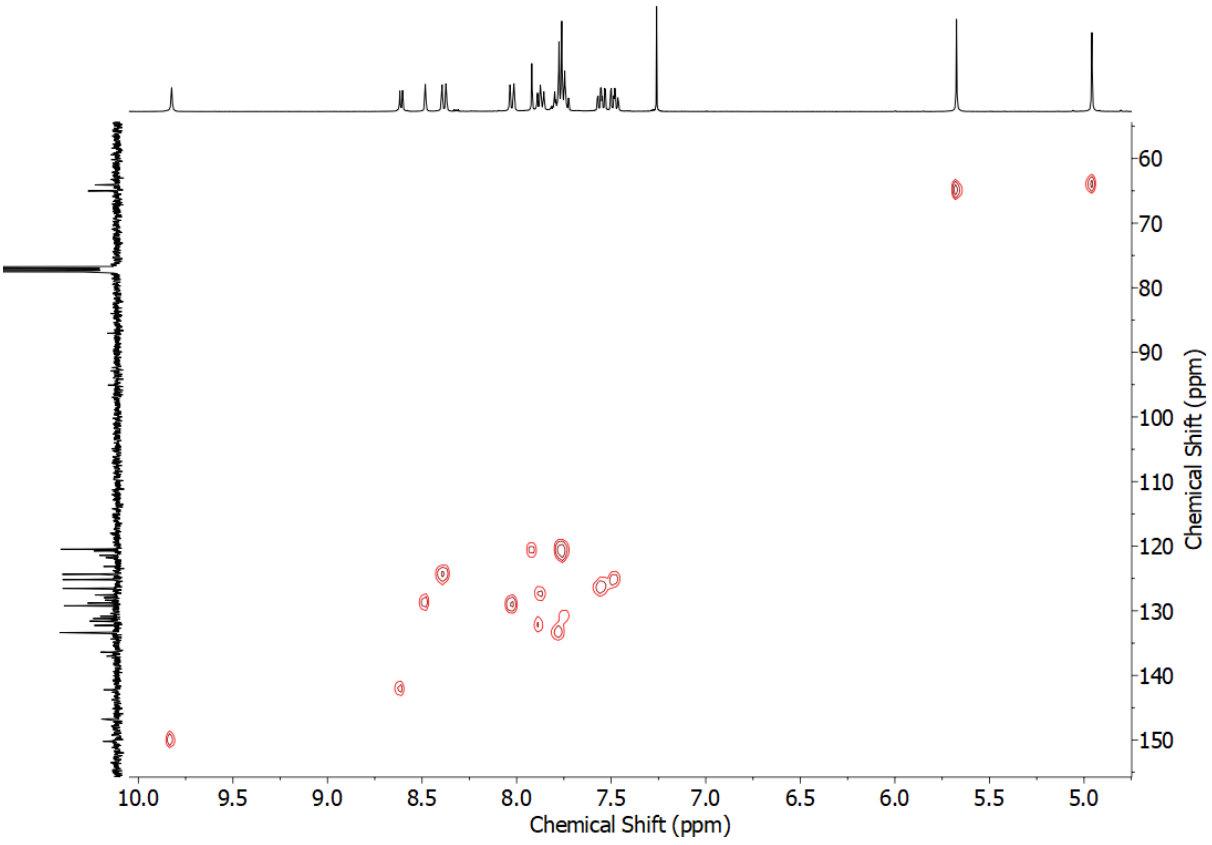

Figure S40 HSQC NMR ($CDCl_3$) of $\mathbf{L^{Anth}}$.

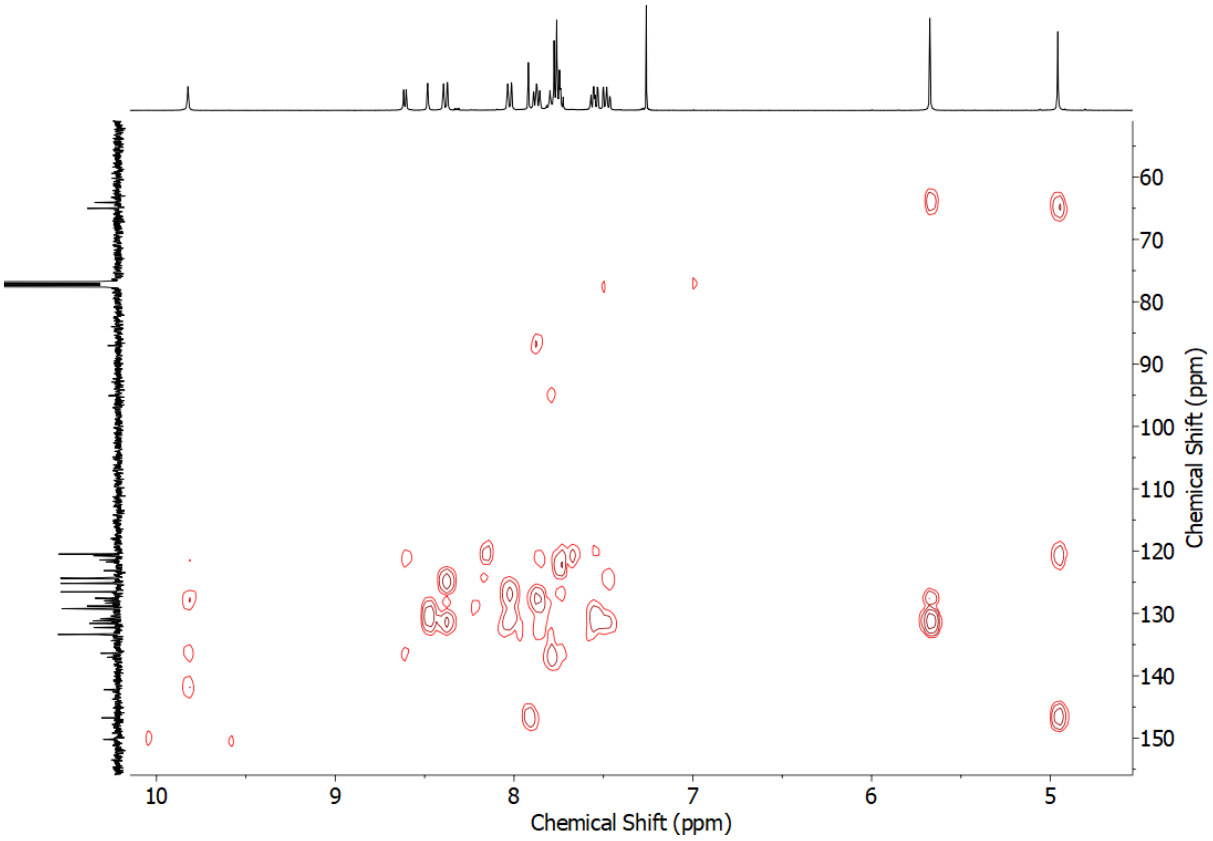

Figure S41 HMBC NMR ($CDCl_3$) of $\mathbf{L^{Anth}}$.

$[Pd_2(L^{Bu})_4](BF_4)_4$

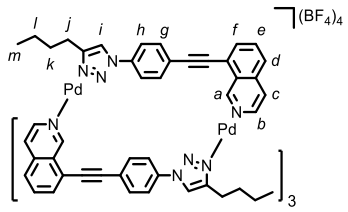

L^{Bu} (10.6 mg, 0.030 mmol, 2.0 eq.) and $[Pd(CH_3CN)_4](BF_4)_2$ (6.7 mg, 0.015 mmol, 1.0 eq.) were sonicated in d_6-DMSO (0.75 mL) until all solids were dissolved, giving a light yellow solution. Quantitative conversion to $[Pd_2(\mathbf{L^{Bu}})_4](BF_4)_4$ was observed by ^{1}H NMR. ^{1}H NMR (500 MHz, d_6-DMSO) δ: 10.30 (s, 4H, H_a), 9.89 (d, J = 6.7 Hz, 4H, H_b), 9.06 (s, 4H, H_i), 8.59 (d, J = 6.6 Hz, 4H, H_c), 8.30-8.21 (m, 20H, H_d, H_g, H_h), 8.10-8.05 (m, 8H, H_e, H_f), 3.30 (m, 1H, H_j), 2.95 (ddd, J = 15.2, 8.8, 6.0 Hz, 1H, $H_{j'}$), 1.49-1.41 (m, 1H, H_k), 1.35-1.27 (m, 2H, H_l), 1.25-1.17 (m, 1H, $H_{k'}$), 0.82 (t, J = 7.3 Hz, 12H, H_m). Diffusion coefficient (500 MHz, d_6-DMSO) D: 1.03 × 10^{-10} m^2s^{-1}. ^{13}C NMR (126 MHz, d_6-DMSO) δ: 155.0, 150.6, 142.9, 136.5, 136.0, 134.4, 133.4, 133.3, 128.2, 127.5, 125.0, 124.1, 123.0, 120.4, 120.3, 96.0, 86.6, 30.0, 24.8, 21.4, 13.7. ESI-MS m/z = 405.12 $\{[Pd_2(L^{Bu})_4]\}^{4+}$ calc. 405.12; 569.17 $\{[Pd_2(L^{Bu})_4](BF_4)\}^{3+}$ calc. 569.16; 897.26 $\{[Pd_2(L^{Bu})_4](BF_4)_2\}^{2+}$ calc. 897.24; 1881.51 $\{[Pd_2(L^{Bu})_4](BF_4)_3\}^{+}$ calc. 1881.49.

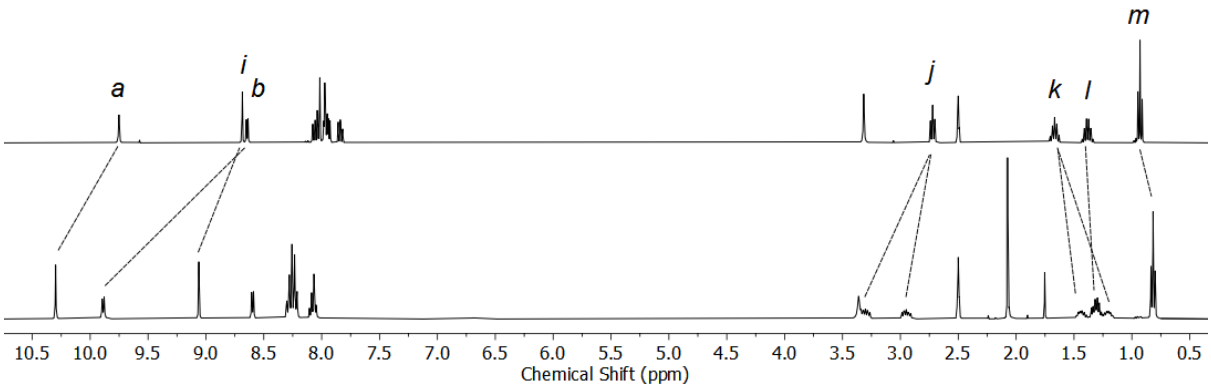

Figure S42 Stacked ^{1}H NMR spectra (d_6-DMSO, 400 MHz) of **L^{Bu}** (top) and $[Pd_2(\mathbf{L^{Bu}})_4](BF_4)_4$ (bottom). Δδ (ppm): H_a 0.50; H_b 1.25; H_i 0.37.

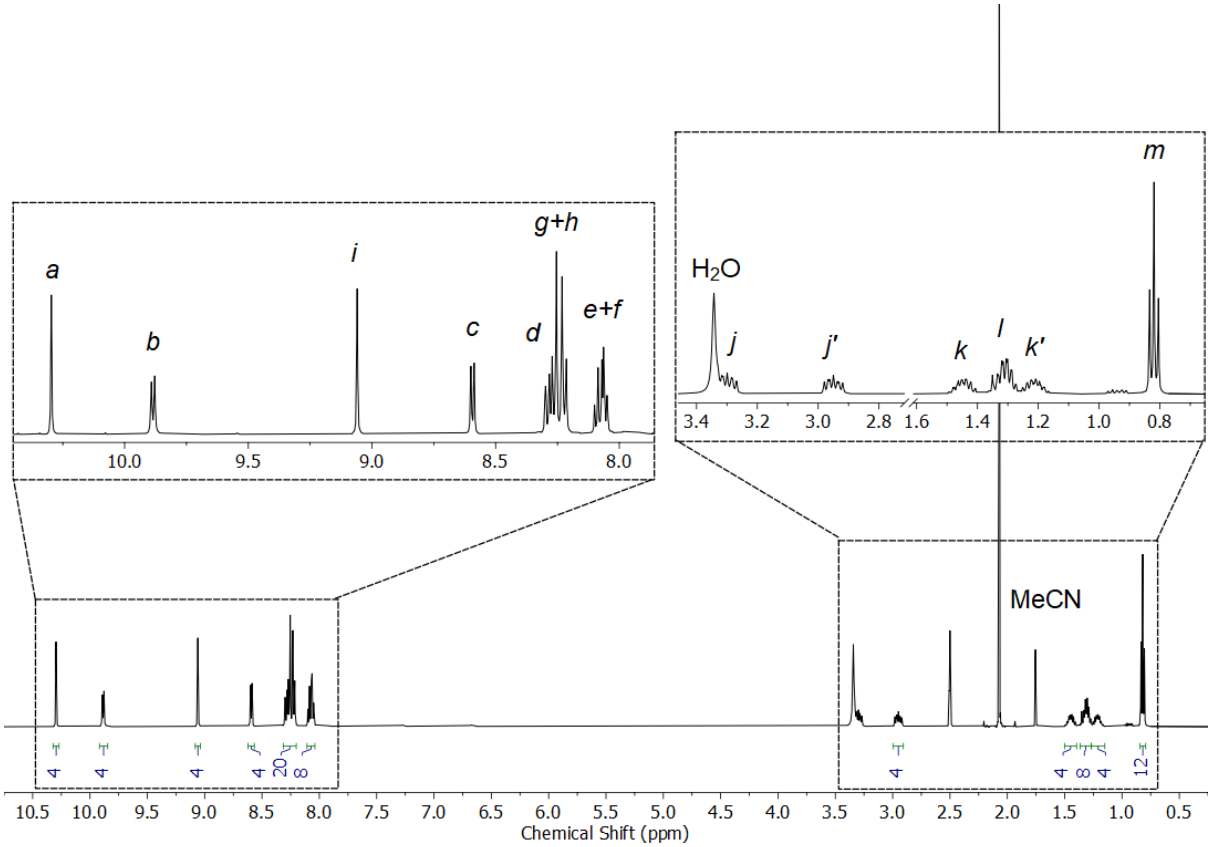

Figure S43 ^{1}H NMR (d_6-DMSO, 500 MHz) of $[Pd_2(\mathbf{L^{Bu}})_4](BF_4)_4$.

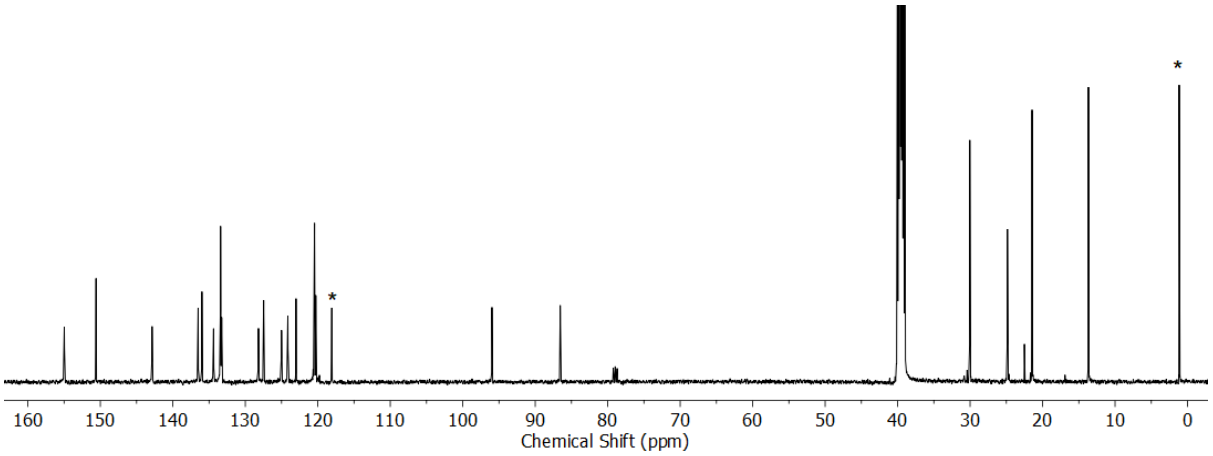

Figure S44 ^{13}C NMR (d_6-DMSO, 126 MHz) of $[Pd_2(\mathbf{L^{Bu}})_4](BF_4)_4$. CH_3CN from the Pd(II) source is indicated(*).

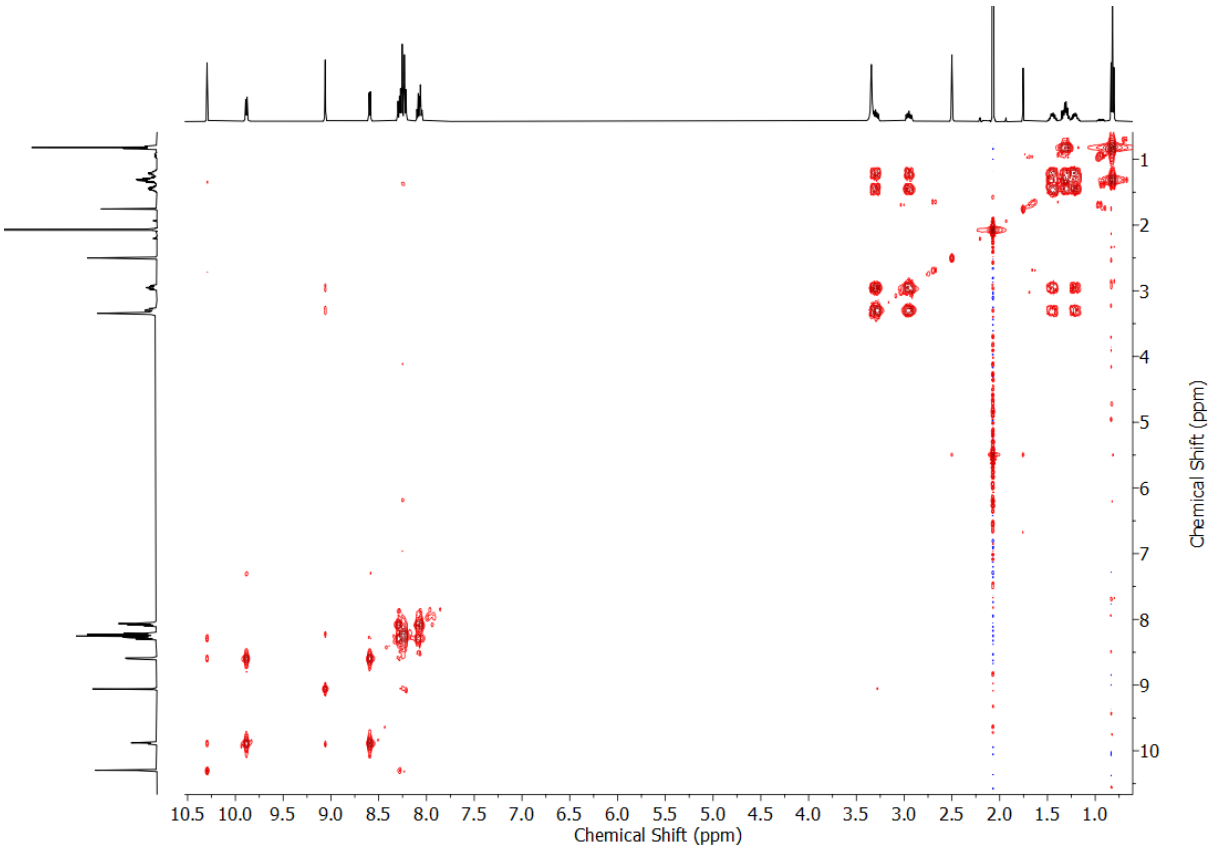

Figure S45 COSY NMR (d_6-DMSO) of $[Pd_2(\mathbf{L}^{\mathbf{Bu}})_4](BF_4)_4$.

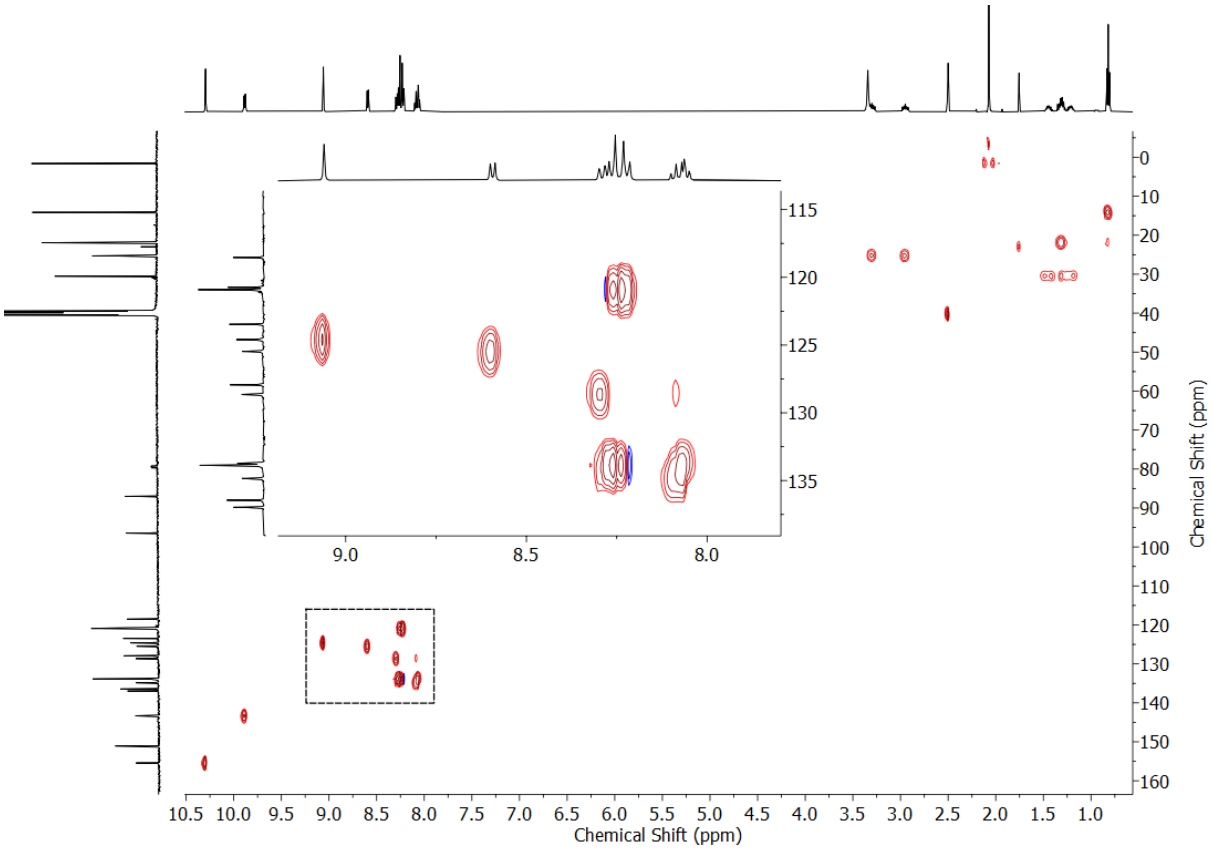

Figure S46 HSQC NMR (d_6-DMSO) of $[Pd_2(\mathbf{L}^{\mathbf{Bu}})_4](BF_4)_4$.

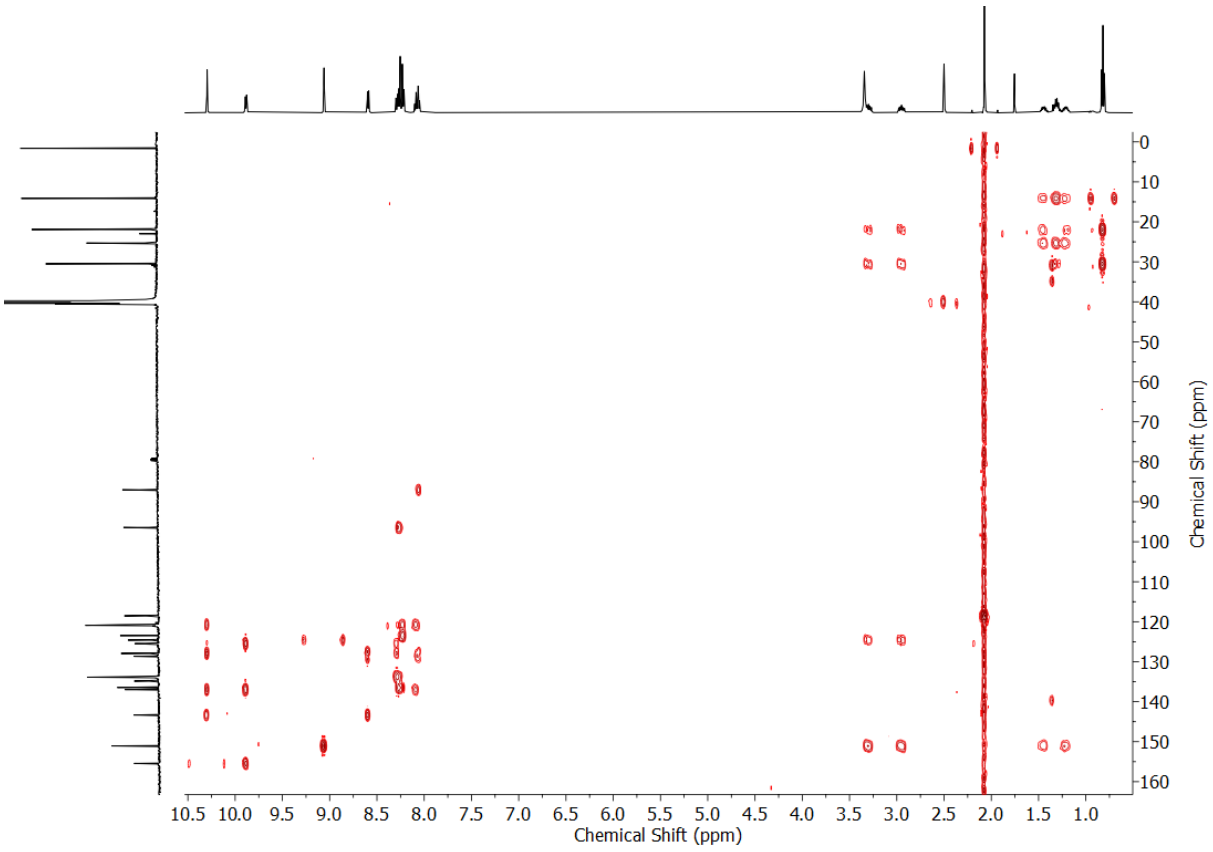

Figure S47 HMBC NMR (d_6-DMSO) of $[Pd_2(\mathbf{L^{Bu}})_4](BF_4)_4$.

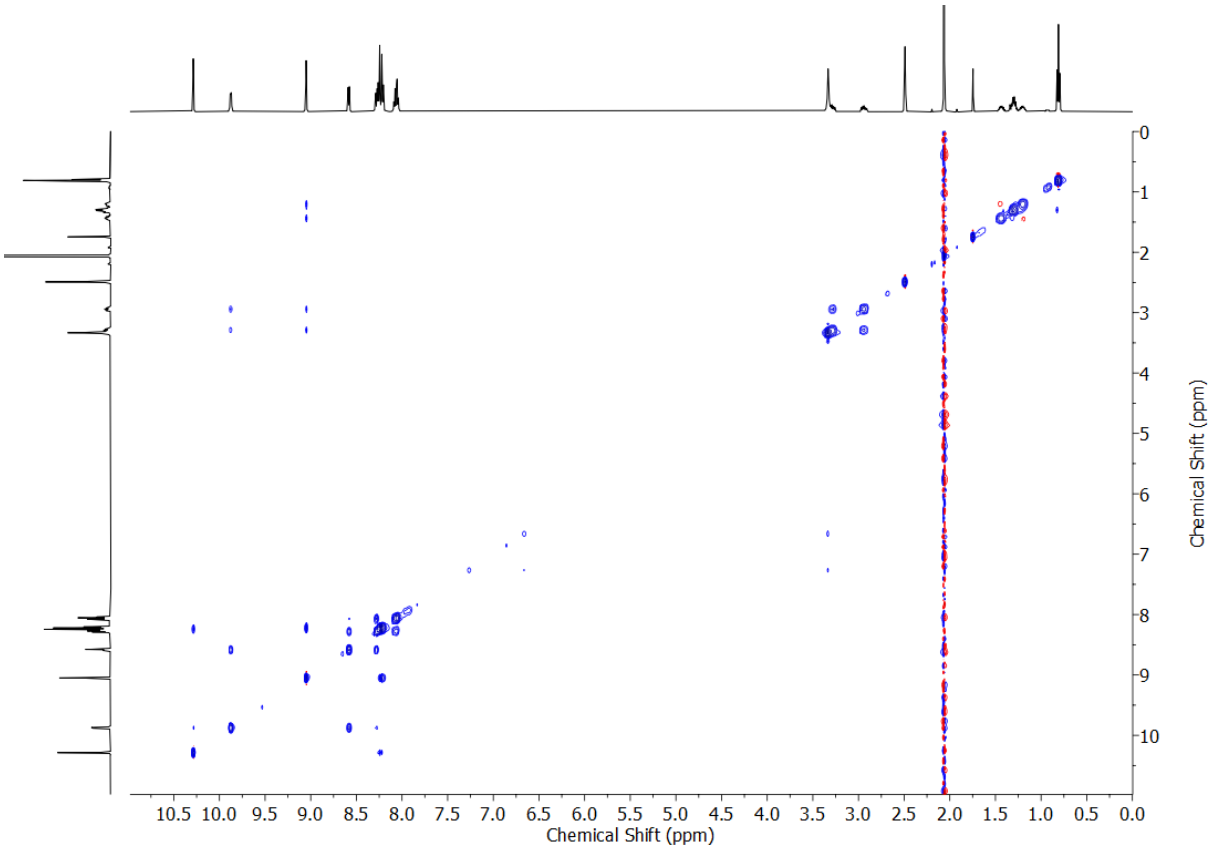

Figure S48 NOESY NMR (d_6-DMSO, 500 MHz) of $[Pd_2(\mathbf{L^{Bu}})_4](BF_4)_4$.

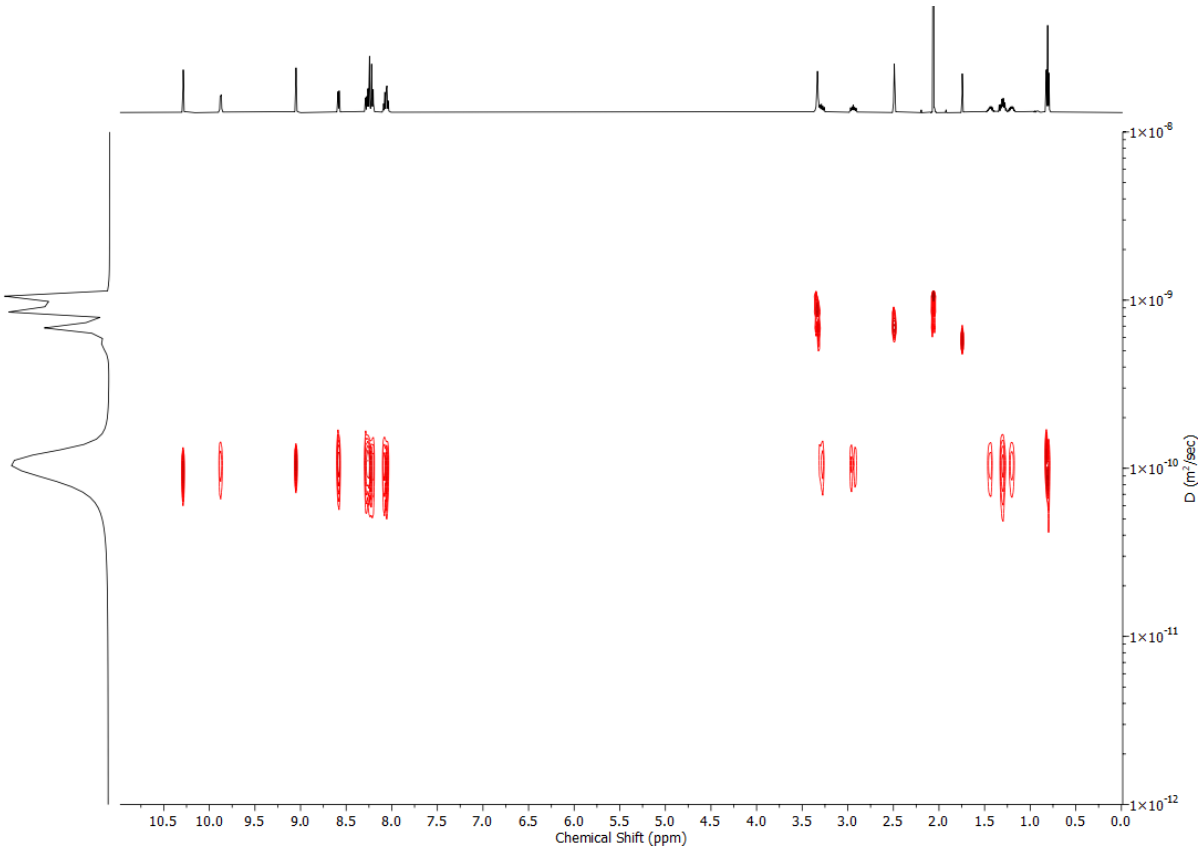

Figure S49 DOSY NMR (d_6-DMSO, 500 MHz) of $[Pd_2(\mathbf{L}^{\mathbf{Bu}})_4](BF_4)_4$.

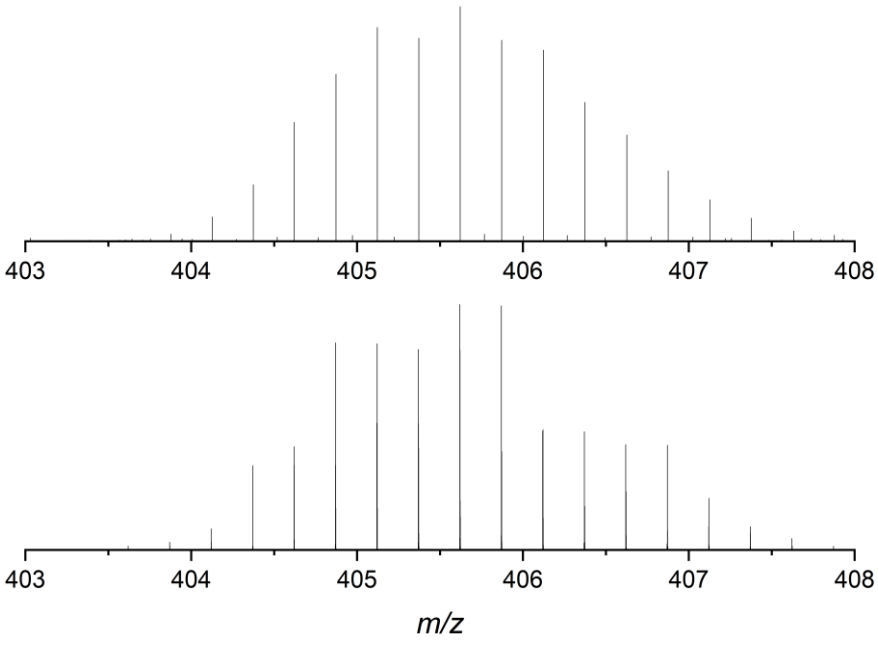

Figure S50 Observed (top) and calculated (bottom) isotopic patterns for $\{[Pd_2(\mathbf{L}^{\mathbf{Bu}})_4]\}^{4+}$.

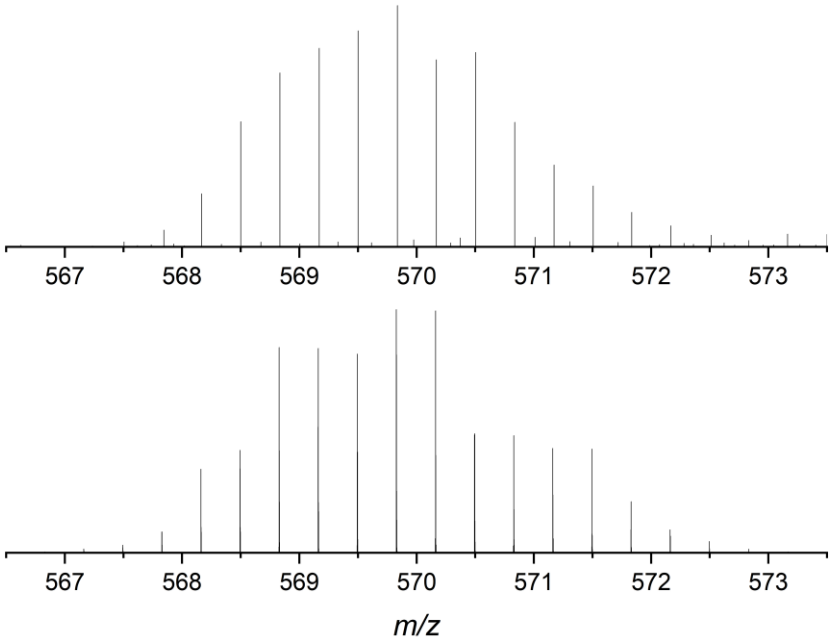

Figure S51 Observed (top) and calculated (bottom) isotopic patterns for $\{[Pd_2(\mathbf{L}^{Bu})_4](BF_4)\}^{3+}$.

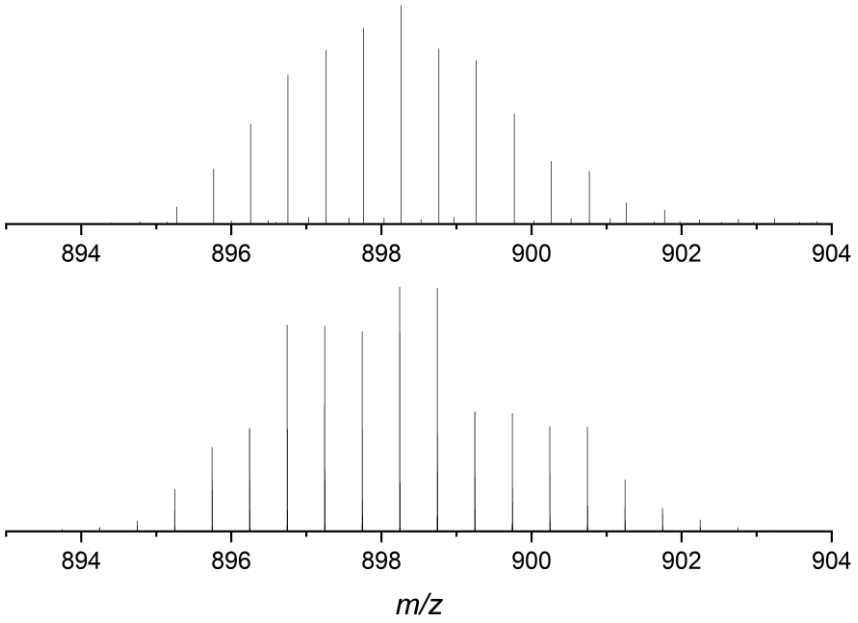

Figure S52 Observed (top) and calculated (bottom) isotopic patterns for $\{[Pd_2(\mathbf{L}^{Bu})_4](BF_4)_2\}^{2+}$.

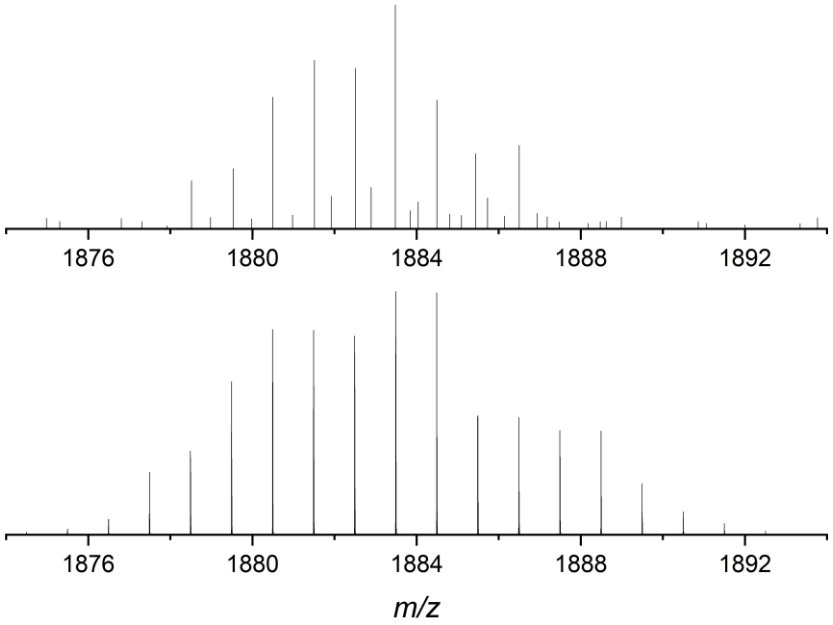

Figure S53 Observed (top) and calculated (bottom) isotopic patterns for $\{[Pd_2(\mathbf{L}^{\mathbf{Bu}})_4](BF_4)_3\}^+$.

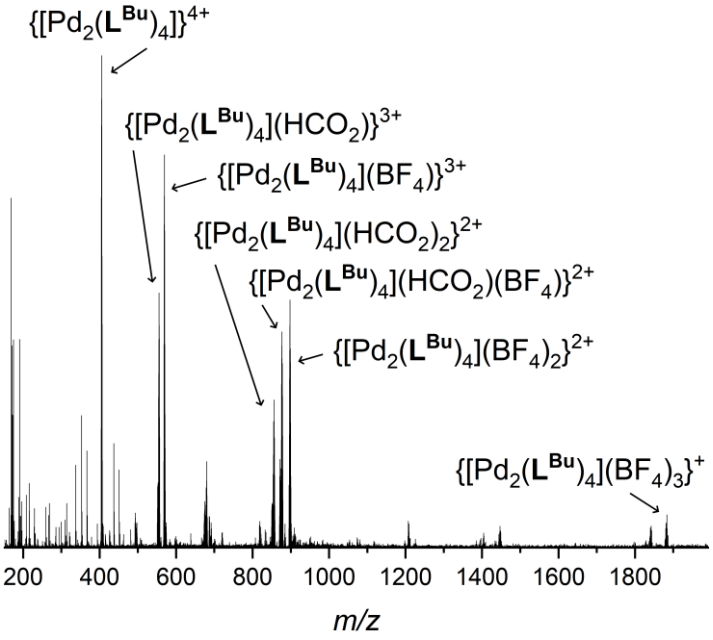

Figure S54 ESI-MS of $[Pd_2(\mathbf{L}^{\mathbf{Bu}})_4](BF_4)_4$.

$[Pd_2(L^{Bn})_4](BF_4)_4$

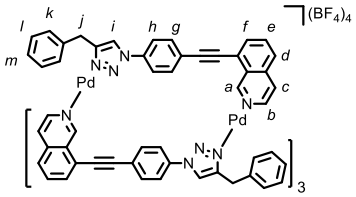

L^{Bn} (11.6 mg, 0.030 mmol, 2.0 eq.) and $[Pd(CH_3CN)_4](BF_4)_2$ (6.7 mg, 0.015 mmol, 1.0 eq.) were sonicated in d_6-DMSO (0.75 mL) until all solids were dissolved, giving a light yellow solution. Quantitative conversion to $[Pd_2(\mathbf{L^{Bn}})_4](BF_4)_4$ was observed by ^{1}H NMR. ^{1}H NMR (400 MHz, d_6-DMSO) δ: 10.31 (s, 4H, H_a), 9.67 (d, J = 6.7 Hz0, 4H, H_b), 9.05 (s, 4H, H_i), 8.33-8.27 (m, 20H, H_c, H_h, H_g), 8.22-8.18 (m, 4H, H_d), 8.08-8.04 (m, 8H, H_e, H_f), 7.16 (t, J = 7.3 Hz, 4H, H_m), 7.08 (app. t, J = 7.4 Hz, 8H, H_l), 6.89 (d, J = 6.8 Hz, 8H, H_k), 4.71 (d, J = 16.9 Hz, 4H, H_j), 4.61 (d, J = 16.8 Hz, 4H, $H_{j'}$). Diffusion coefficient (500 MHz, d_6-DMSO) D: 9.53 × 10^{-11} m^2s^{-1}. ^{13}C NMR (101 MHz, d_6-DMSO) δ: 154.8, 149.0, 142.6, 136.4, 136.3, 136.0, 134.2, 133.3, 133.2, 128.4, 128.2, 127.9, 127.4, 126.9, 125.3, 125.0, 123.1, 120.6, 120.2, 96.0, 86.7, 30.6. ESI-MS m/z = 439.11 $\{[Pd_2(L^{Bn})_4]\}^{4+}$ calc. 439.10; 614.49 $\{[Pd_2(L^{Bn})_4](BF_4)\}^{3+}$ calc. 614.47; 965.23 $\{[Pd_2(L^{Bn})_4](BF_4)_2\}^{2+}$ calc. 965.21.

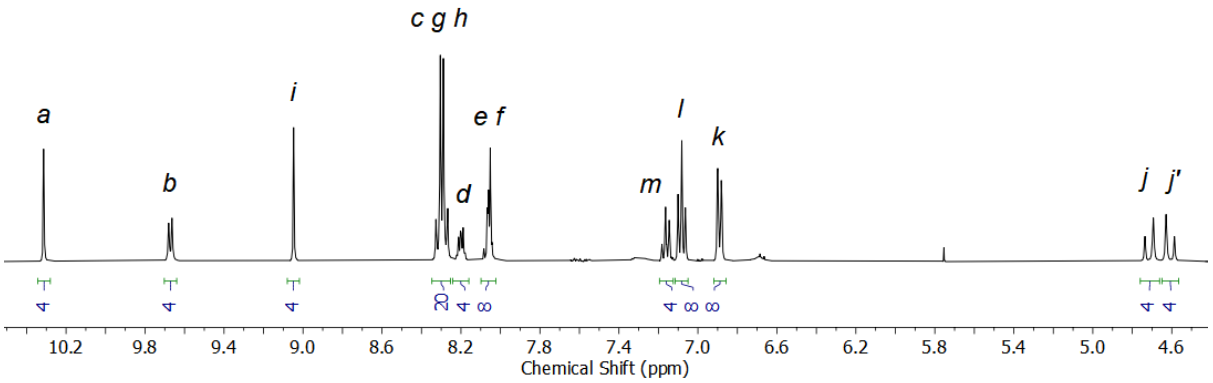

Figure S55 ^{1}H NMR (d_6-DMSO, 400 MHz) of $[Pd_2(\mathbf{L^{Bn}})_4](BF_4)_4$.

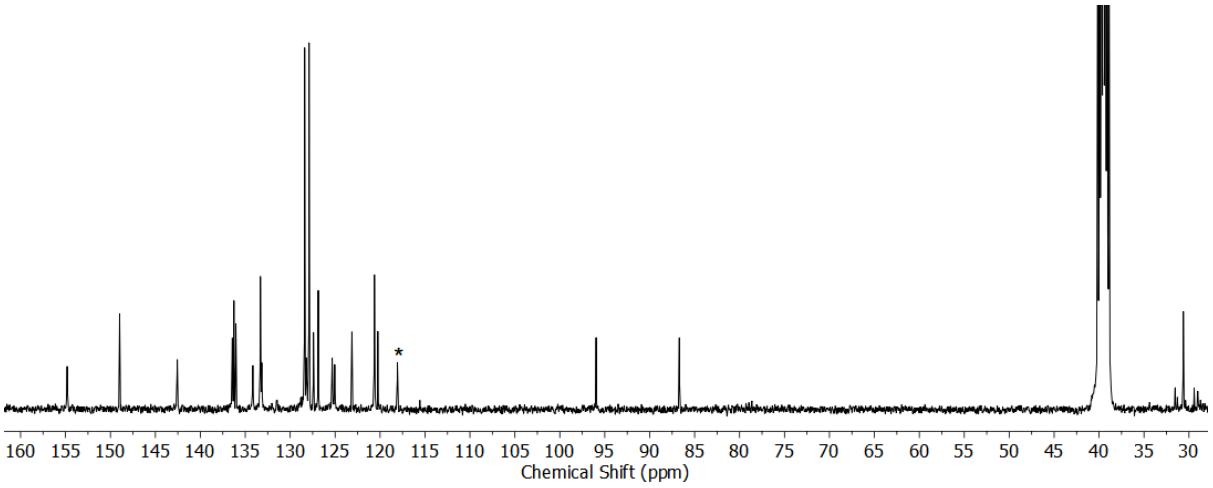

Figure S56 ^{13}C NMR (d_6-DMSO, 101 MHz) of $[Pd_2(\mathbf{L^{Bn}})_4](BF_4)_4$. CH_3CN from the Pd(II) source is indicated(*).

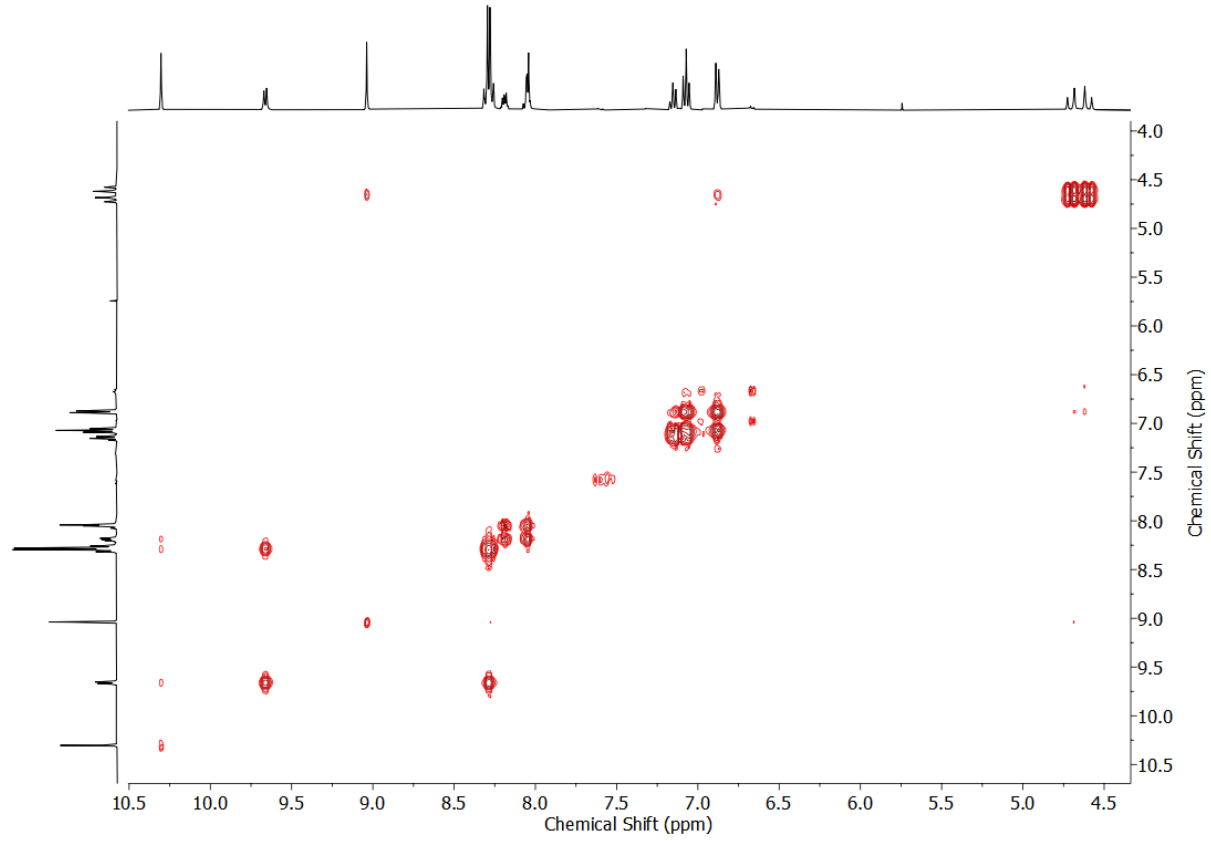

Figure S57 COSY NMR (d_6-DMSO) of $[Pd_2(\mathbf{L^{Bn}})_4](BF_4)_4$.

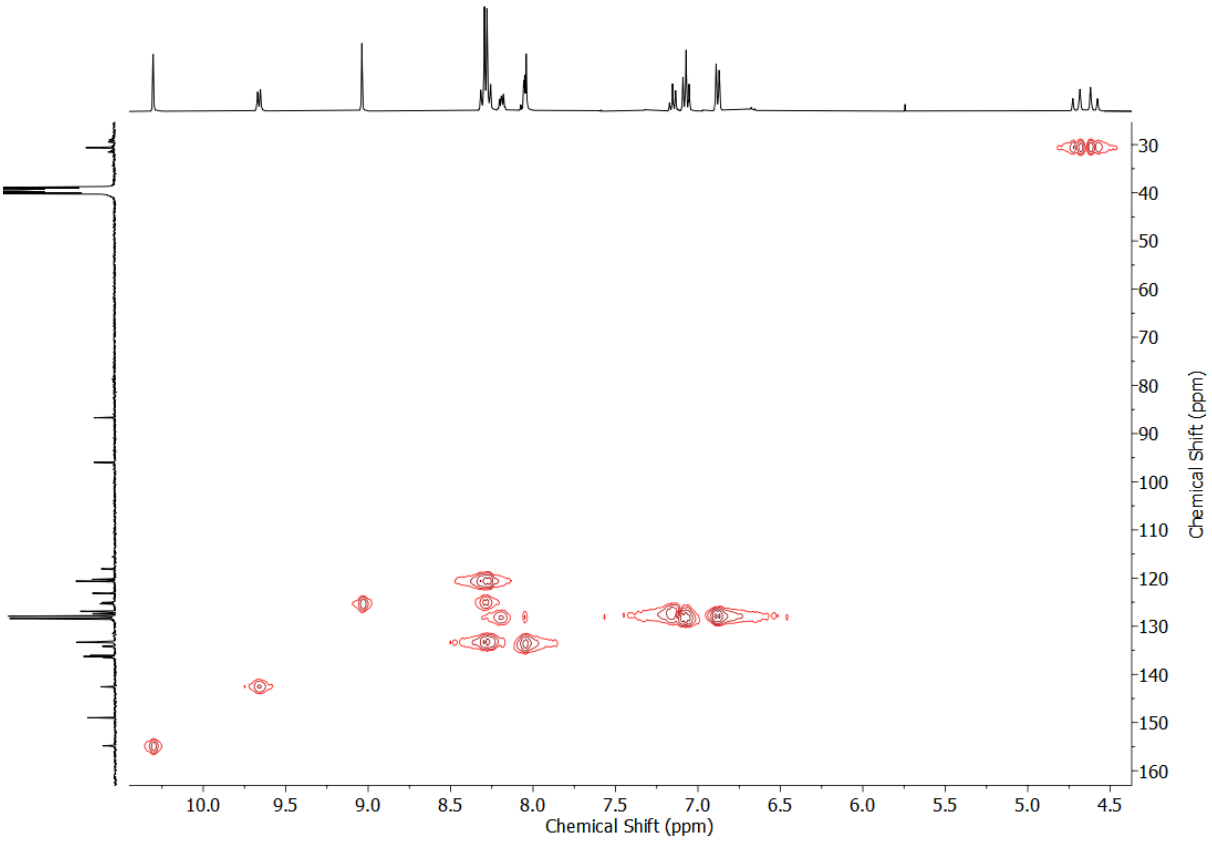

Figure S58 HSQC NMR (d_6-DMSO) of $[Pd_2(\mathbf{L^{Bn}})_4](BF_4)_4$.

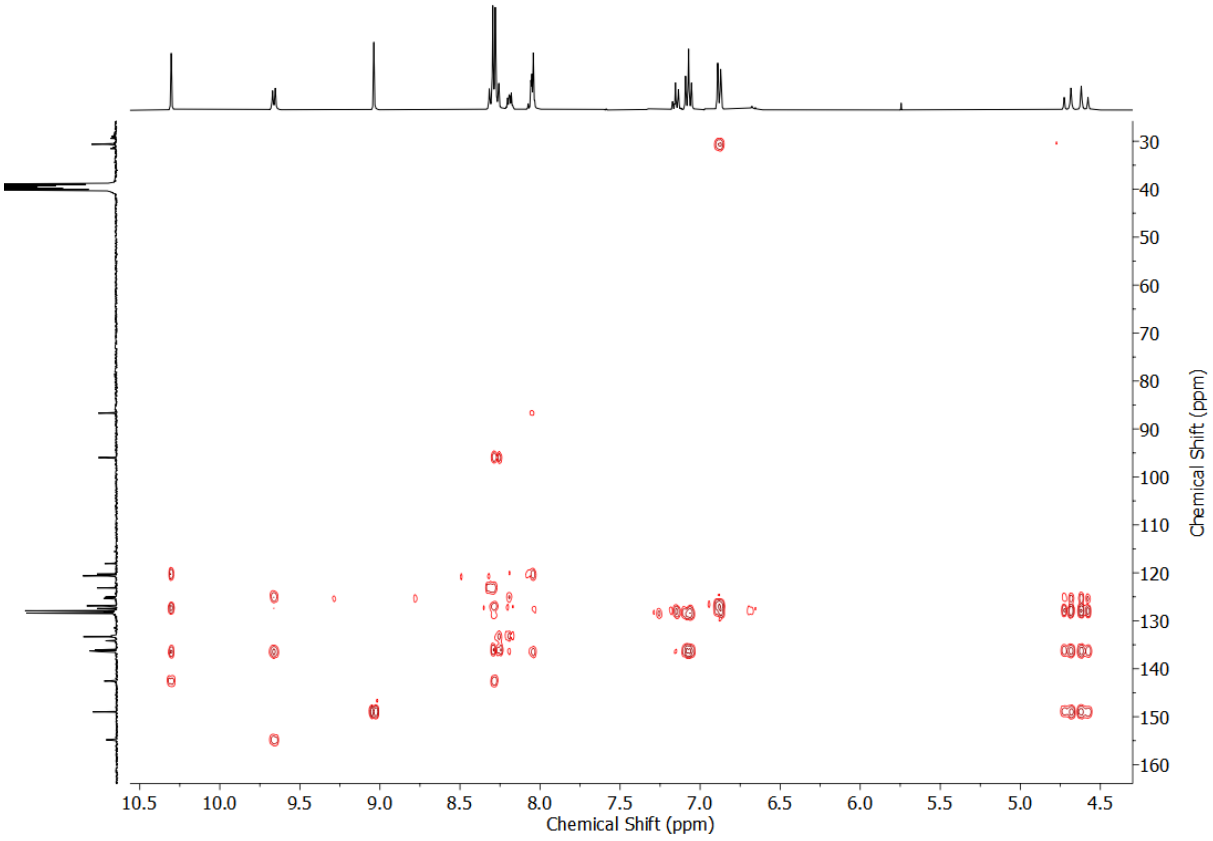

Figure S59 HMBC NMR (d_6-DMSO) of $[Pd_2(\mathbf{L}^{\mathbf{Bn}})_4](BF_4)_4$.

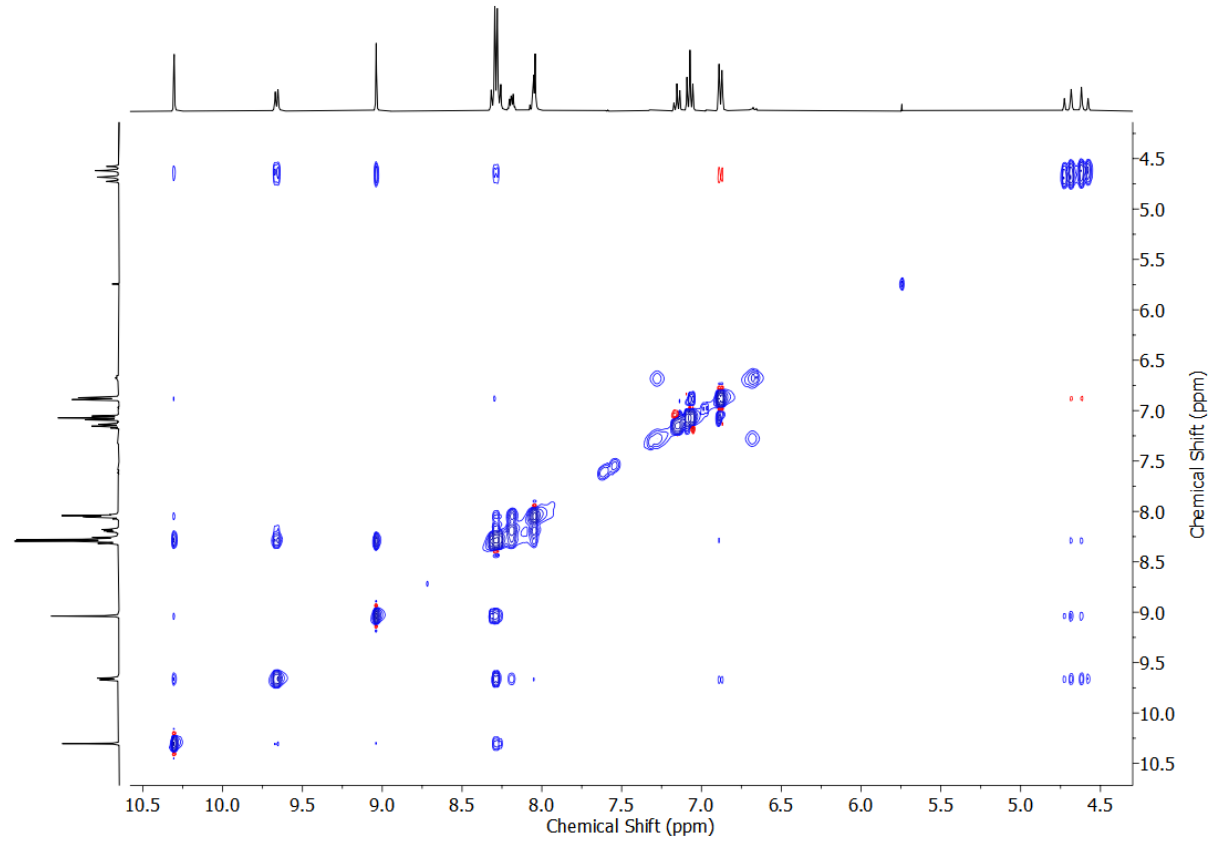

Figure S60 NOESY NMR (d_6-DMSO, 400 MHz) of $[Pd_2(\mathbf{L}^{\mathbf{Bn}})_4](BF_4)_4$.

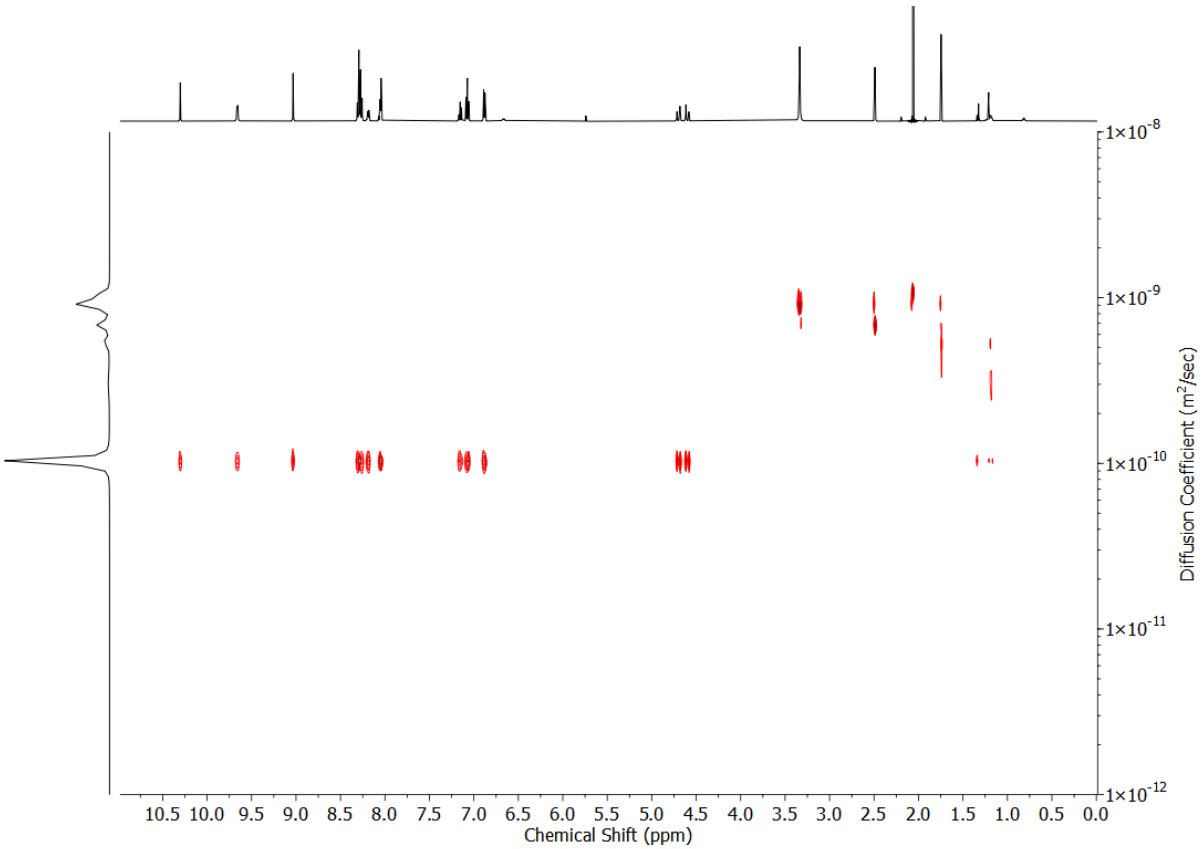

Figure S61 DOSY NMR (d_6-DMSO, 500 MHz) of $[Pd_2(\mathbf{L^{Bn}})_4](BF_4)_4$.

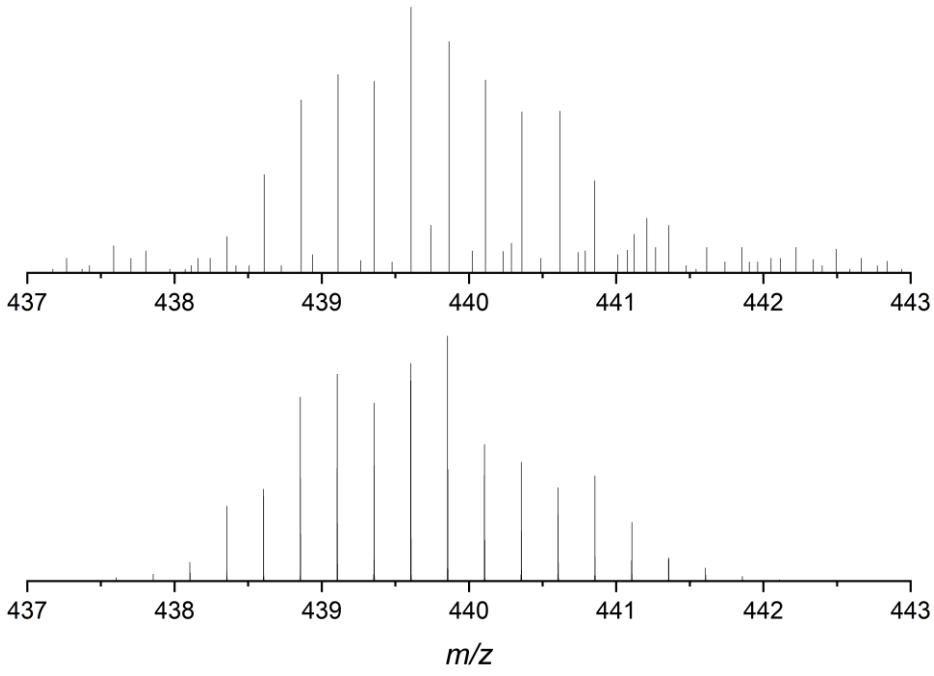

Figure S62 Observed (top) and calculated (bottom) isotopic patterns for $\{[Pd_2(\mathbf{L^{Bn}})_4]\}^{4+}$.

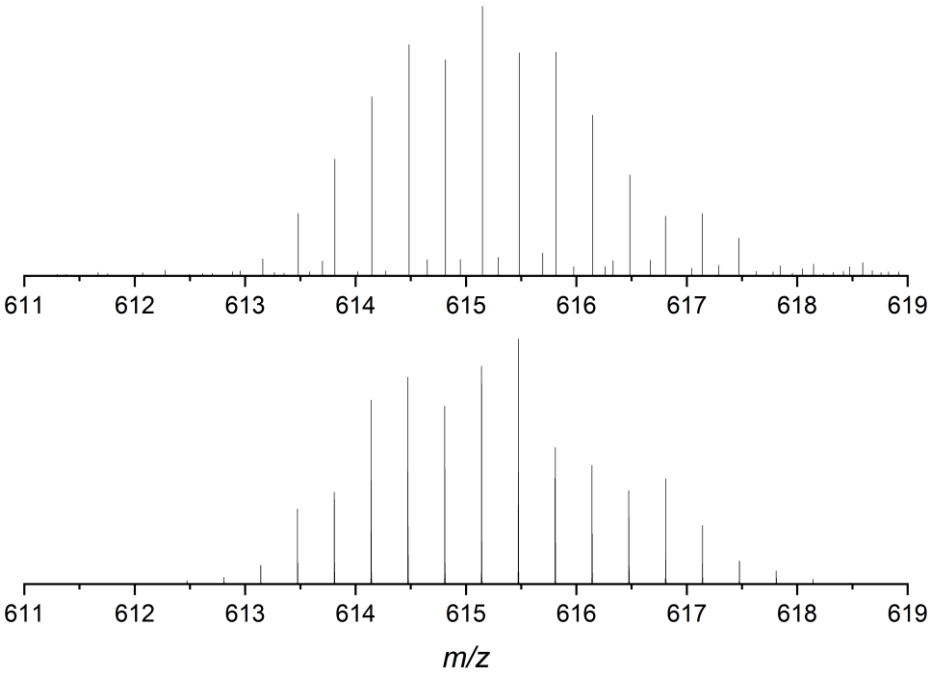

Figure S63 Observed (top) and calculated (bottom) isotopic patterns for $\{[Pd_2(\mathbf{L}^{Bn})_4](BF_4)\}^{3+}$.

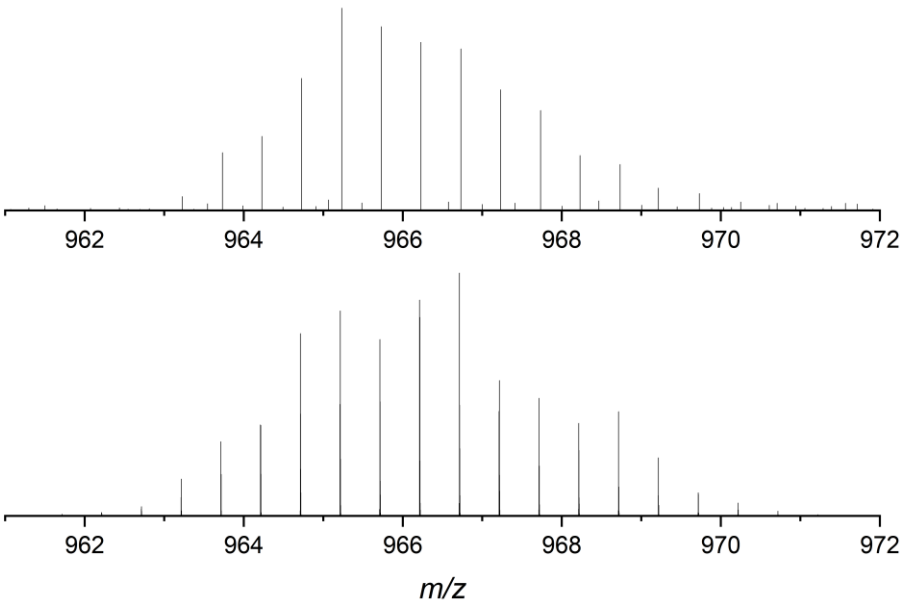

Figure S64 Observed (top) and calculated (bottom) isotopic patterns for $\{[Pd_2(\mathbf{L}^{Bn})_4](BF_4)_2\}^{2+}$.

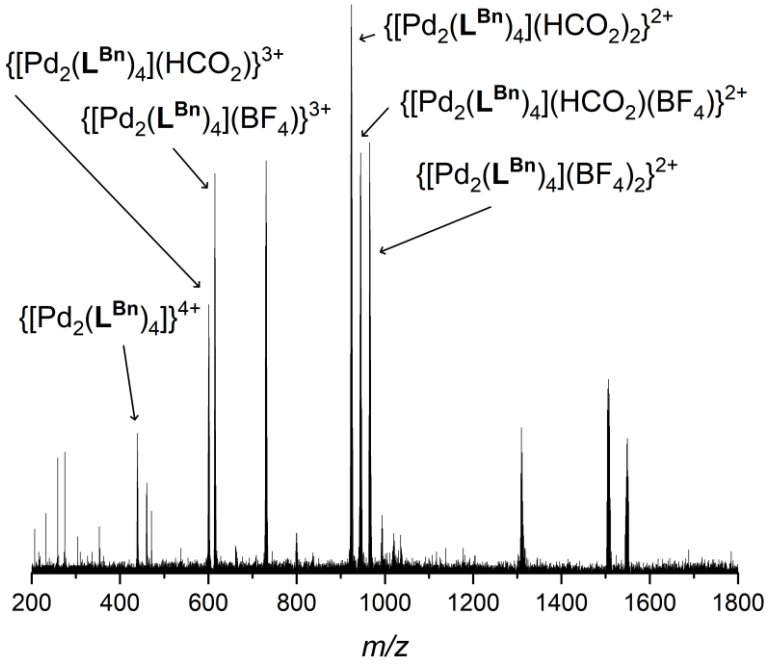

Figure S65 ESI-MS of $[Pd_2(\mathbf{L^{Bn}})_4](BF_4)_4$.

$[Pd_2(L^{OH})_4](BF_4)_4$

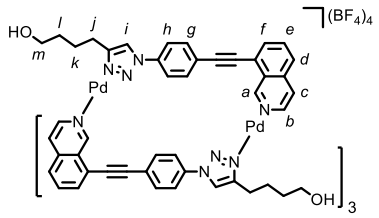

L^{OH} (11.1 mg, 0.030 mmol, 2.0 eq.) and $[Pd(CH_3CN)_4](BF_4)_2$ (6.7 mg, 0.015 mmol, 1.0 eq.) were sonicated in d_6-DMSO (0.75 mL) until all solids were dissolved, giving a light yellow solution. Quantitative conversion to $[Pd_2(\mathbf{L^{OH}})_4](BF_4)_4$ was observed by ^{1}H NMR. ^{1}H NMR (400 MHz, d_6-DMSO) δ: 10.29 (s, 4H, H_a), 9.87 (d, J = 6.7 Hz, 4H, H_b), 9.07 (s, 4H, H_i), 8.58 (d, J = 6.5 Hz, 4H, H_c), 8.29-8.22 (m, 20H, H_d/H_e, H_g, H_h), 8.12-8.04 (m, 8H, H_d/H_e, H_f), 4.45 (br. S, 4H, H_{OH}), 3.30 (m, 12H, H_j, H_m), 3.01-2.94 (m, 4H, $H_{j'}$), 1.60-1.51 (m, 4H, H_k), 1.48-1.41 (m, 8H, H_l), 1.31-1.21 (m, 4H, $H_{k'}$). Diffusion coefficient (500 MHz, d_6-DMSO) D: 9.64 × 10^{-11} m^2s^{-1}. ^{13}C NMR (101 MHz, d_6-DMSO) δ: 154.9, 150.7, 142.8, 136.5, 136.0, 134.3, 133.4, 133.3, 128.2, 127.5, 125.1, 124.1, 123.0, 120.4, 120.3, 95.9, 86.6, 60.1, 31.4, 24.9, 24.7. ESI-MS m/z = 421.12 $\{[Pd_2(L^{OH})_4]\}^{4+}$ calc. 421.11; 576.49 $\{[Pd_2(L^{OH})_4](HCO_2)\}^{3+}$ calc. 576.49; 887.24 $\{[Pd_2(L^{OH})_4](HCO_2)_2\}^{2+}$ calc. 887.23.

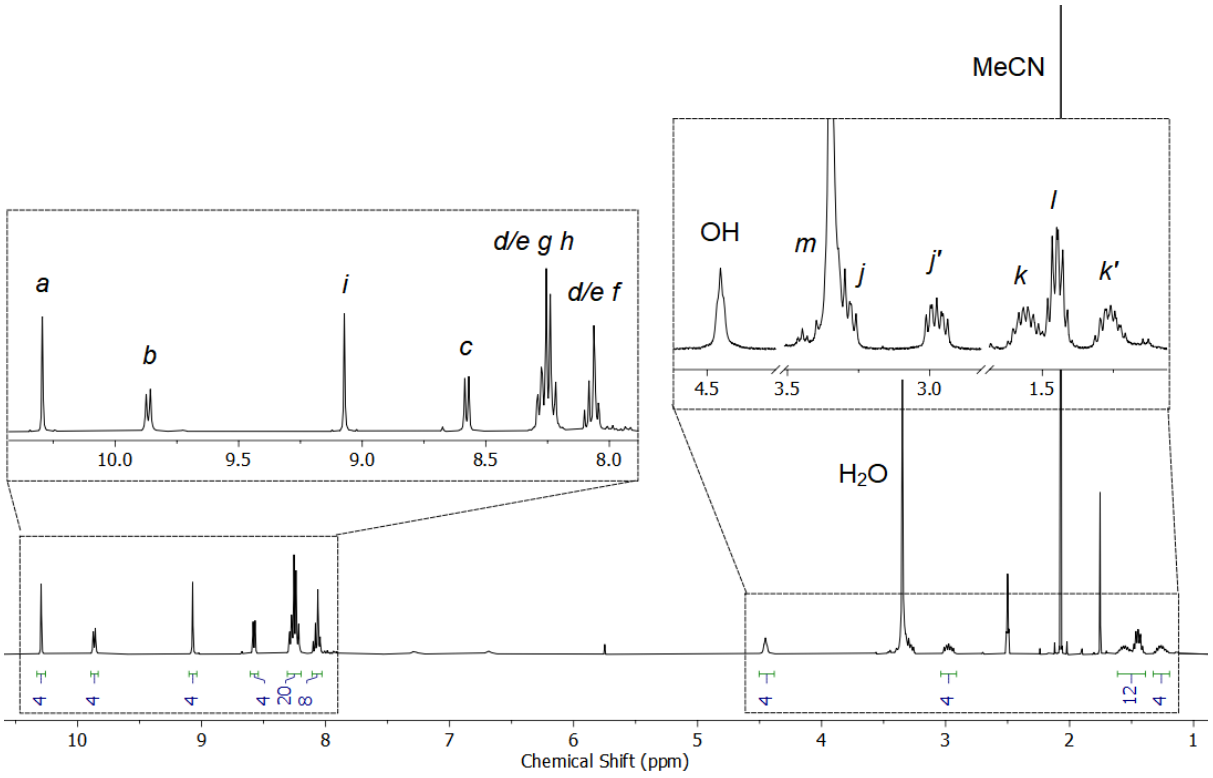

Figure S66 ^{1}H NMR (d_6-DMSO, 400 MHz) of $[Pd_2(\mathbf{L^{OH}})_4](BF_4)_4$.

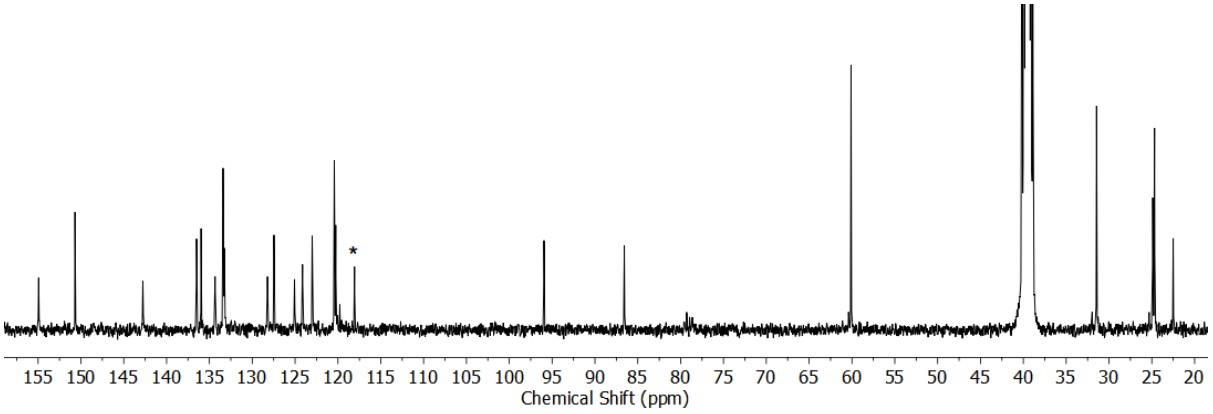

Figure S67 ^{13}C NMR (d_6-DMSO, 101 MHz) of $[Pd_2(\mathbf{L^{OH}})_4](BF_4)_4$. CH_3CN from the Pd(II) source is indicated(*).

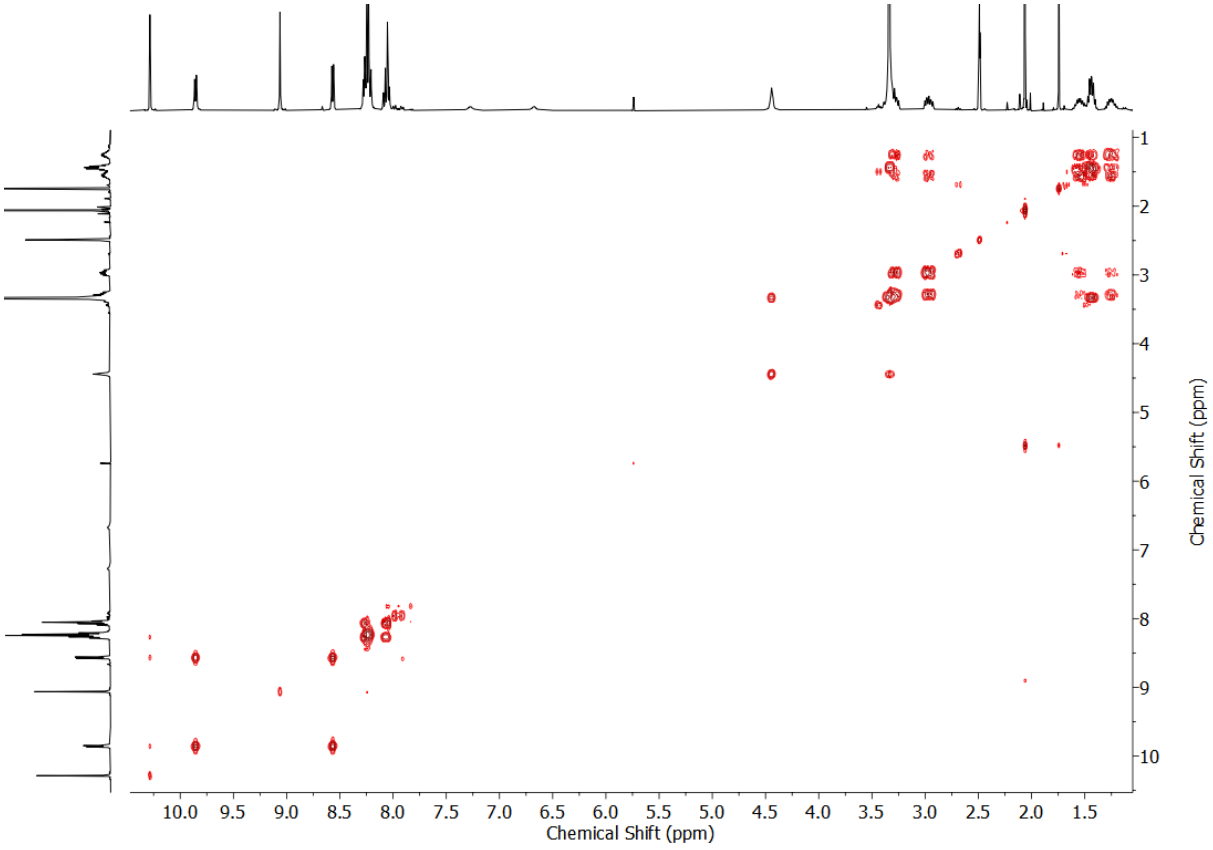

Figure S68 COSY NMR (d_6-DMSO) of $[Pd_2(\mathbf{L^{OH}})_4](BF_4)_4$.

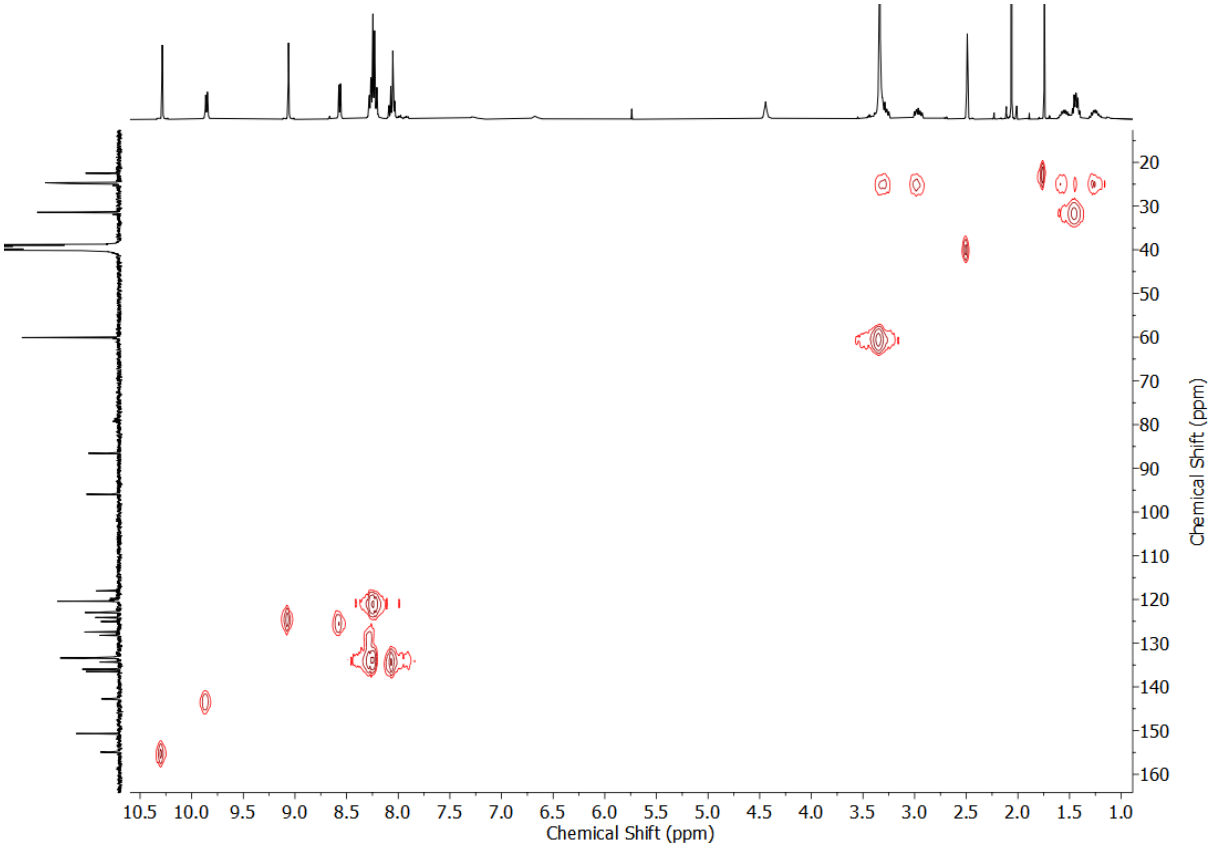

Figure S69 HSQC NMR (d_6-DMSO) of $[Pd_2(\mathbf{L}^{\mathbf{OH}})_4](BF_4)_4$.

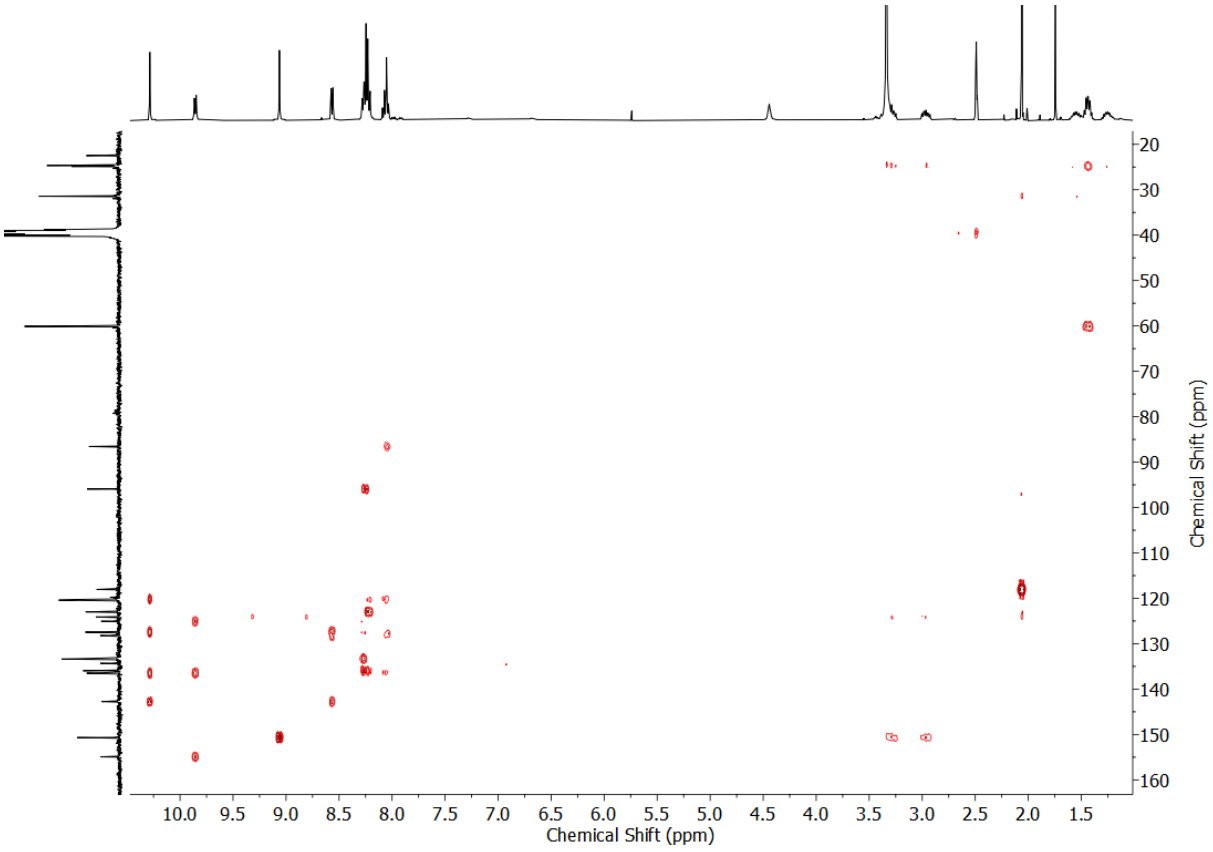

Figure S70 HMBC NMR (d_6-DMSO) of $[Pd_2(\mathbf{L}^{\mathbf{OH}})_4](BF_4)_4$.

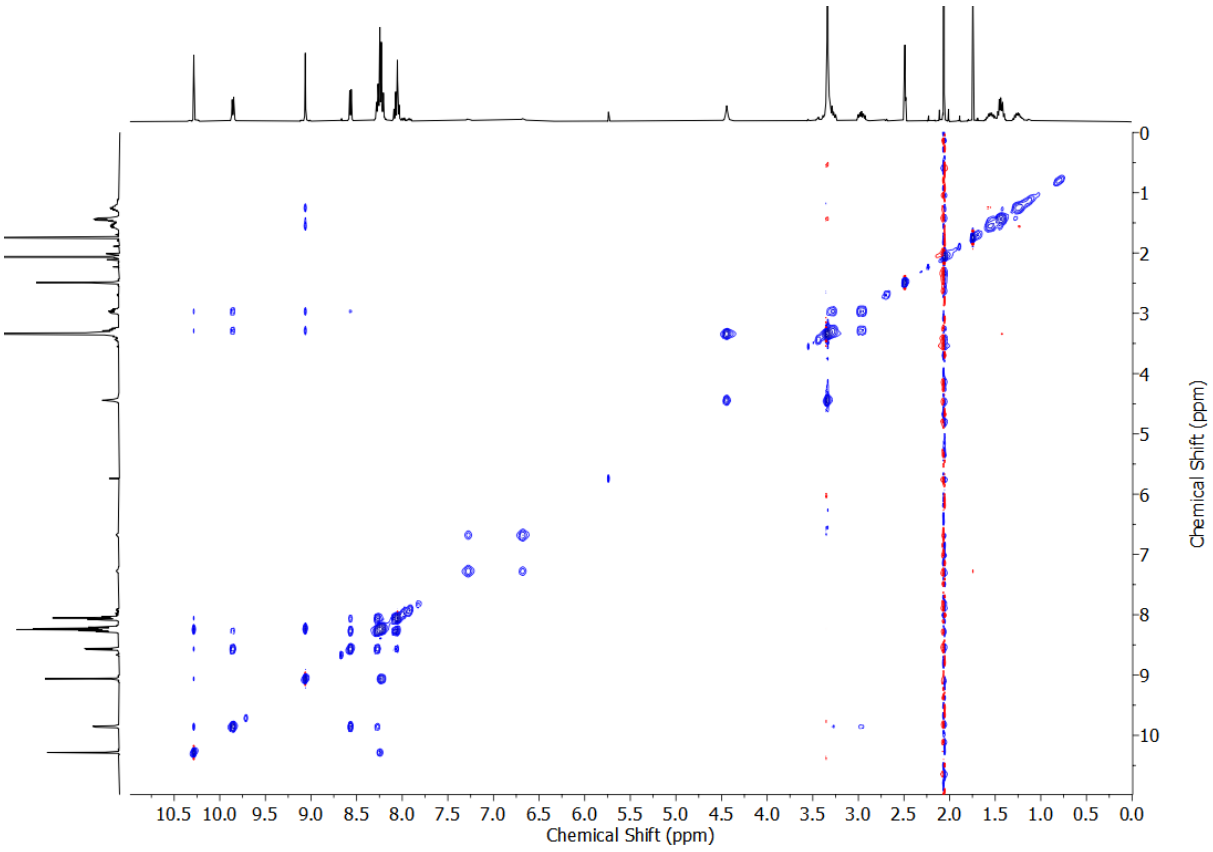

Figure S71 NOESY NMR (d_6-DMSO, 400 MHz) of $[Pd_2(\mathbf{L^{OH}})_4](BF_4)_4$.

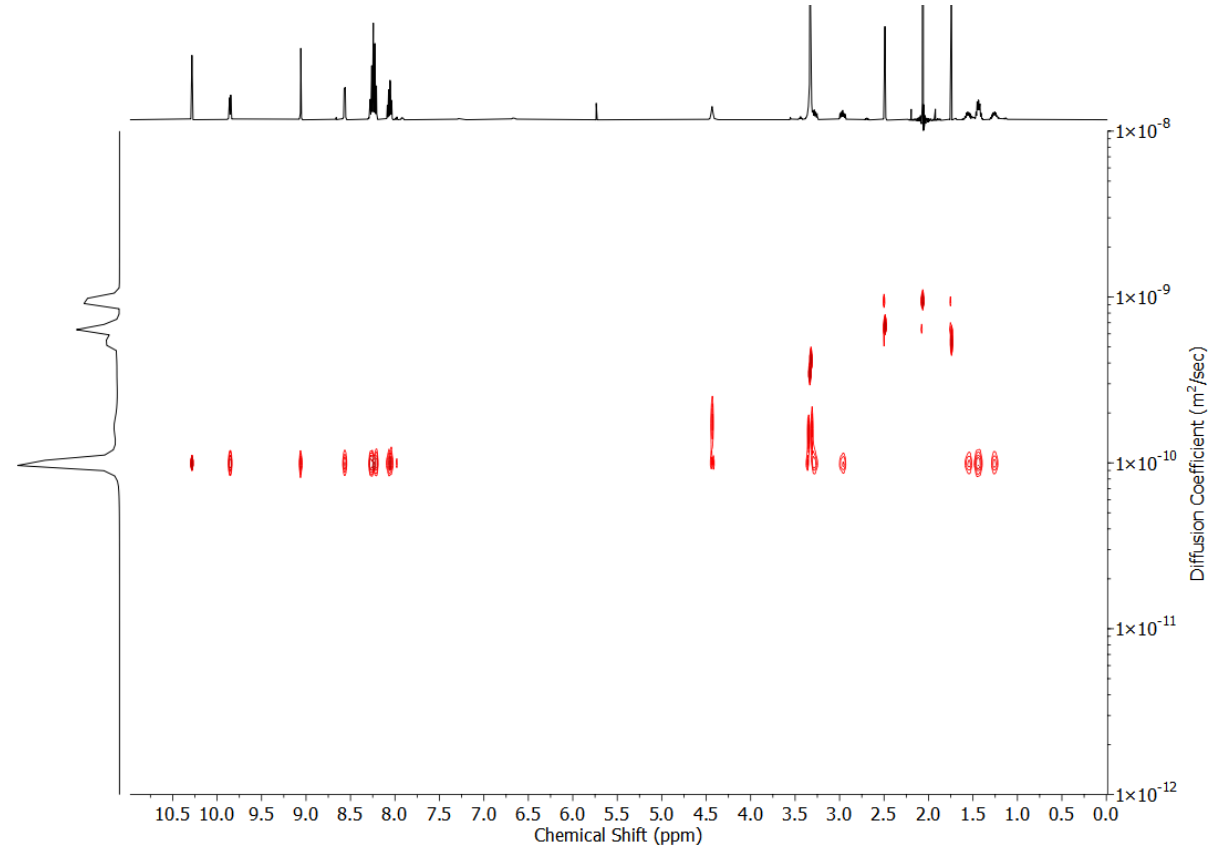

Figure S72 DOSY NMR (d_6-DMSO, 500 MHz) of $[Pd_2(\mathbf{L^{OH}})_4](BF_4)_4$.

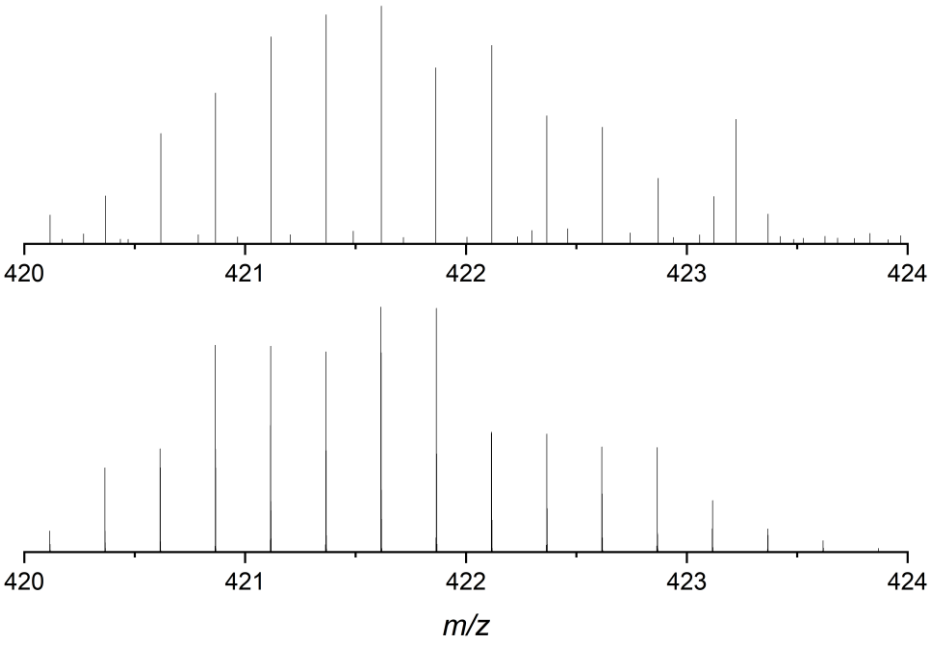

Figure S73 Observed (top) and calculated (bottom) isotopic patterns for $\{[Pd_2(\mathbf{L^{OH}})_4]\}^{4+}$.

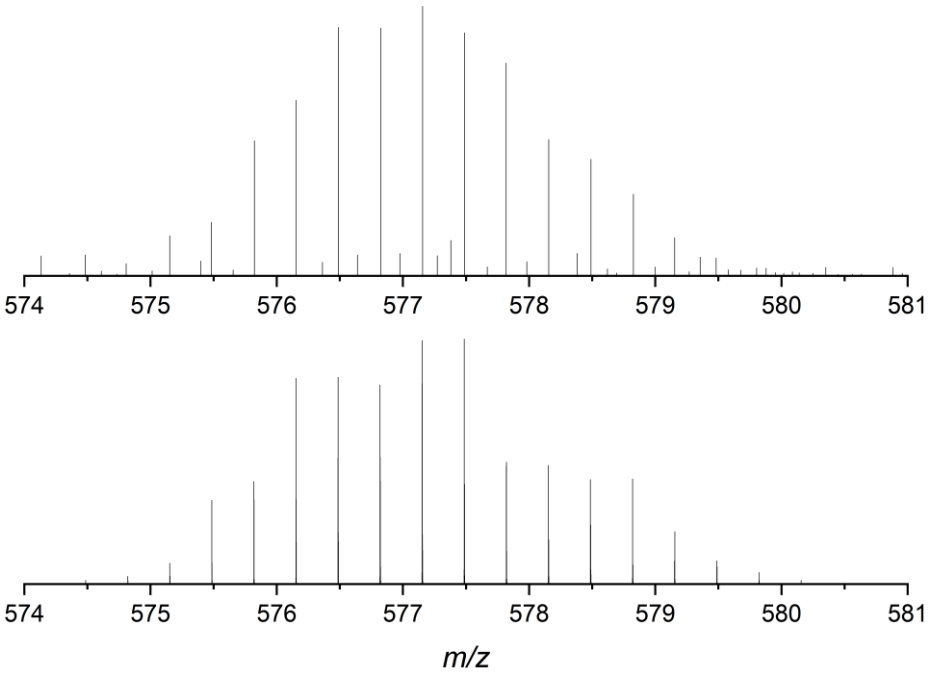

Figure S74 Observed (top) and calculated (bottom) isotopic patterns for $\{[Pd_2(\mathbf{L^{OH}})_4](HCO_2)\}^{3+}$.

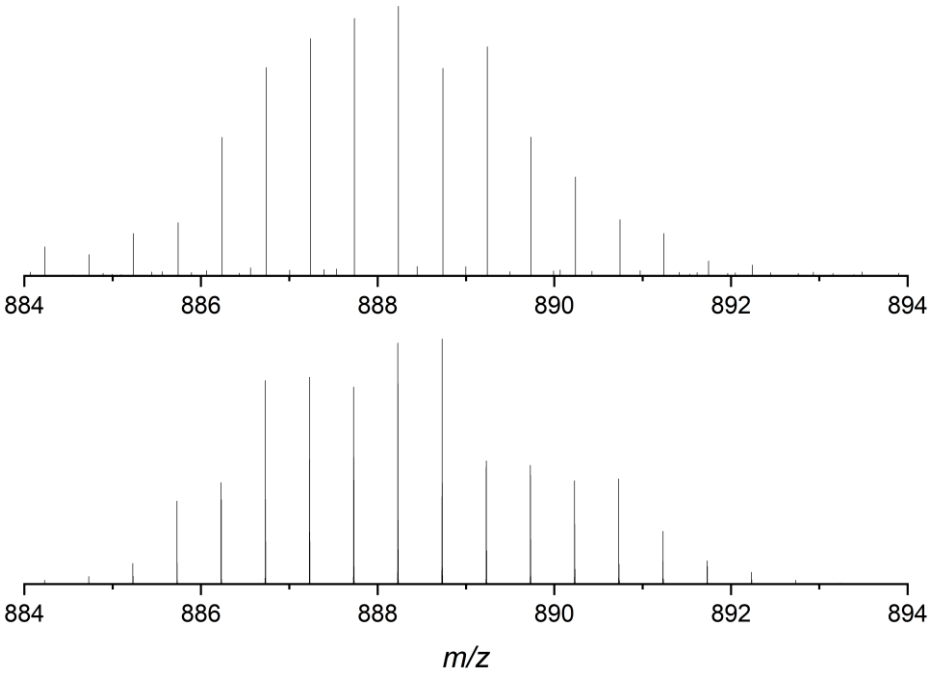

Figure S75 Observed (top) and calculated (bottom) isotopic patterns for $\{[Pd_2(\mathbf{L}^{OH})_4](HCO_2)_2\}^{2+}$.

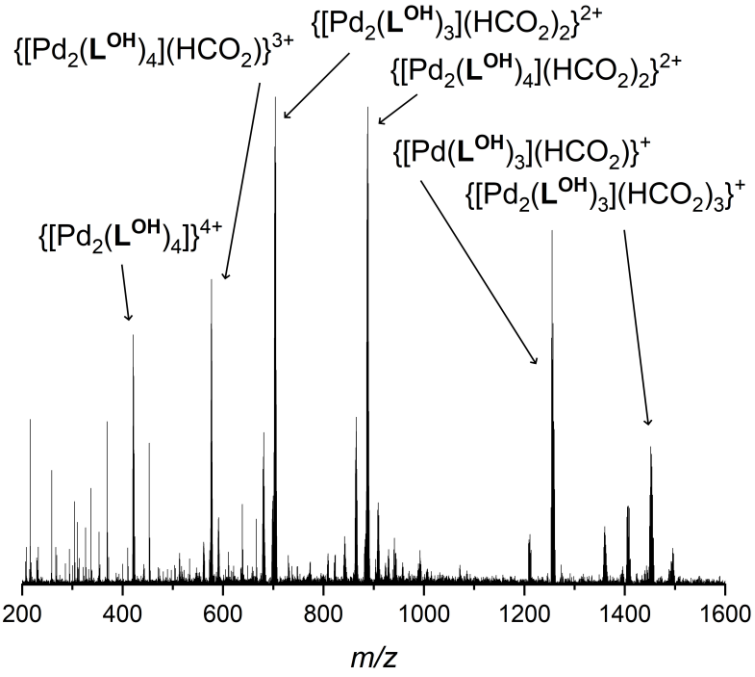

Figure S76 ESI-MS of $[Pd_2(\mathbf{L}^{OH})_4](BF_4)_4$.

$[Pd_2(L^{Ene})_4](BF_4)_4$

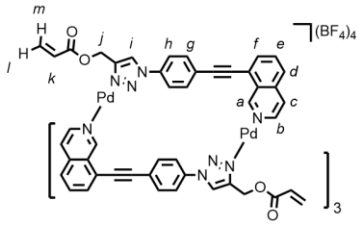

L^{Ene} (11.4 mg, 0.030 mmol, 2.0 eq.) and $[Pd(CH_3CN)_4](BF_4)_2$ (6.7 mg, 0.015 mmol, 1.0 eq.) were sonicated in d_6-DMSO (0.75 mL) until all solids were dissolved, giving a light yellow solution. Quantitative conversion to $[Pd_2(\mathbf{L}^{Ene})_4](BF_4)_4$ was observed by ^{1}H NMR. ^{1}H NMR (400 MHz, d_6-DMSO) δ: 10.27 (d, J = 0.8 Hz, 4H, H_a), 9.78 (d, J = 6.7 Hz, 4H, H_b), 9.32 (s, 4H, H_i), 8.50 (d, J = 6.3 Hz, 4H, H_c), 8.29-8.25 (m, 20H, H_d, H_g, H_h), 8.10-8.05 (m, 8H, H_e, H_f), 6.12 (dd, J = 17.2, 1.4 Hz, 4H, H_m), 5.87 (dd, J = 10.4, 1.4 Hz, 4H, H_l), 5.83 (br.s, 8H, H_j), 5.70 (dd, J = 17.2, 10.5 Hz, 4H, H_k). Diffusion coefficient (500 MHz, d_6-DMSO) D: 9.89 × 10^{-11} m^2s^{-1}. ^{13}C NMR (101 MHz, d_6-DMSO) δ: 164.7, 155.0, 145.1, 142.8, 136.6, 135.8, 134.3, 133.4, 133.2, 132.9, 128.3, 127.5, 127.1, 126.9, 125.1, 123.4, 120.7, 120.3, 95.8, 86.7, 56.1. ESI-MS m/z = 606.44 $\{[Pd_2(\mathbf{L}^{Ene})_4](BF_4)\}^{3+}$ calc. 606.44; 953.18 $\{[Pd_2(\mathbf{L}^{Ene})_4](BF_4)_2\}^{2+}$ calc. 953.16.

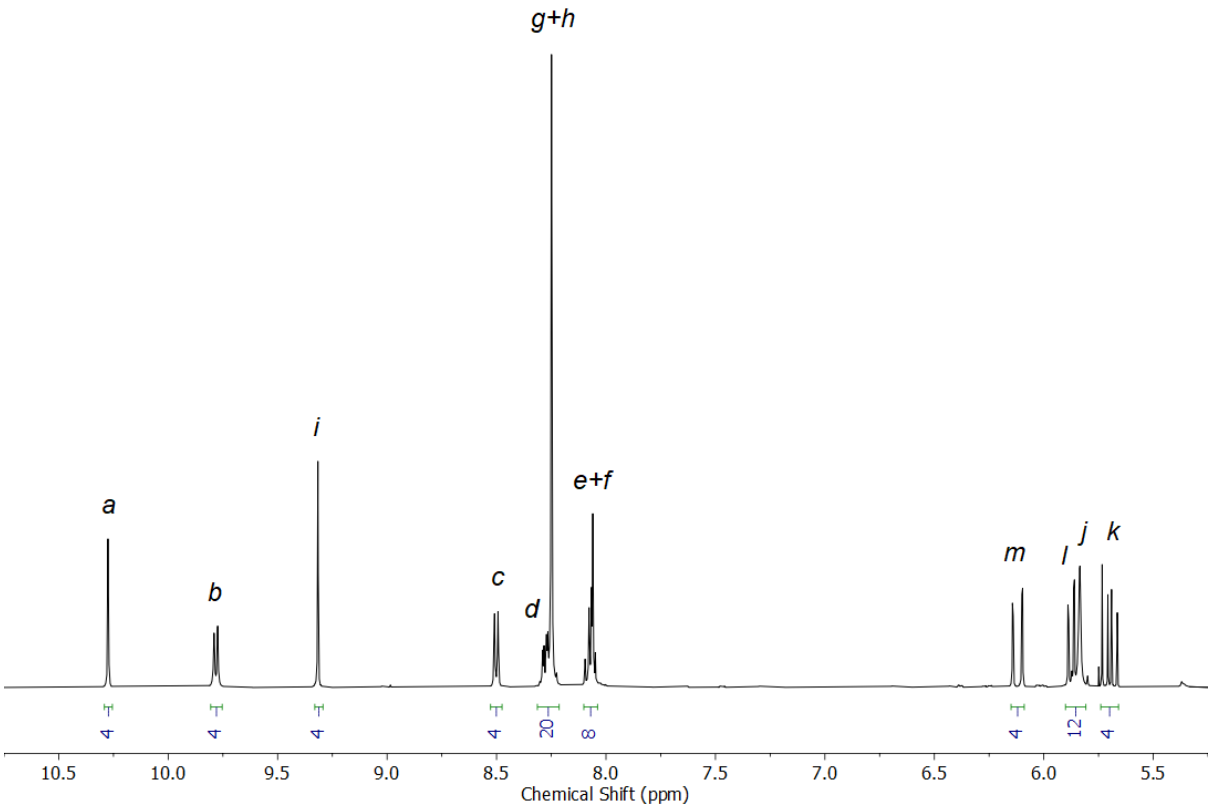

Figure S77 ^{1}H NMR (d_6-DMSO, 400 MHz) of $[Pd_2(\mathbf{L}^{Ene})_4](BF_4)_4$.

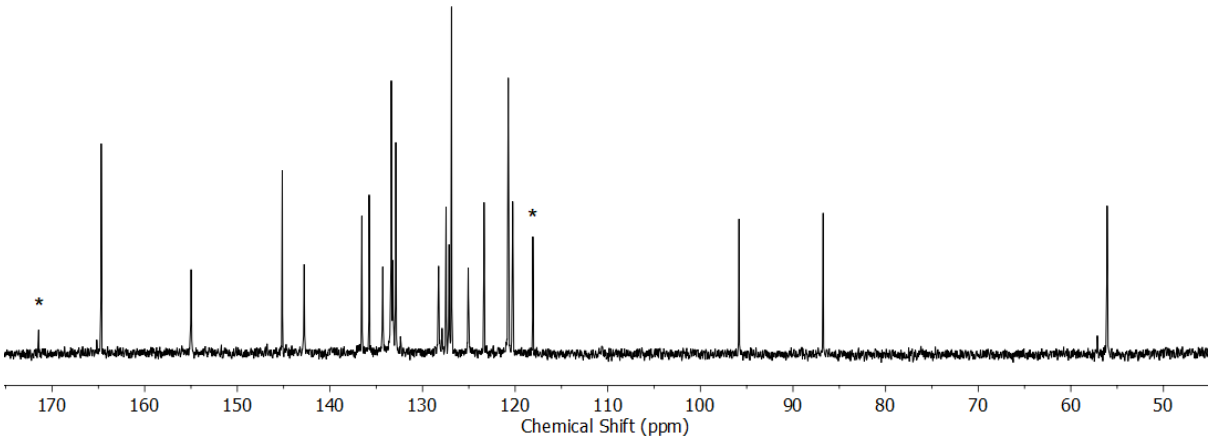

Figure S78 ^{13}C NMR (d_6-DMSO, 101 MHz) of $[Pd_2(\mathbf{L^{Ene}})_4](BF_4)_4$. Impurities and CH_3CN from the Pd(II) source are indicated(*).

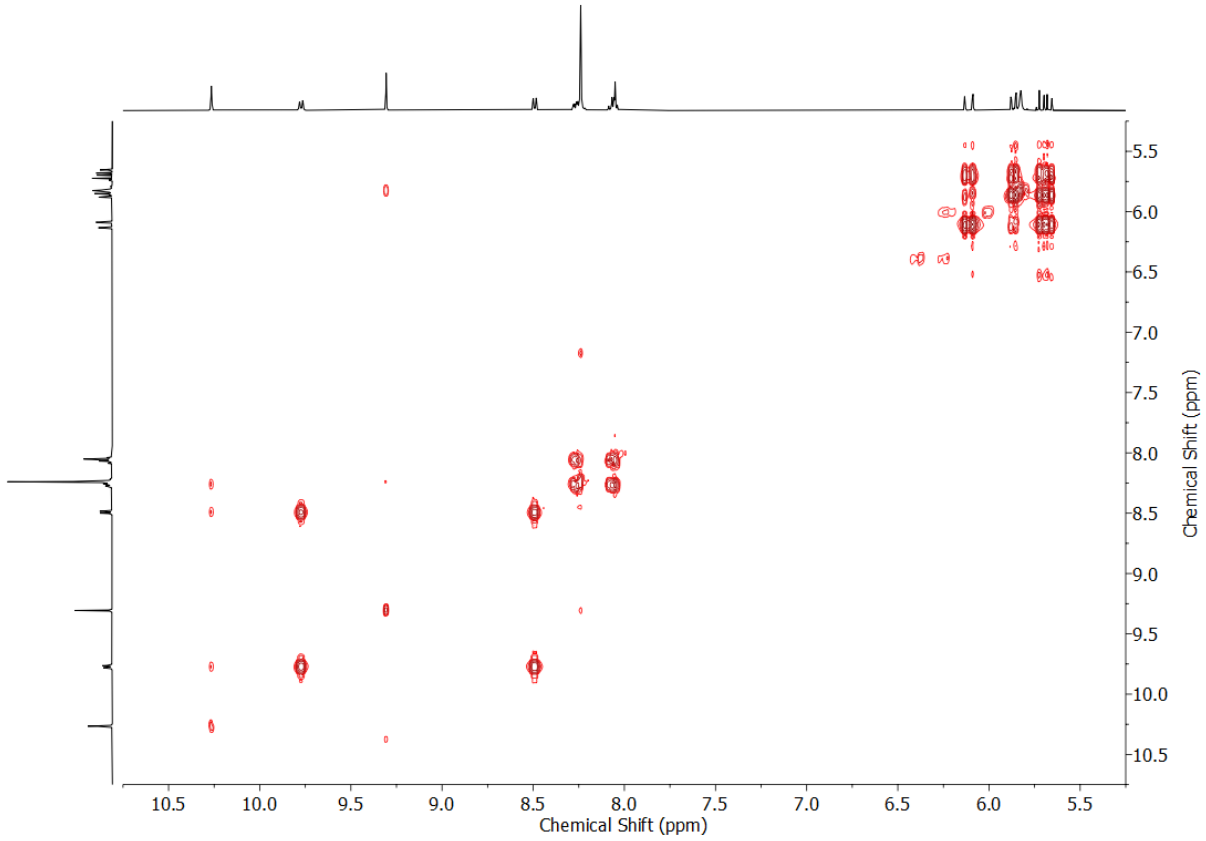

Figure S79 COSY NMR (d_6-DMSO) of $[Pd_2(\mathbf{L^{Ene}})_4](BF_4)_4$.

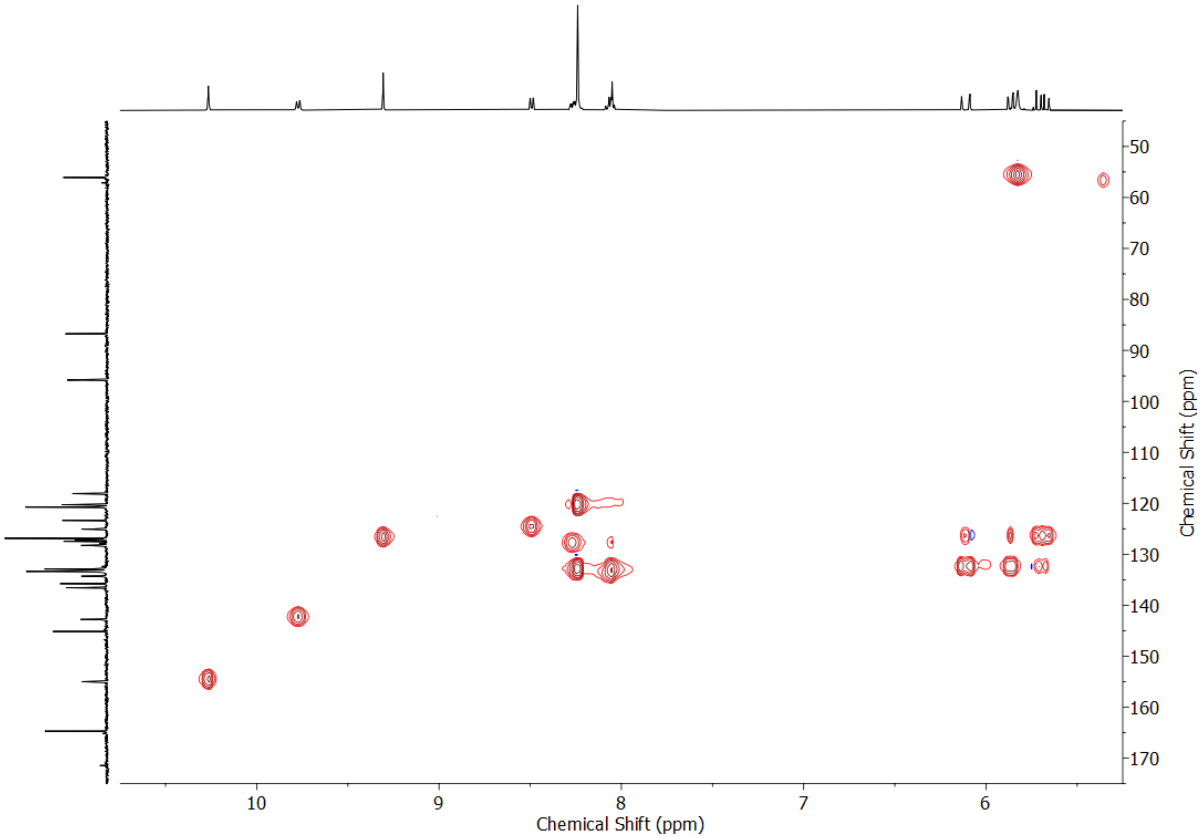

Figure S80 HSQC NMR (d_6-DMSO) of $[Pd_2(\mathbf{L}^{\mathbf{Ene}})_4](BF_4)_4$.

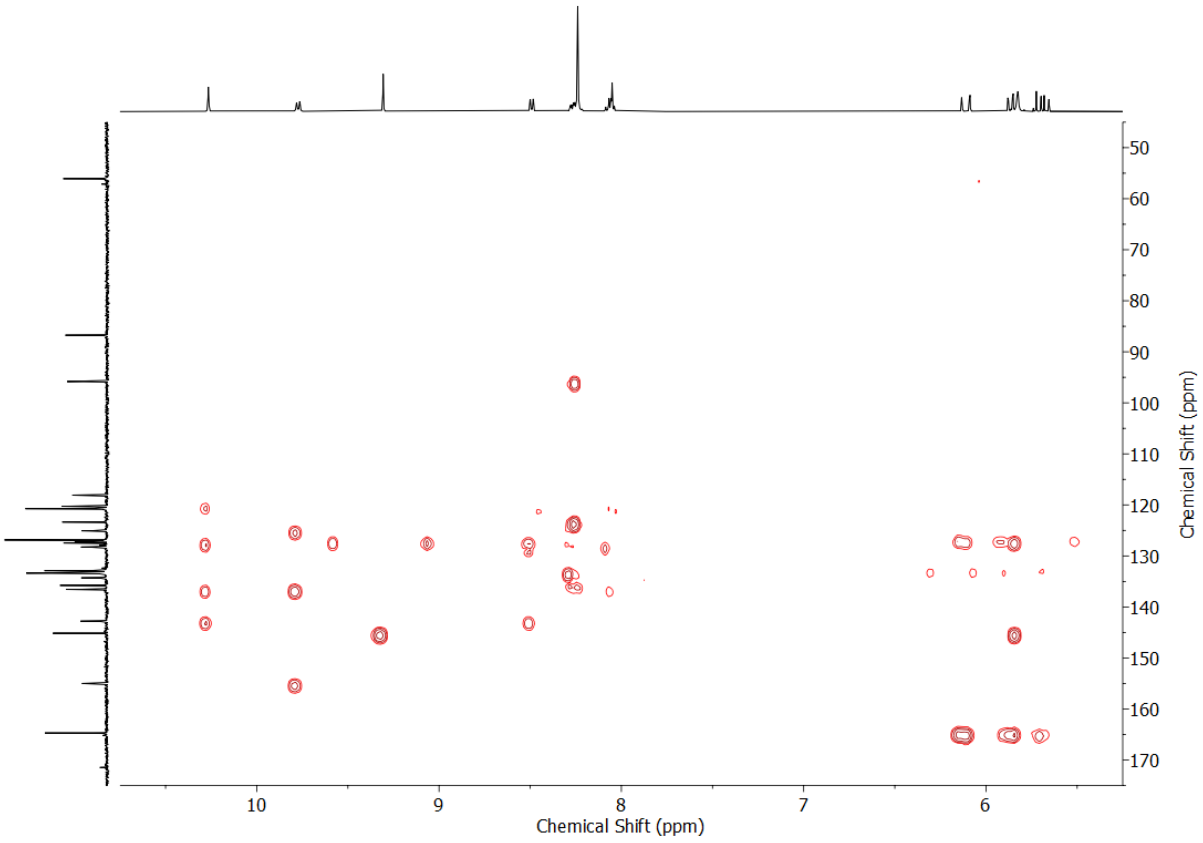

Figure S81 HMBC NMR (d_6-DMSO) of $[Pd_2(\mathbf{L}^{\mathbf{Ene}})_4](BF_4)_4$.

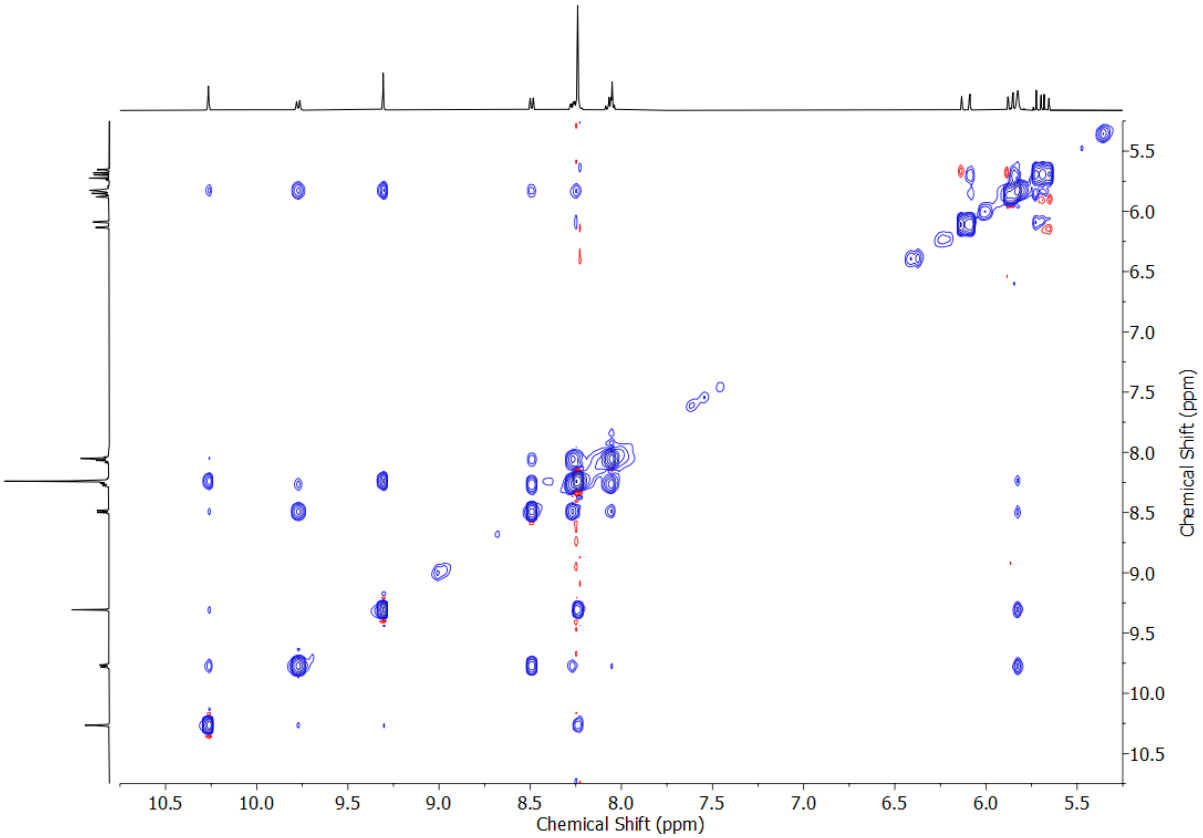

Figure S82 NOESY NMR (d_6-DMSO, 400 MHz) of $[Pd_2(\mathbf{L}^{Ene})_4](BF_4)_4$.

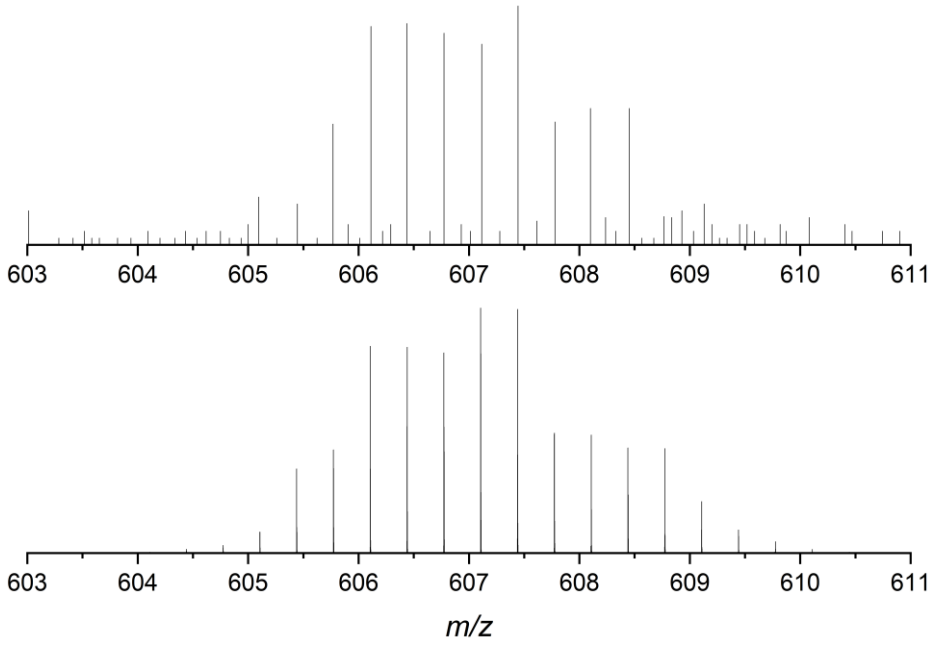

Figure S83 Observed (top) and calculated (bottom) isotopic patterns for $\{[Pd_2(\mathbf{L}^{Ene})_4](BF_4)\}^{3+}$.

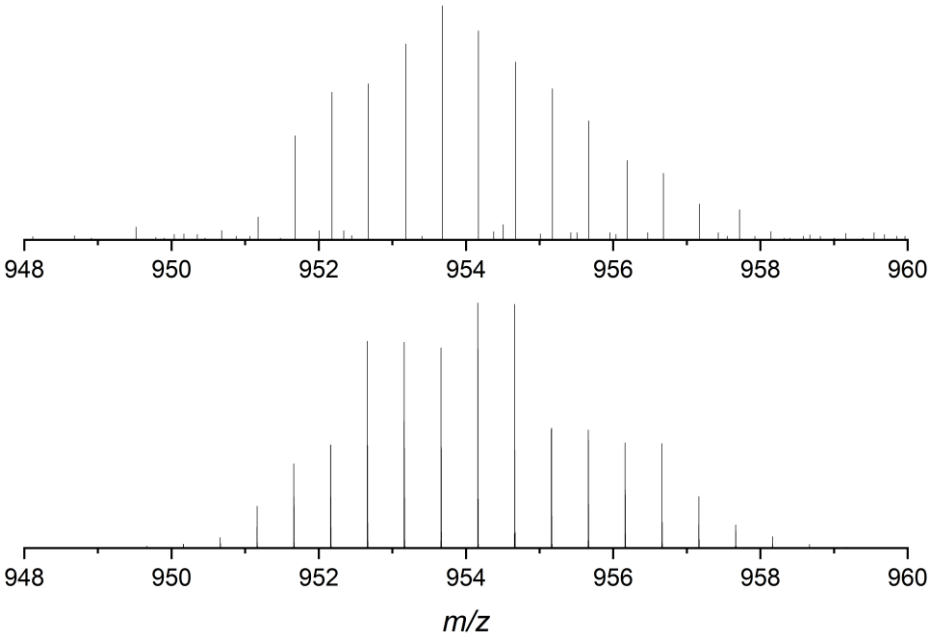

Figure S84 Observed (top) and calculated (bottom) isotopic patterns for $\{[Pd_2(\mathbf{L}^{Ene})_4](BF_4)_2\}^{2+}$.

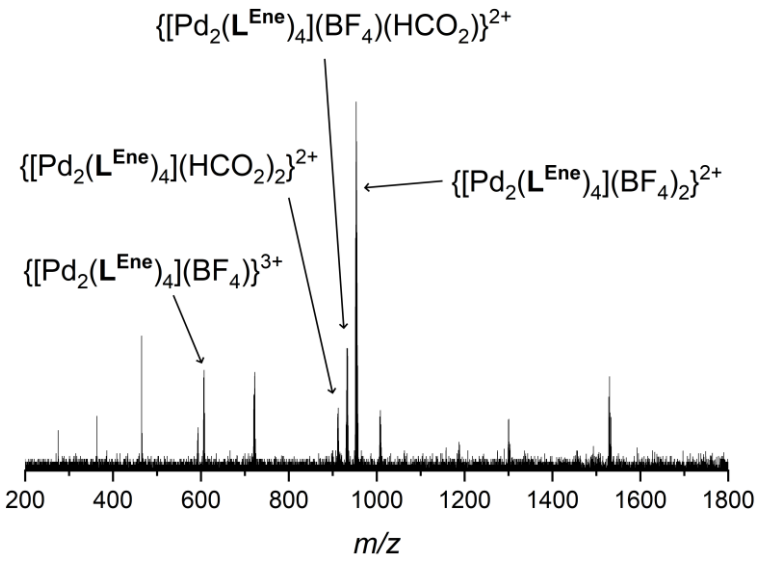

Figure S85 ESI-MS of $[Pd_2(\mathbf{L}^{Ene})_4](BF_4)_4$.

$[Pd_2(L^{Phth})_4](BF_4)_4$

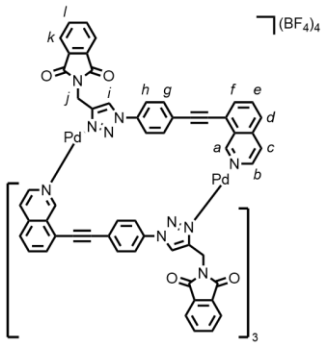

L^{Phth} (13.7 mg, 0.030 mmol, 2.0 eq.) and $[Pd(CH_3CN)_4](BF_4)_2$ (6.7 mg, 0.015 mmol, 1.0 eq.) were sonicated in d_6-DMSO (0.75 mL) until all solids were dissolved, giving a light yellow solution. Quantitative conversion to $[Pd_2(L^{Phth})_4](BF_4)_4$ was observed by ^{1}H NMR. ^{1}H NMR (500 MHz, d_6-DMSO) δ: 10.31 (s, 4H, H_a), 9.83 (d, J = 6.7 Hz, 4H, H_b), 9.24 (s, 4H, H_i), 8.55 (d, J = 6.5 Hz, 4H, H_c), 8.34 (d, J = 7.3 Hz, 4H, H_d), 8.24 (d, J = 8.7 Hz, 8H, H_g), 8.18 (d, J = 8.8 Hz, 8H, H_h), 8.12-8.07 (m, 8H, H_e, H_f), 7.83 (s, 8H, H_k, H_l), 5.54 (d, J = 16.5 Hz, 4H, H_j), 5.03 (d, J = 16.5 Hz, 4H, $H_{j'}$). Diffusion coefficient (500 MHz, d_6-DMSO) D: 8.89 × 10^{-11} m^2s^{-1}. ^{13}C NMR (126 MHz, d_6-DMSO) δ: 167.2, 155.2, 146.8, 142.7, 136.7, 135.7, 134.7, 134.3, 133.4, 133.3, 131.5, 128.4, 127.8, 125.4, 125.3, 123.4, 123.4, 120.4, 120.4, 95.7, 86.9, 32.7. ESI-MS m/z = 706.45 $\{[Pd_2(L^{Phth})_4](BF_4)\}^{3+}$ calc. 706.45; 1103.18 $\{[Pd_2(L^{Phth})_4](BF_4)_2\}^{2+}$ calc. 1103.18.

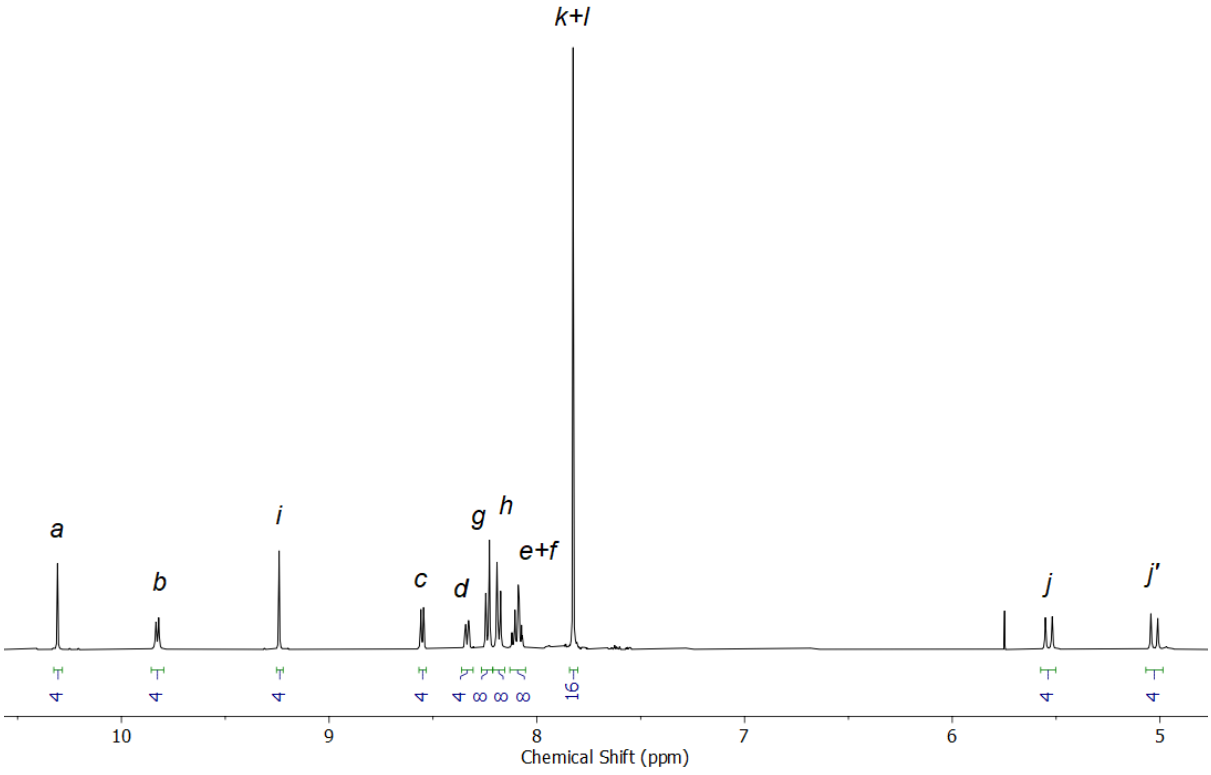

Figure S86 ^{1}H NMR (d_6-DMSO, 500 MHz) of $[Pd_2(L^{Phth})_4](BF_4)_4$.

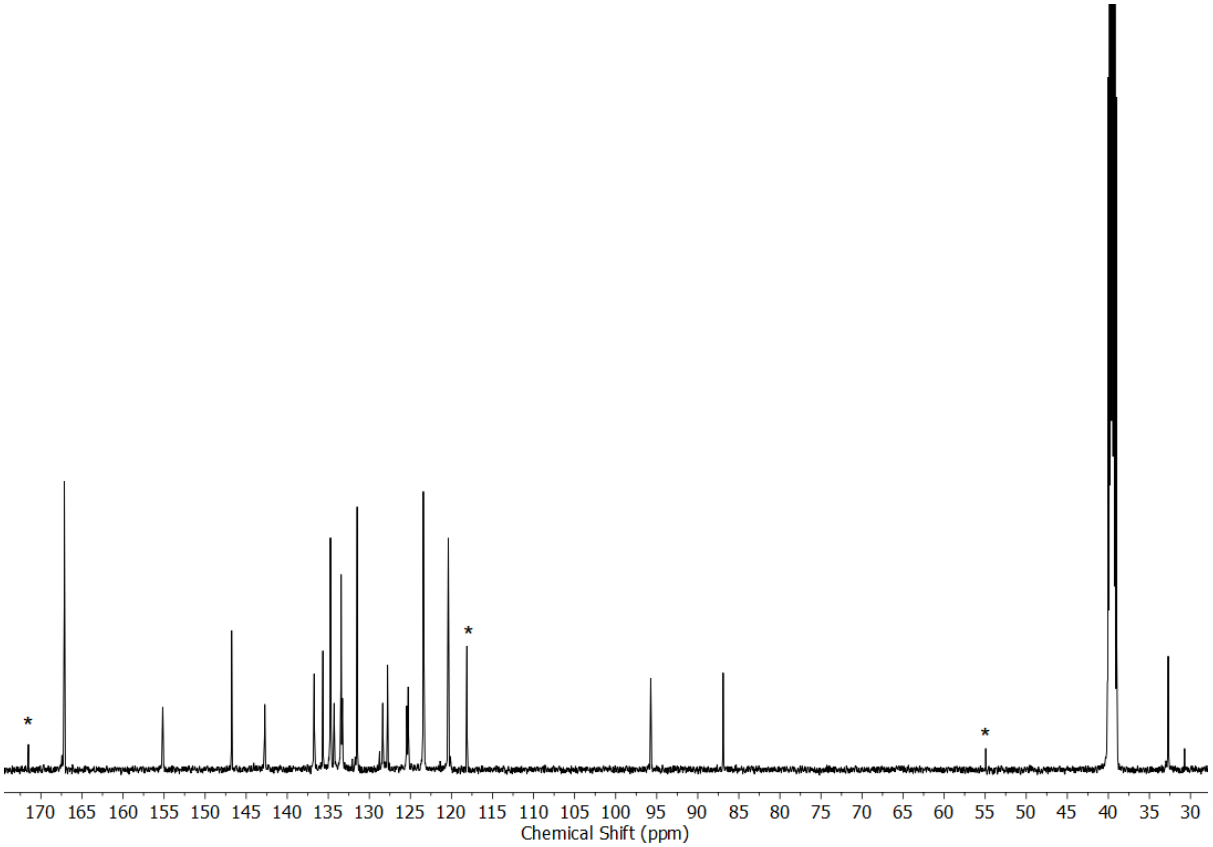

Figure S87 ^{13}C NMR (d_6-DMSO, 126 MHz) of $[Pd_2(\mathbf{L}^{\mathbf{Phth}})_4](BF_4)_4$. Impurities and CH_3CN from the Pd(II) source are indicated(*).

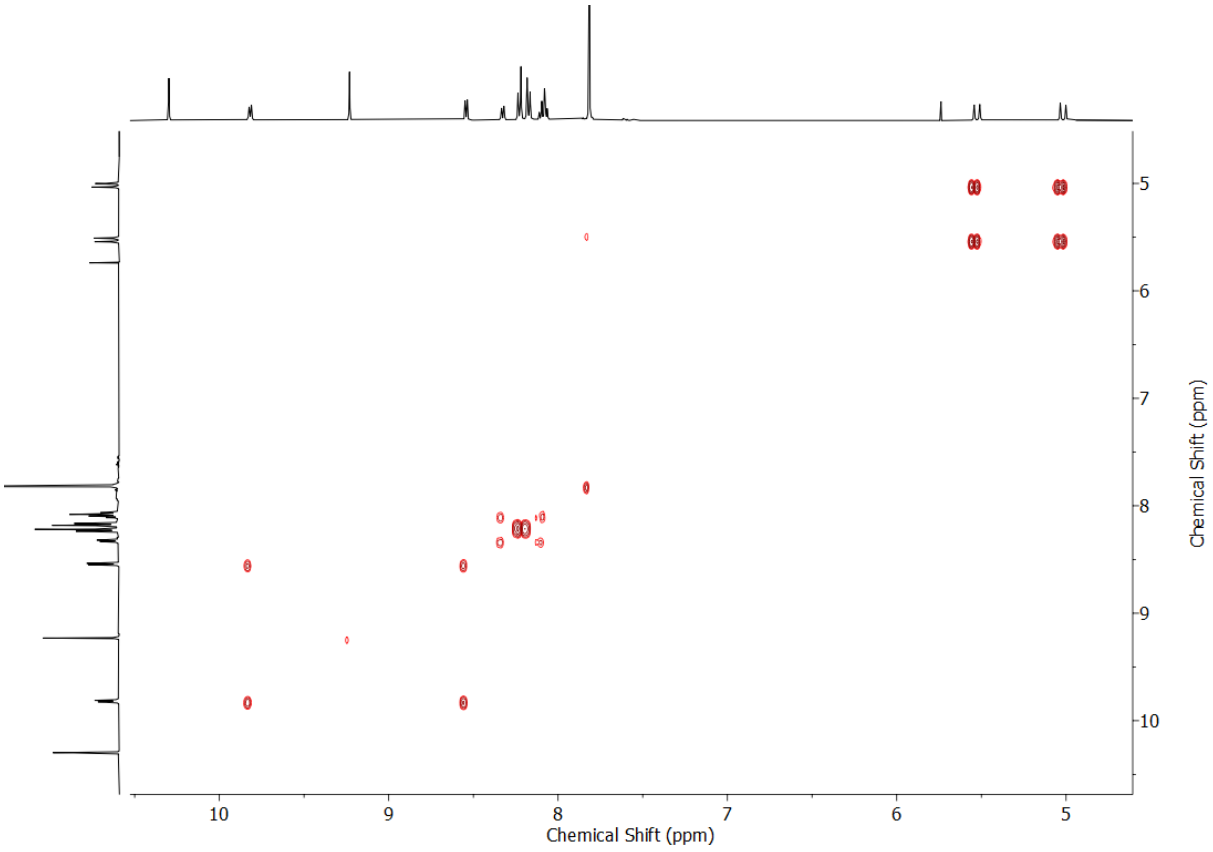

Figure S88 COSY NMR (d_6-DMSO) of $[Pd_2(\mathbf{L}^{\mathbf{Phth}})_4](BF_4)_4$.

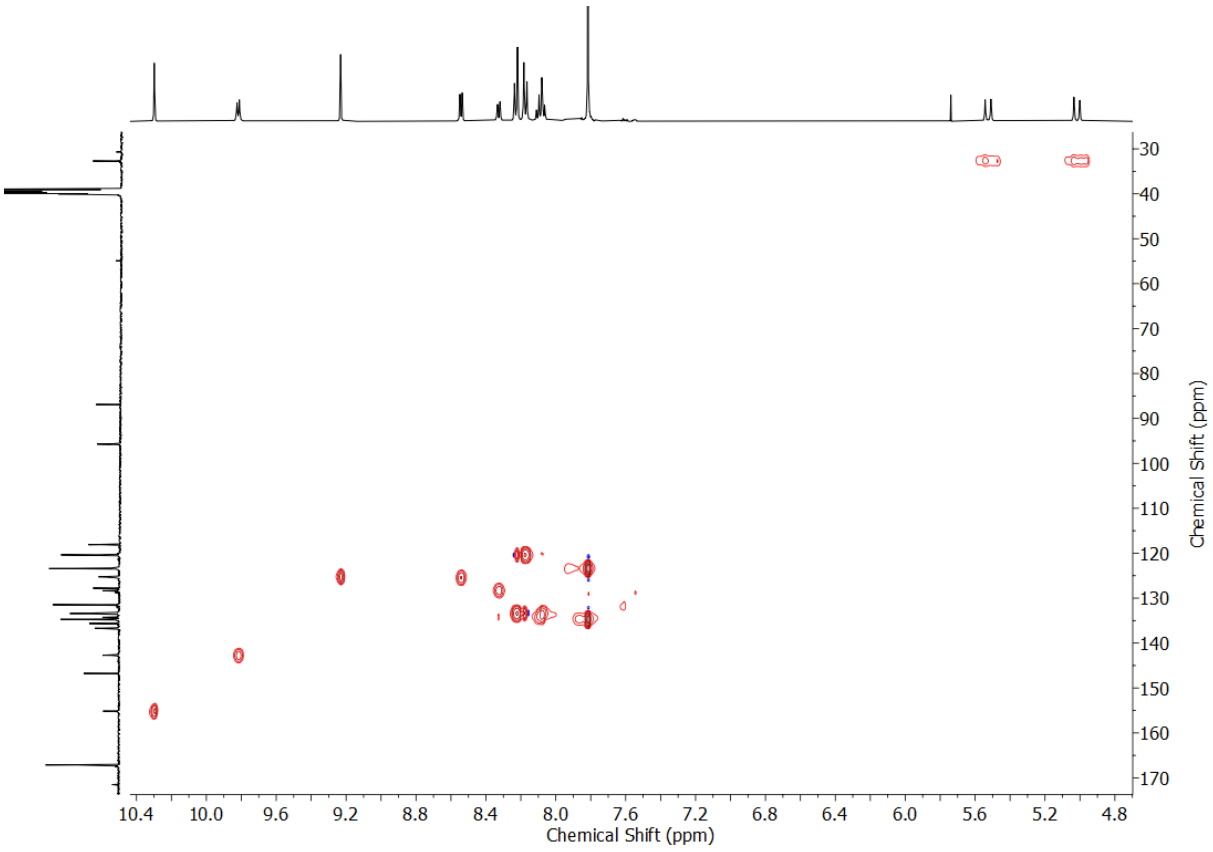

Figure S89 HSQC NMR (d_6-DMSO) of $[Pd_2(\mathbf{L}^{\mathbf{Phth}})_4](BF_4)_4$.

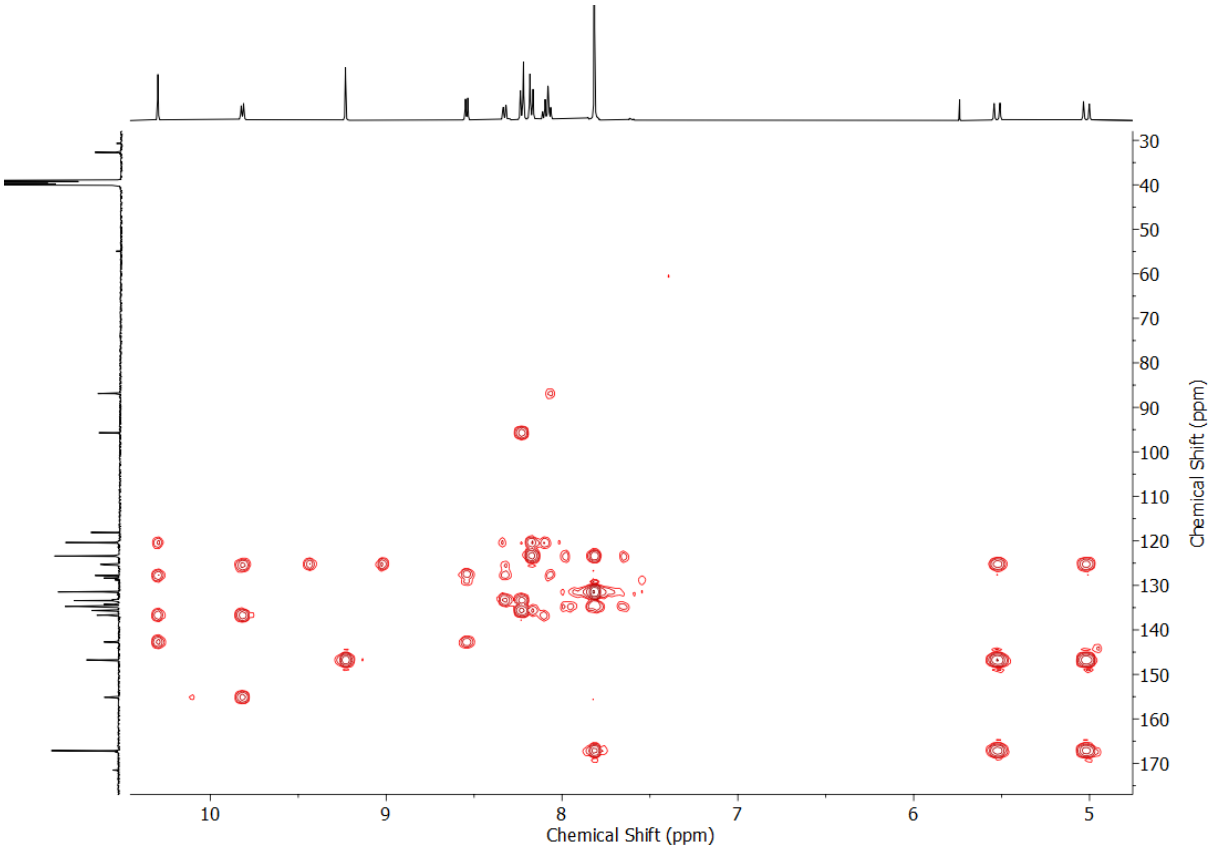

Figure S90 HMBC NMR (d_6-DMSO) of $[Pd_2(\mathbf{L}^{\mathbf{Phth}})_4](BF_4)_4$.

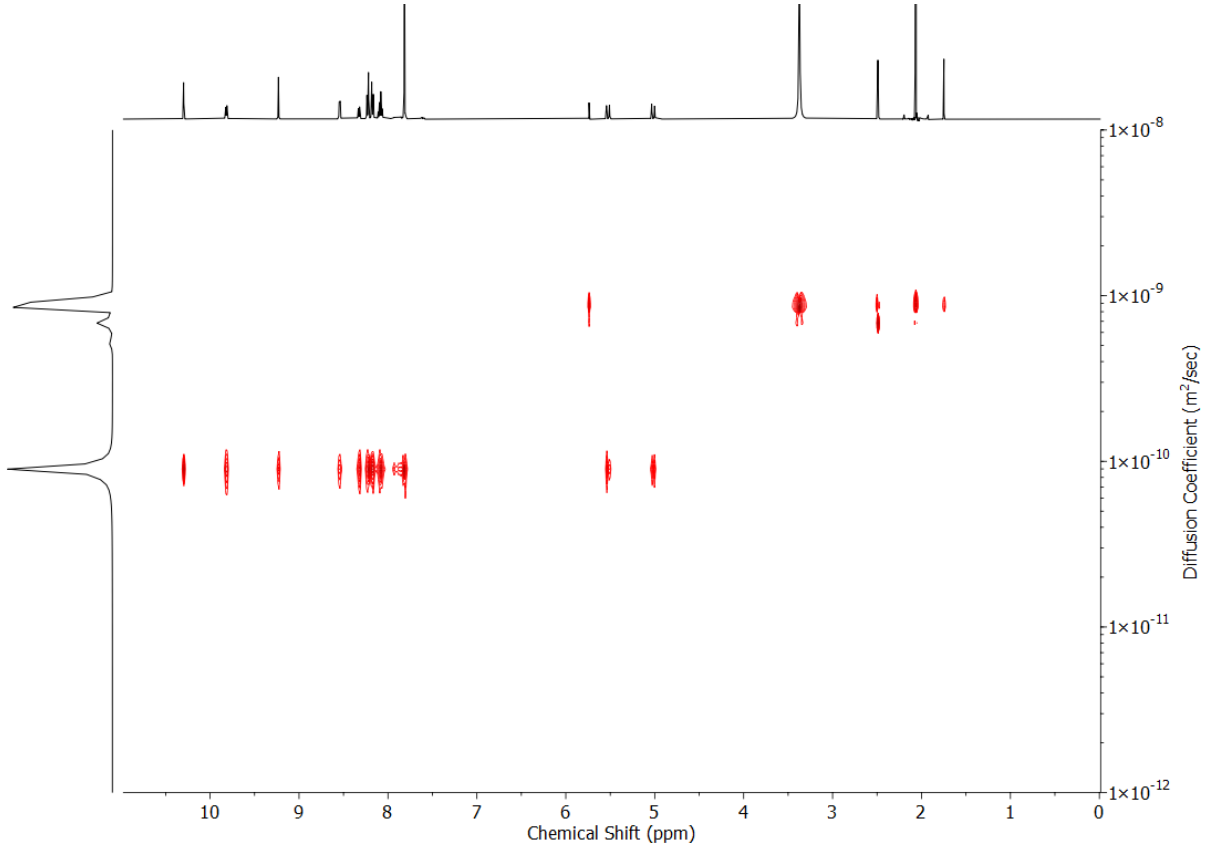

Figure S91 DOSY NMR (d_6-DMSO, 500 MHz) of $[Pd_2(\mathbf{L}^{\mathbf{Phth}})_4](BF_4)_4$.

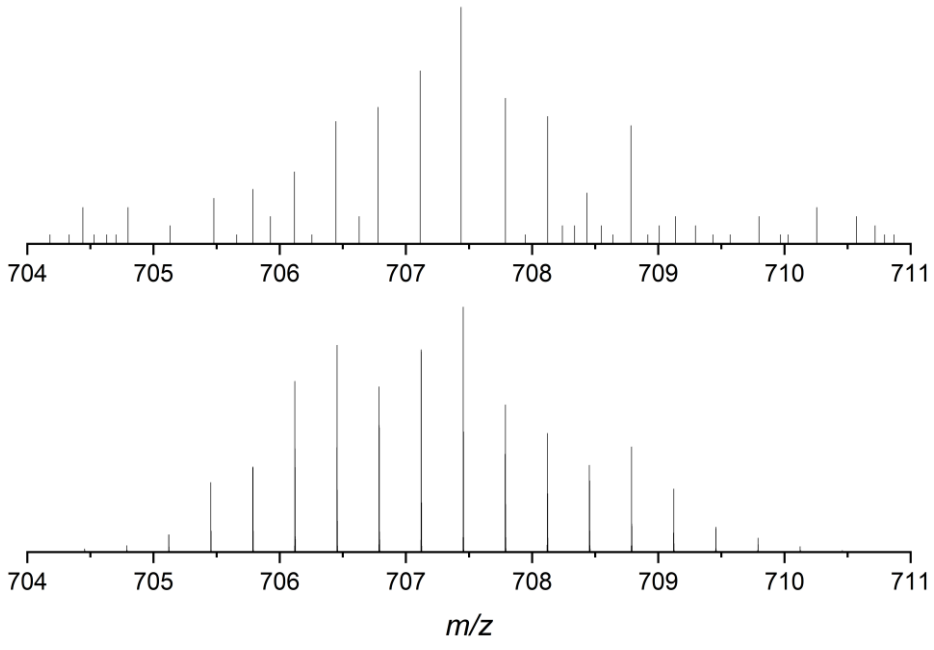

Figure S92 Observed (top) and calculated (bottom) isotopic patterns for $\{[Pd_2(\mathbf{L}^{\mathbf{Phth}})_4](BF_4)\}^{3+}$.

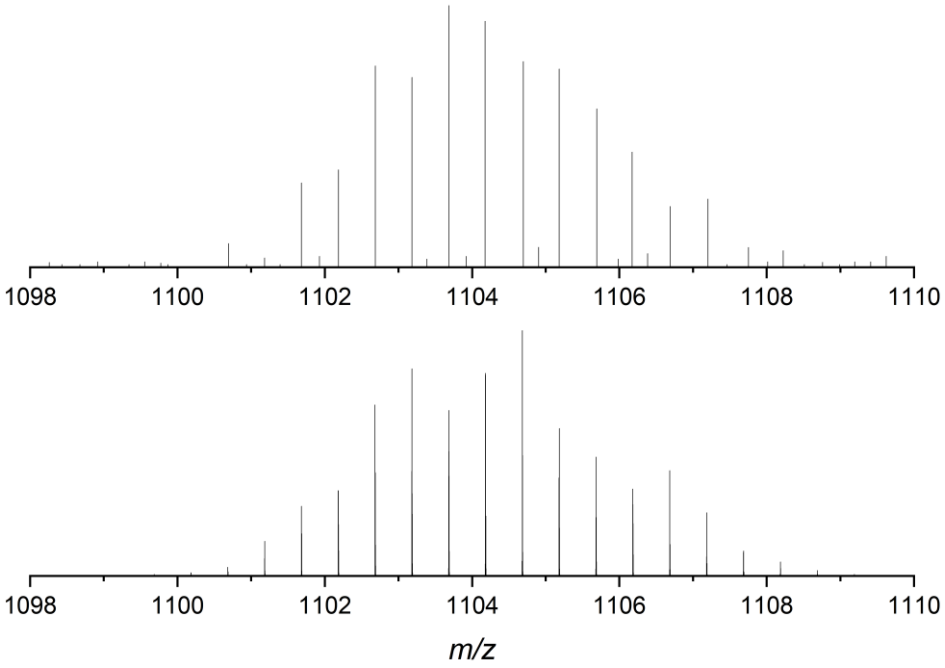

Figure S93 Observed (top) and calculated (bottom) isotopic patterns for $\{[Pd_2(\mathbf{L}^{Phth})_4](BF_4)_2\}^{2+}$.

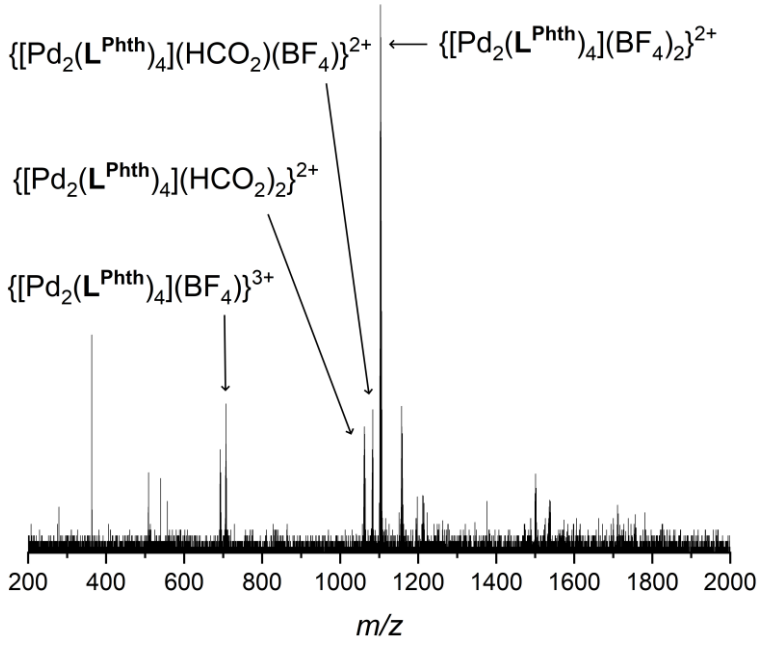

Figure S94 ESI-MS of $[Pd_2(\mathbf{L}^{Phth})_4](BF_4)_4$.

$[Pd_2(L^{Anth})_4](BF_4)_4$

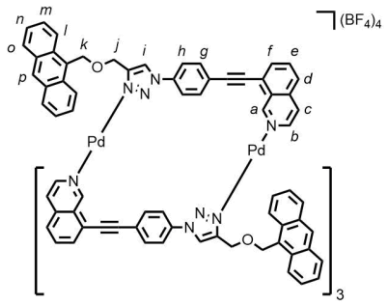

L^{Anth} (15.5 mg, 0.030 mmol, 2.0 eq.) and $[Pd(CH_3CN)_4](BF_4)_2$ (6.7 mg, 0.015 mmol, 1.0 eq.) were sonicated in d_6-DMSO (0.75 mL) until all solids were dissolved, giving a light yellow solution. Quantitative conversion to $[Pd_2(L^{Anth})_4](BF_4)_4$ was observed by ^{1}H NMR. ^{1}H NMR (500 MHz, d_6-DMSO) δ: 10.19 (s, 4H, H_a), 9.49 (d, J = 6.7 Hz, 4H, H_b), 9.17 (s, 4H, H_i), 8.64 (s, 4H, H_p), 8.33 (d, J = 8.6 Hz, 8H, H_g), 8.27 (d, J = 8.7 Hz, 8H, H_h), 8.10 (d, J = 8.9 Hz, 4H, H_o), 8.00 (d, J = 6.5 Hz, 4H, H_c), 7.89-7.83 (m, 16H, H_e, H_f, H_l), 7.79 (d, J = 8.0 Hz, 4H, H_d), 7.44 (m, 8H, H_n), 7.36 (ddd, J = 8.8, 6.5, 1.4 Hz, 8H, H_m), 5.33 (d, J = 13.2 Hz, 4H, H_j), 5.22 (d, J = 11.0 Hz, 4H, H_k), 5.51 (d, J = 10.9 Hz, 4H, $H_{k'}$), 4.68 (d, J = 13.3 Hz, 4H, $H_{j'}$). Diffusion coefficient (500 MHz, d_6-DMSO) D: 9.07 × 10^{-11} m^2s^{-1}. ^{13}C NMR (126 MHz, d_6-DMSO) δ: 154.6, 146.6, 142.4, 136.1, 135.7, 134.0, 133.5, 133.0, 130.8, 130.1, 129.0, 128.7, 127.7, 127.4, 127.2, 126.3, 125.9, 125.1, 124.7, 123.7, 123.5, 120.6, 119.9, 95.6, 86.9, 63.5, 61.7. ESI-MS m/z = 787.85 $\{[Pd_2(L^{Anth})_4](BF_4)\}^{3+}$ calc. 787.86; 1225.29 $\{[Pd_2(L^{Anth})_4](BF_4)_2\}^{2+}$ calc. 1225.30.

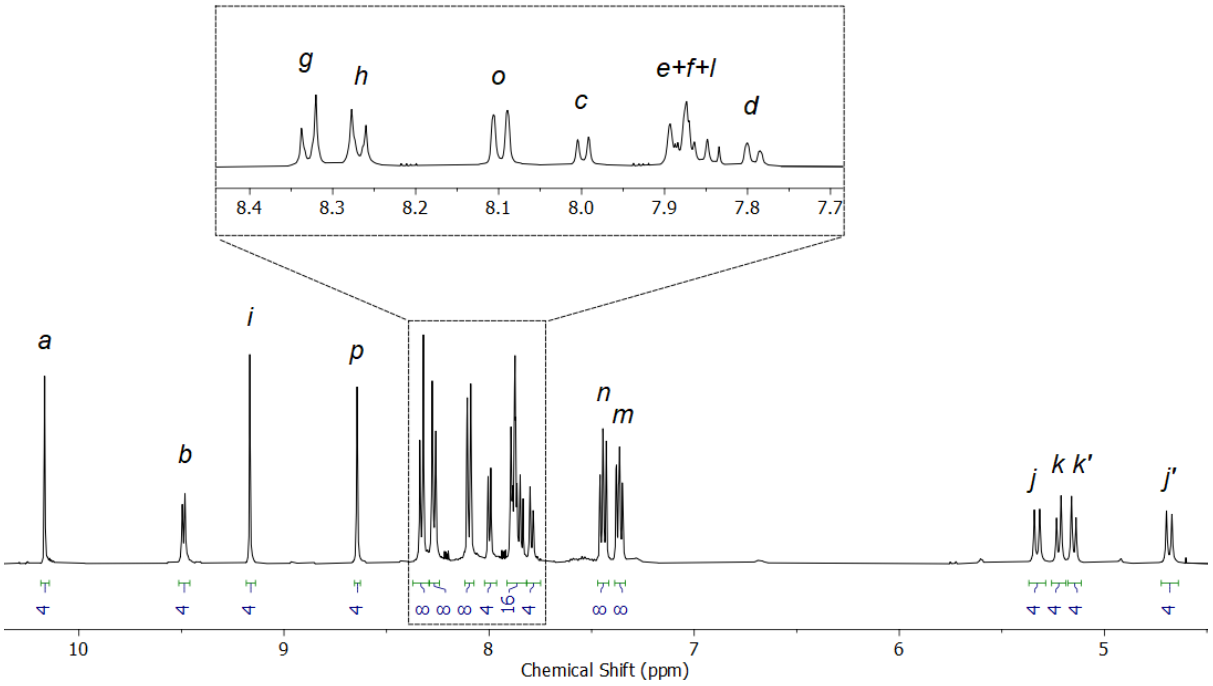

Figure S95 ^{1}H NMR (d_6-DMSO, 500 MHz) of $[Pd_2(L^{Anth})_4](BF_4)_4$.

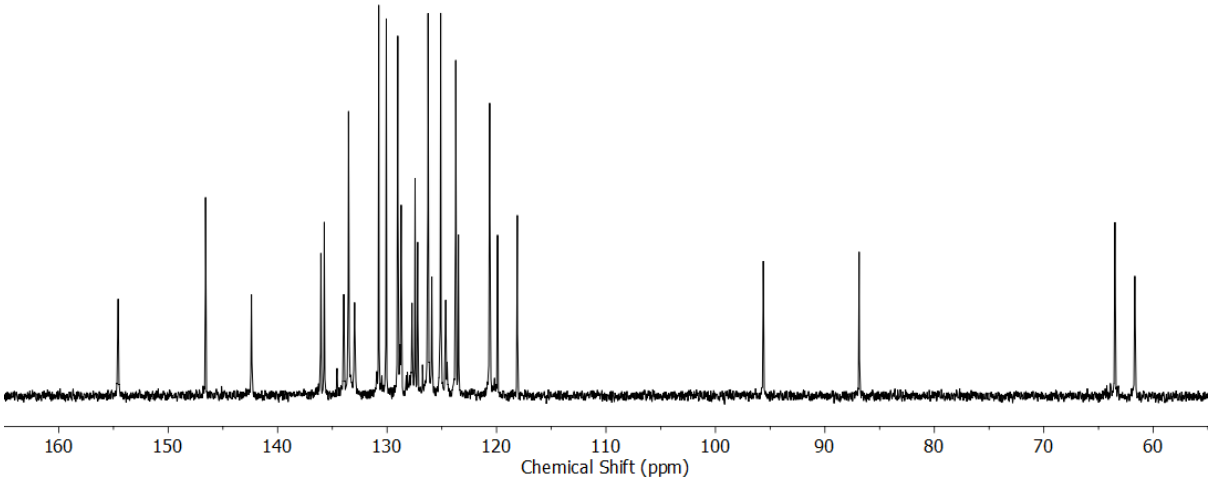

Figure S96 ^{13}C NMR (d_6-DMSO, 126 MHz) of $[Pd_2(\mathbf{L}^{\mathbf{Anth}})_4](BF_4)_4$.

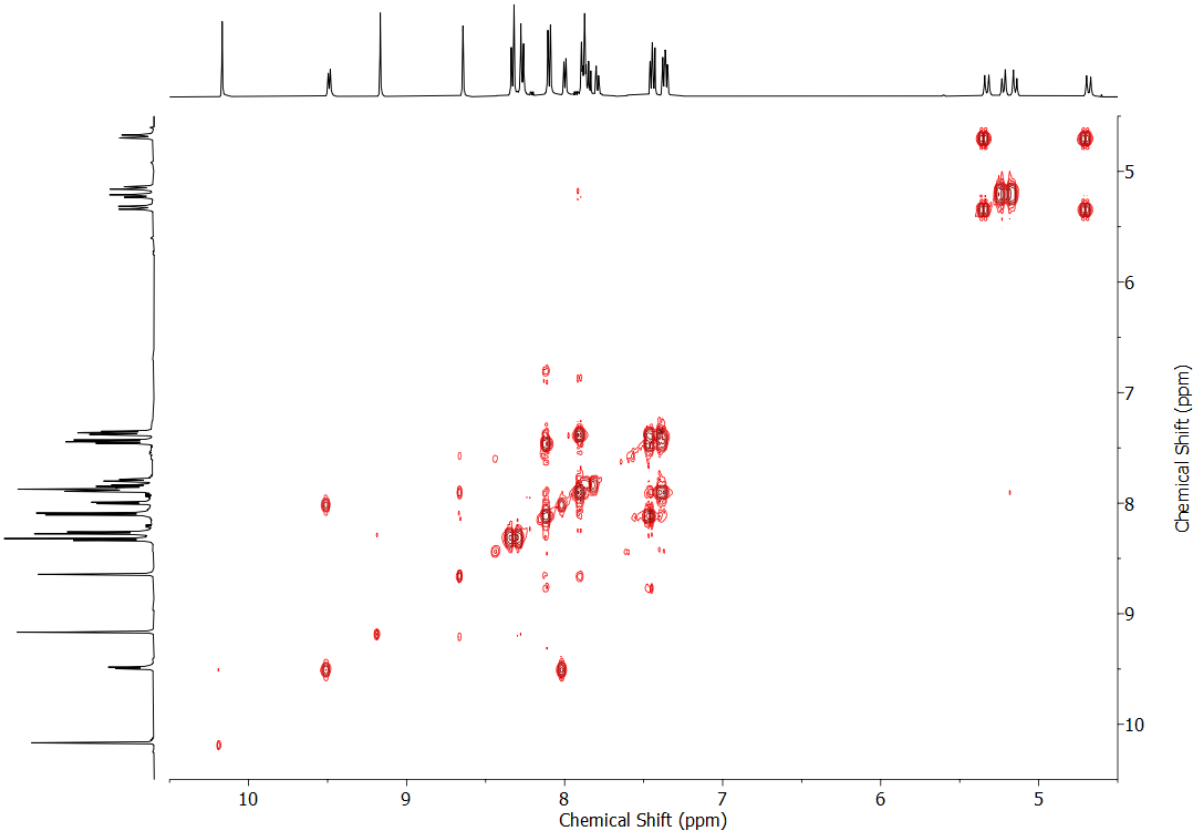

Figure S97 COSY NMR (d_6-DMSO) of $[Pd_2(\mathbf{L}^{\mathbf{Anth}})_4](BF_4)_4$.

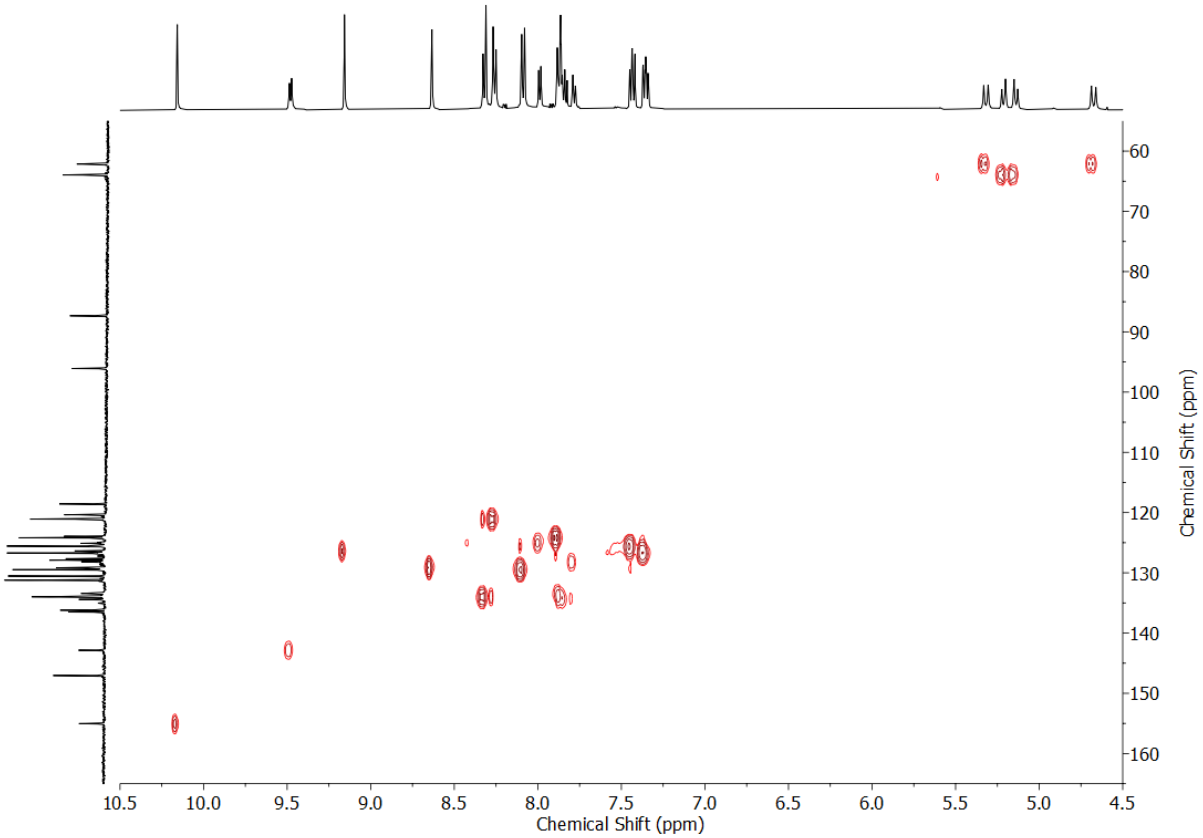

Figure S98 HSQC NMR (d_6-DMSO) of $[Pd_2(\mathbf{L}^{Anth})_4](BF_4)_4$.

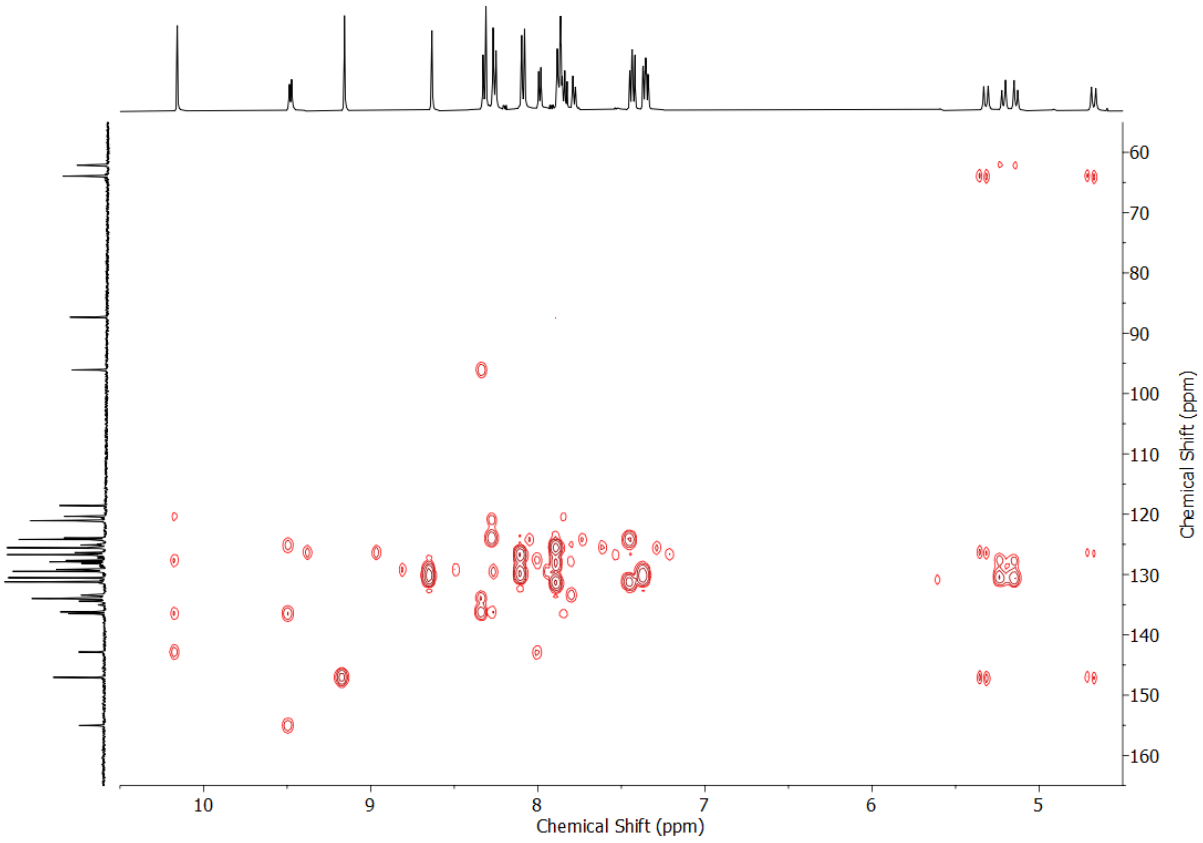

Figure S99 HMBC NMR (d_6-DMSO) of $[Pd_2(\mathbf{L}^{Anth})_4](BF_4)_4$.

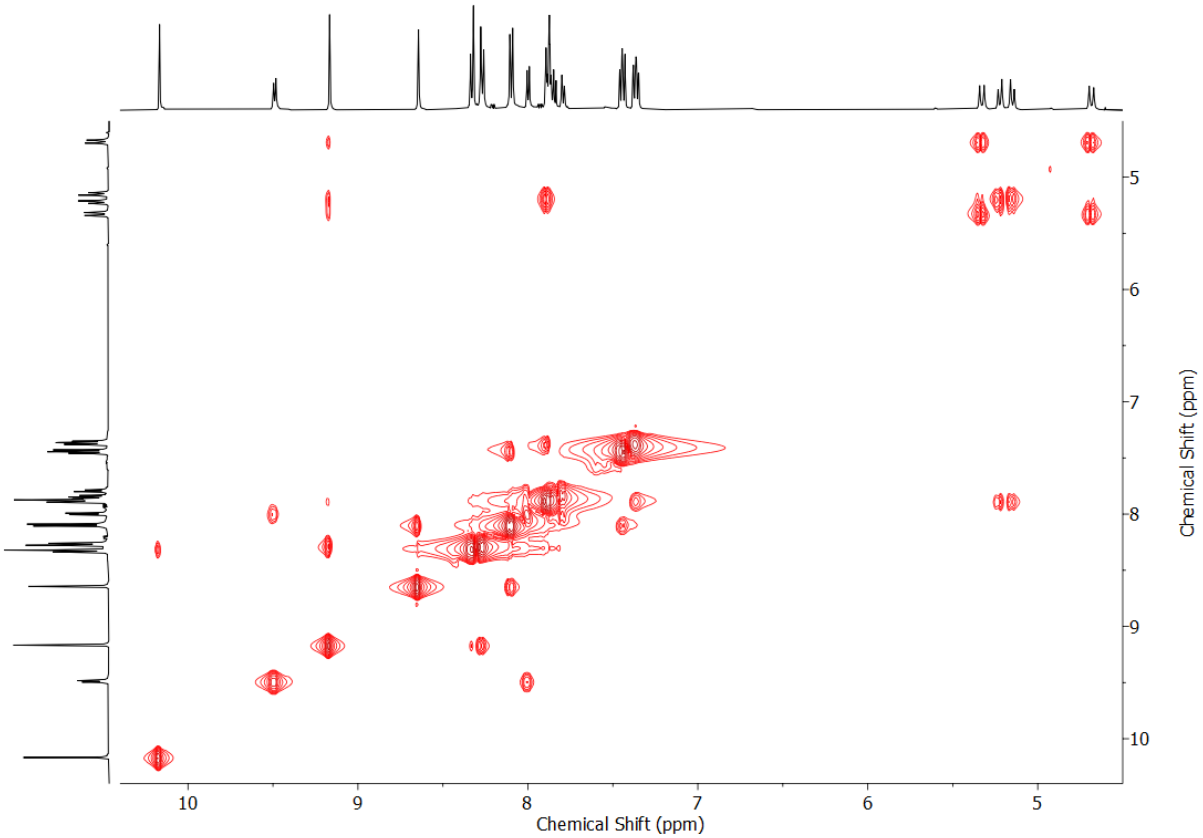

Figure S100 NOESY NMR (d_6-DMSO, 500 MHz) of $[Pd_2(\mathbf{L}^{Anth})_4](BF_4)_4$.

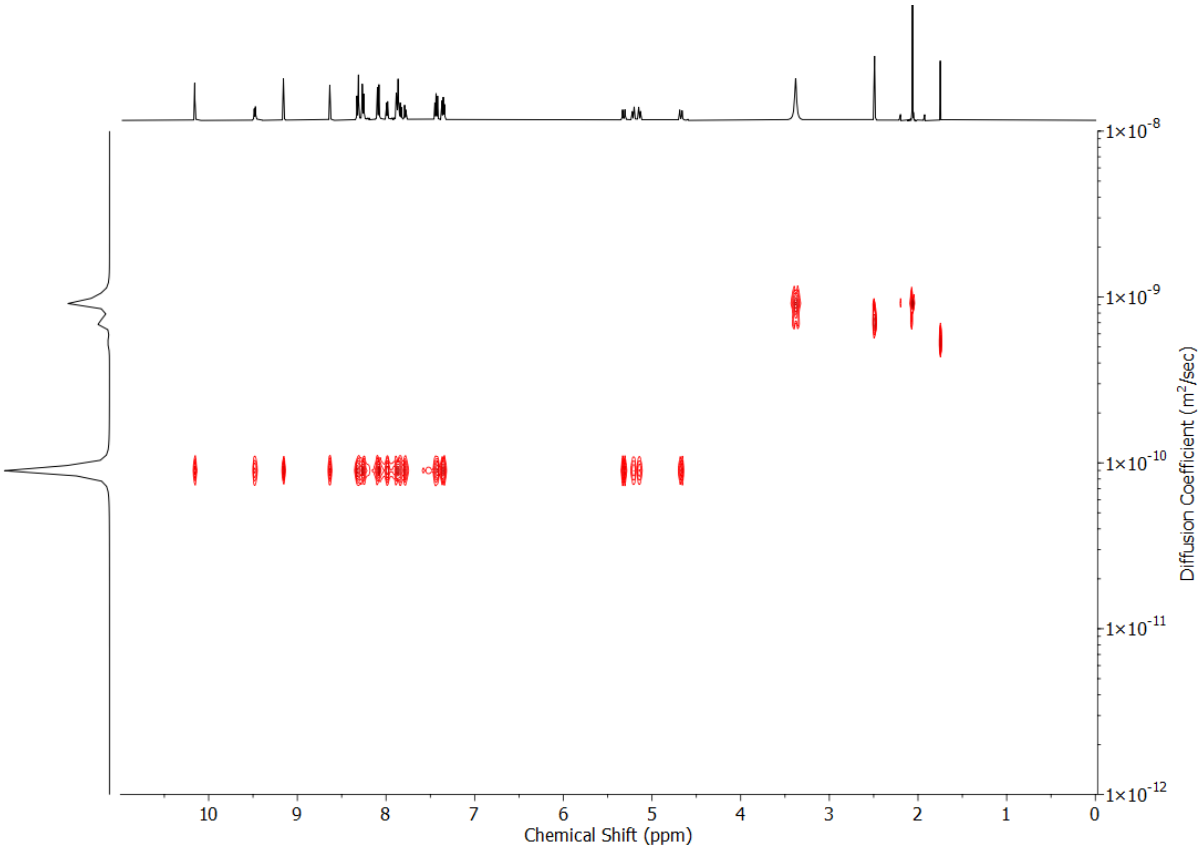

Figure S101 DOSY NMR (d_6-DMSO, 500 MHz) of $[Pd_2(\mathbf{L}^{Anth})_4](BF_4)_4$.

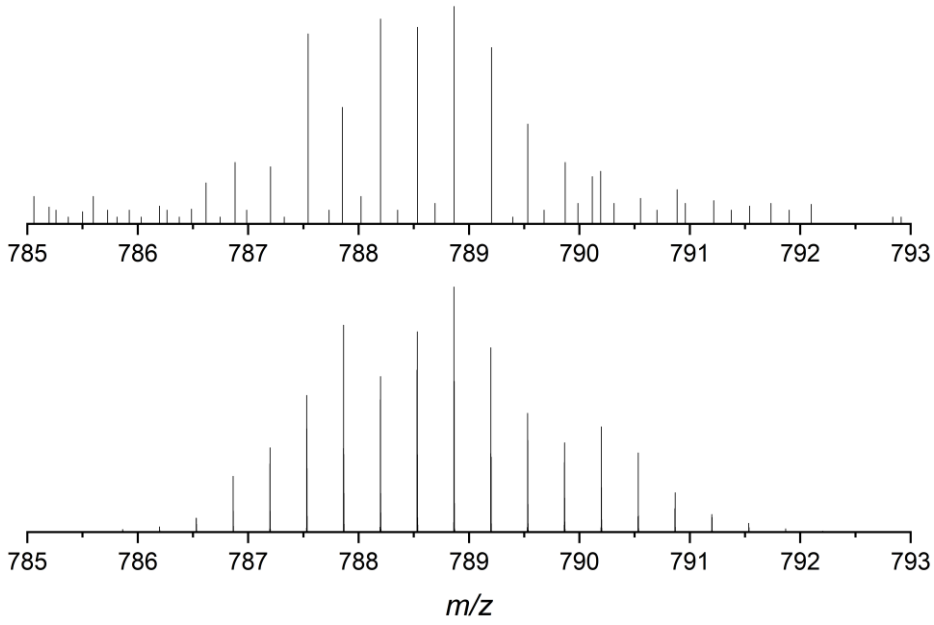

Figure S102 Observed (top) and calculated (bottom) isotopic patterns for $\{[Pd_2(\mathbf{L}^{\mathbf{Anth}})_4](BF_4)\}^{3+}$.

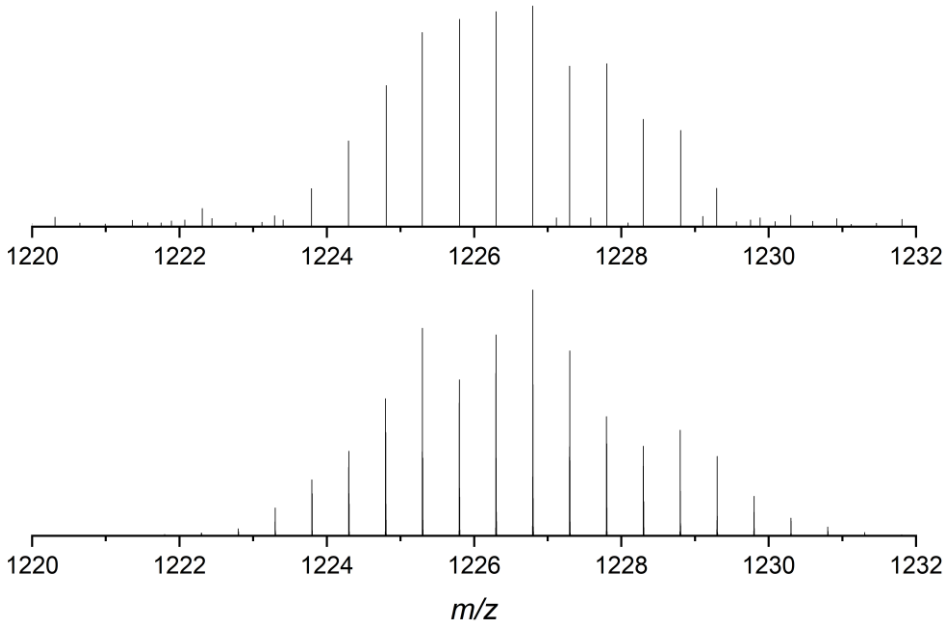

Figure S103 Observed (top) and calculated (bottom) isotopic patterns for $\{[Pd_2(\mathbf{L}^{\mathbf{Anth}})_4](BF_4)_2\}^{2+}$.

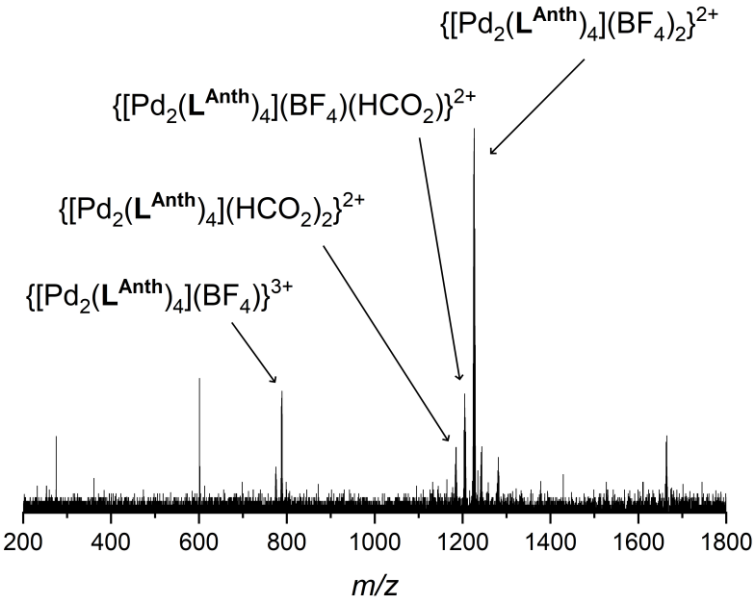

Figure S104 ESI-MS of $[Pd_2(\mathbf{L}^{Anth})_4](BF_4)_4$.

Comparison of L^{Bu} and L^{Phth} Self-assembly

L^{Bu} + 0.25 eq. Pd(II)

L^{Bu} (10.6 mg, 0.030 mmol, 2.0 eq.) and $[Pd(CH_3CN)_4](BF_4)_2$ (3.3 mg, 0.0075 mmol, 1.0 eq.) were sonicated in d_6-DMSO (0.75 mL) until all solids were dissolved, giving a light yellow solution.

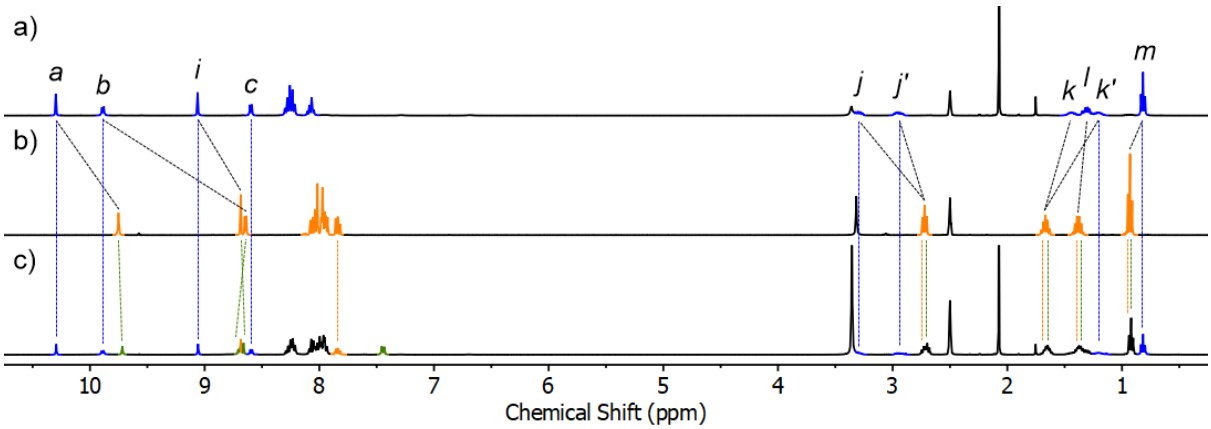

Figure S105 ^{1}H NMR spectra (400 MHz, d_6-DMSO) of a) $[Pd_2(L^{Bu})_4](BF_4)_4$, b) L^{Bu}, and c) L^{Bu} + 0.25 eq. Pd(II) ($[L^{Bu}]$ = 40 mM). Non-overlapping peaks have been colour-coded: $[Pd_2(L^{Bu})_4](BF_4)_4$ = blue, L^{Bu} = orange, $[Pd(L^{Bu})_4](BF_4)_2$ = green.

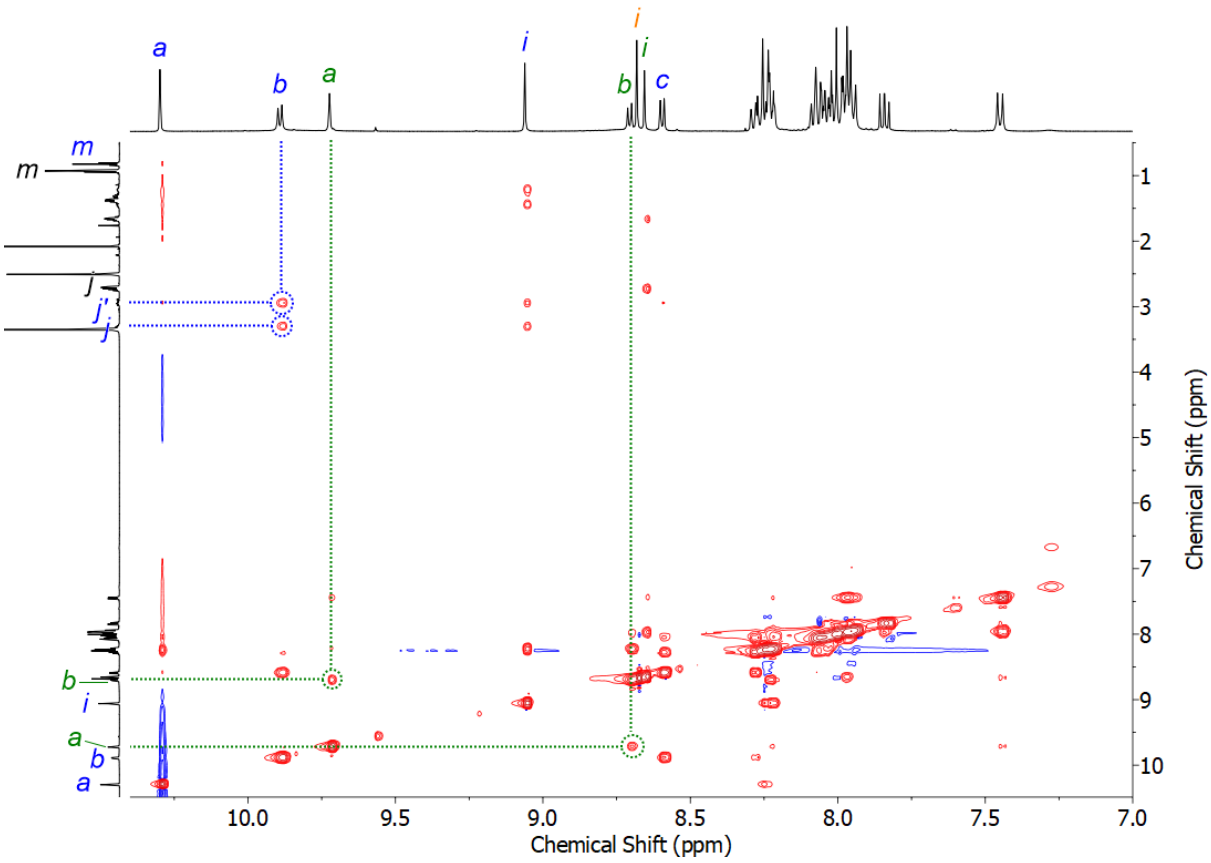

Figure S106 NOESY NMR spectrum (500 MHz, d_6-DMSO) of L^{Bu} + 0.25 eq. Pd(II). Peak labels have been colour-coded: $[Pd_2(L^{Bu})_4](BF_4)_4$ = blue, L^{Bu} = orange, $[Pd(L^{Bu})_4](BF_4)_2$ = green.

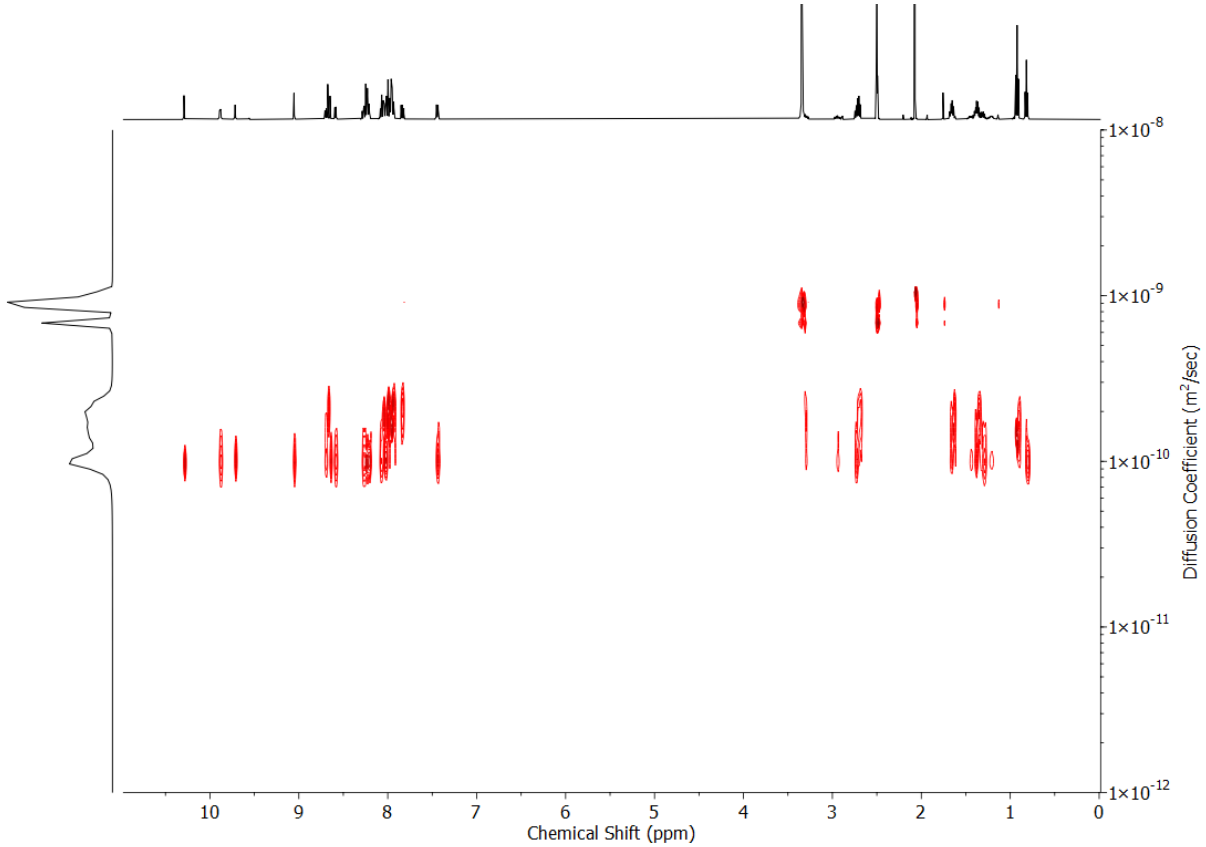

Figure S107 DOSY NMR spectrum (500 MHz, d_6-DMSO) of $\mathbf{L^{Bu}}$ + 0.25 eq. Pd(II).

L^{Phth} + 0.25 eq. Pd(II)

L^{Phth} (13.7 mg, 0.030 mmol, 2.0 eq.) and $[Pd(CH_3CN)_4](BF_4)_2$ (3.3 mg, 0.0075 mmol, 1.0 eq.) were sonicated in d_6-DMSO (0.75 mL) until all solids were dissolved, giving a light yellow solution.

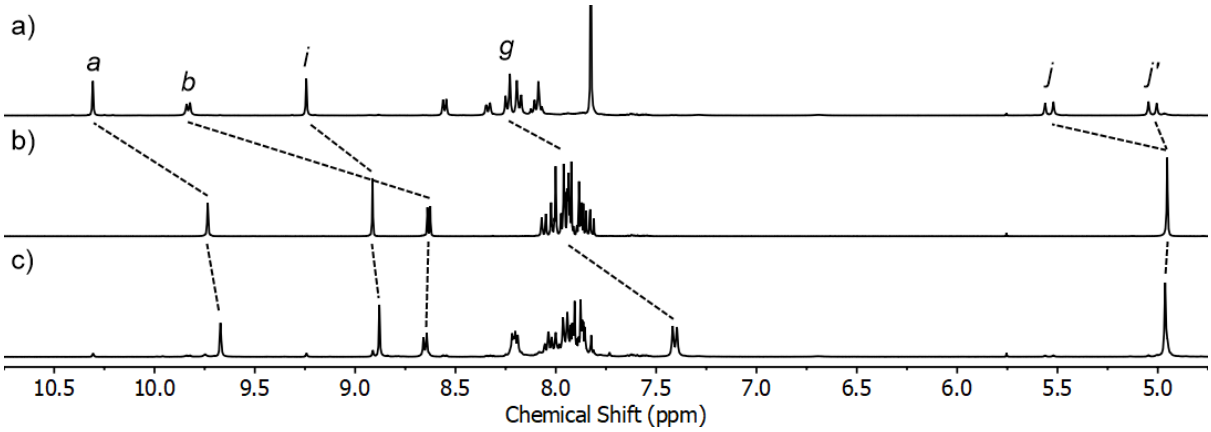

Figure S108 ^{1}H NMR spectra (400 MHz, d_6-DMSO) of a) $[Pd_2(\mathbf{L}^{Phth})_4](BF_4)_4$, b) **L**^{Phth}, and c) $[Pd(\mathbf{L}^{Phth})_4](BF_4)_2$ ([**L**^{Phth}] = 40 mM).

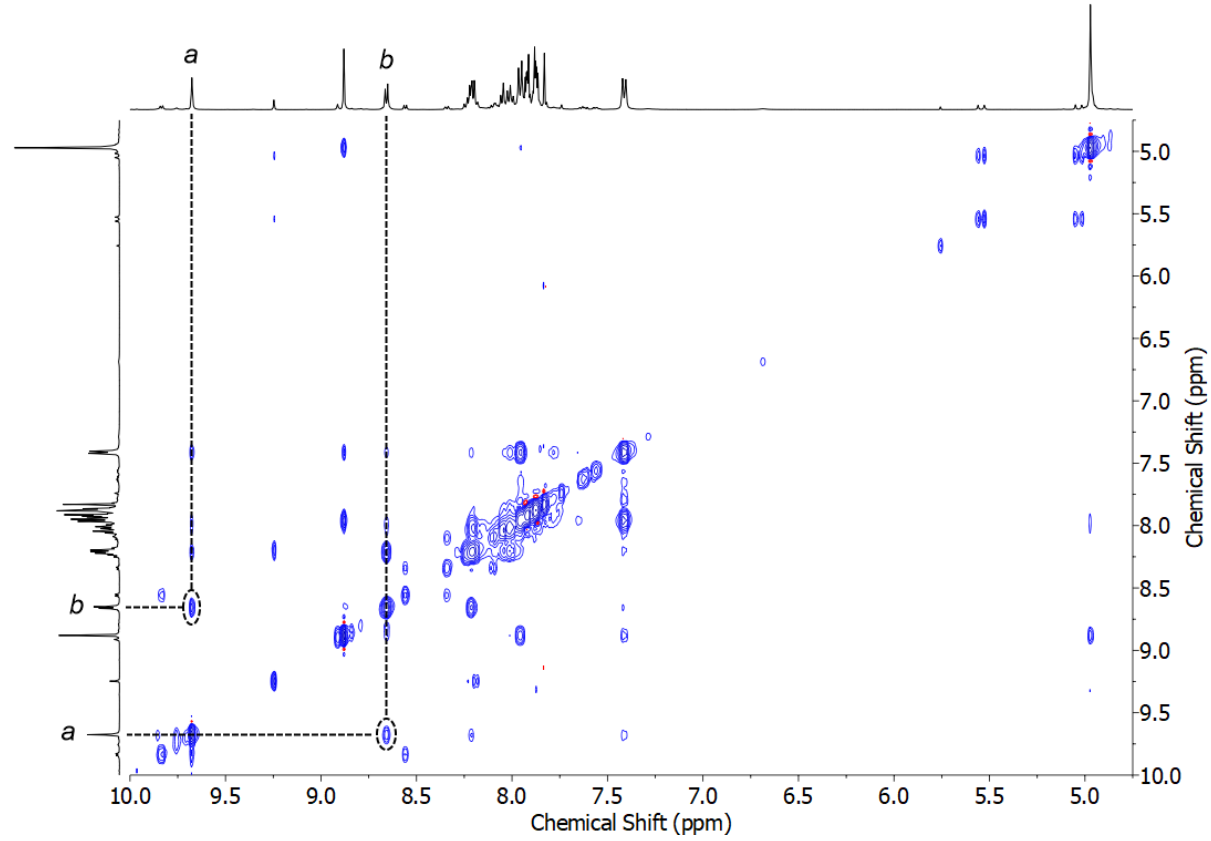

Figure S109 NOESY NMR spectrum (500 MHz, d_6-DMSO) of $[Pd(\mathbf{L}^{Phth})_4](BF_4)_2$.

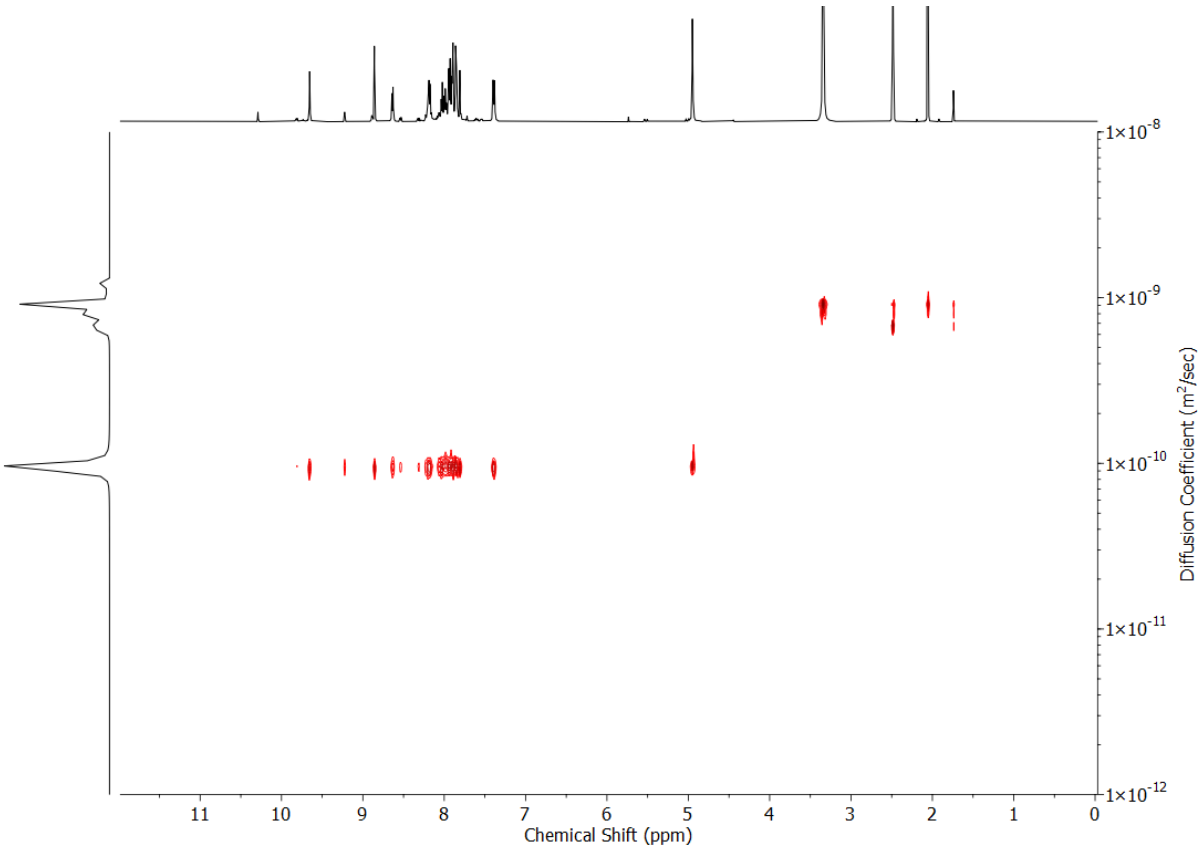

Figure S110 DOSY NMR spectrum (500 MHz, d_6-DMSO) of [Pd(**L**$^{\mathbf{Phth}}$)$_4$](BF$_4$)$_2$.

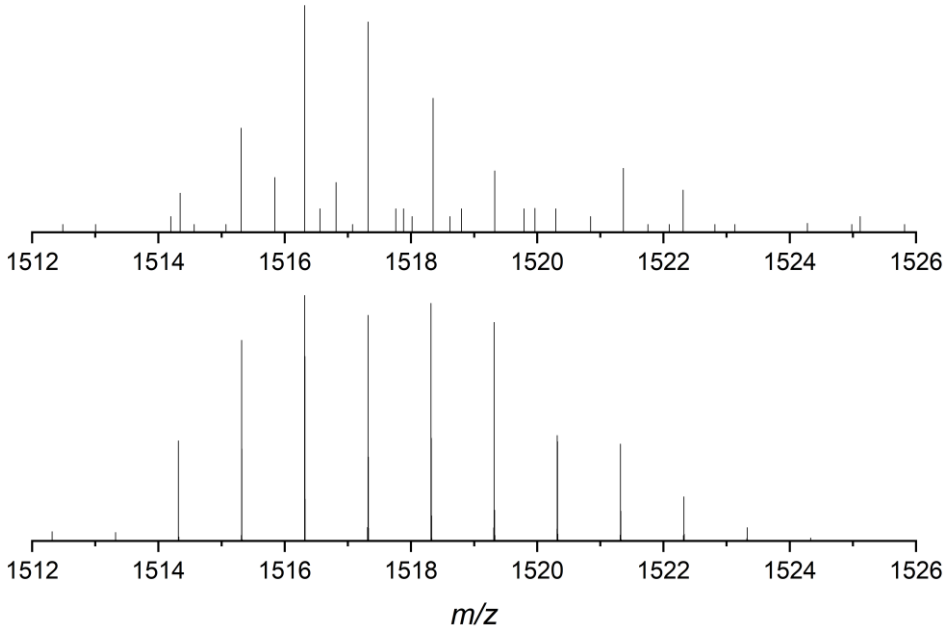

Figure S111 Observed (top) and calculated (bottom) isotopic patterns for {[Pd$_2$(**L**$^{\mathbf{Phth}}$)$_3$](HCO$_2$)}$^+$.

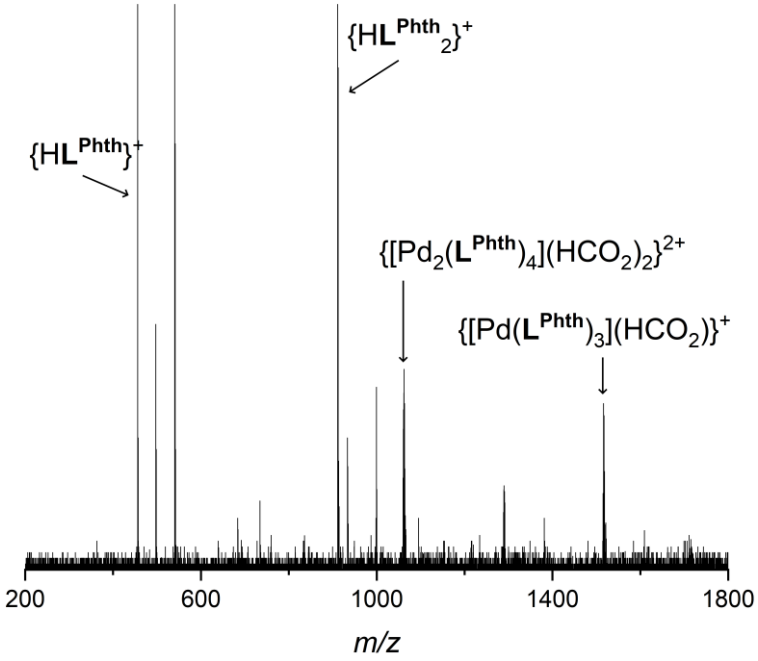

Figure S112 ESI-MS of $[Pd(\mathbf{L}^{Phth})_4](BF_4)_2$.

Model Mononuclear Complexes

$[Pd(\mathbf{1})_4](BF_4)_2$

1 (8.1 mg, 0.030 mmol, 4 eq.) and $[Pd(CH_3CN)_4](BF_4)_2$ (3.3 mg, 0.0075 mmol, 1 eq.) were sonicated in d_6-DMSO (0.75 mL) until all solids were dissolved, giving an orange solution. Quantitative conversion to $[Pd(\mathbf{1})_4](BF_4)_2$ was observed by ^{1}H NMR.

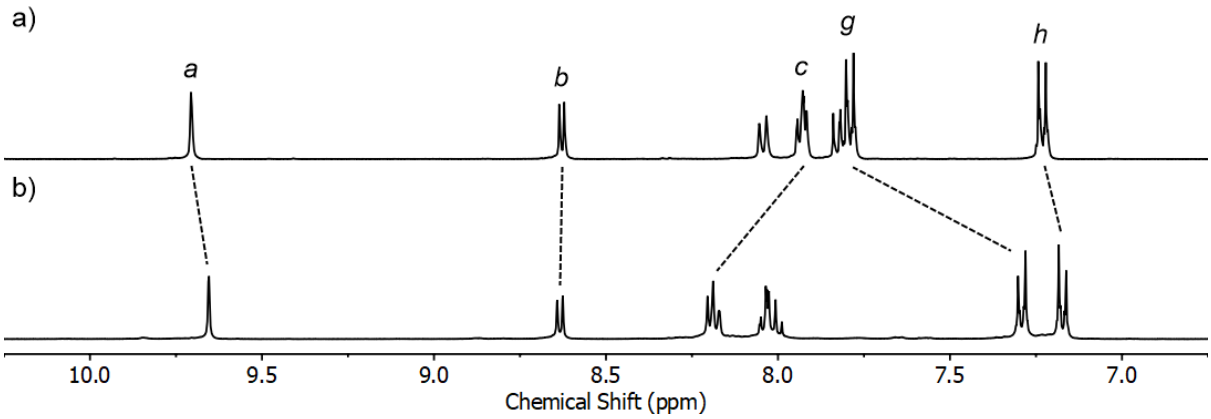

Figure S113 ^{1}H NMR spectrum (400 MHz, d_6-DMSO) of a) **1**, and b) **1** + 0.25 eq. Pd(II) ([**1**] = 40 mM).

$[Pd(\mathbf{S2})_4](BF_4)_2$

S2 (7.3 mg, 0.030 mmol, 4 eq.) and $[Pd(CH_3CN)_4](BF_4)_2$ (3.3 mg, 0.0075 mmol, 1 eq.) were sonicated in d_6-DMSO (0.75 mL) until all solids were dissolved, giving an orange solution. Quantitative conversion to $[Pd(\mathbf{S2})_4](BF_4)_2$ was observed by ^{1}H NMR.

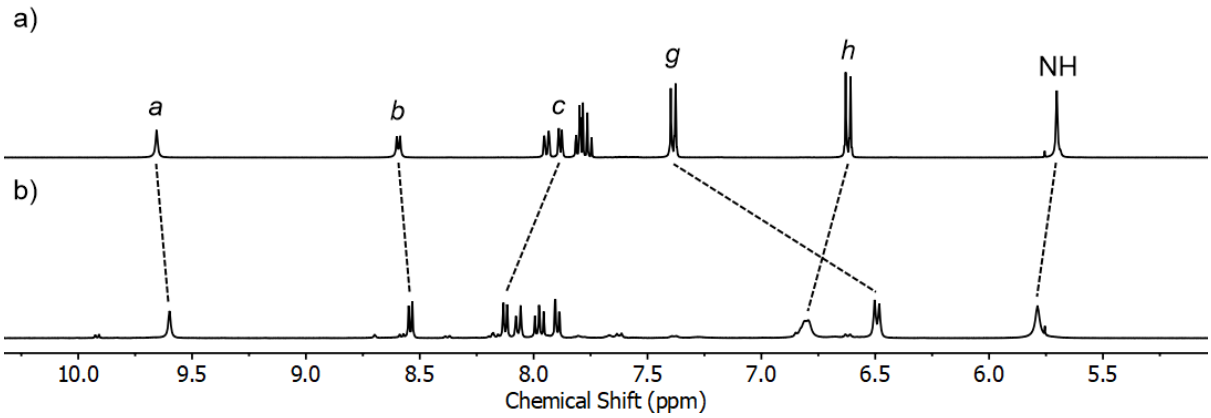

Figure S114 ^{1}H NMR spectrum (400 MHz, d_6-DMSO) of a) **S2**, and b) **S2** + 0.25 eq. Pd(II) ([**S2**] = 40 mM).

Combinatorial Libraries

$[Pd_2(\mathbf{L^{Bu}})_x(\mathbf{L^{Bn}})_{(4-x)}](BF_4)_4$

$\mathbf{L^{Bu}}$ (5.3 mg, 0.015 mmol, 1 eq.), $\mathbf{L^{Bn}}$ (5.8 mg, 0.015 mmol, 1 eq.) and $[Pd(CH_3CN)_4](BF_4)_2$ (6.7 mg, 0.015 mmol, 1 eq.) were sonicated in d_6-DMSO (0.75 mL) until a homogenous solution was obtained.

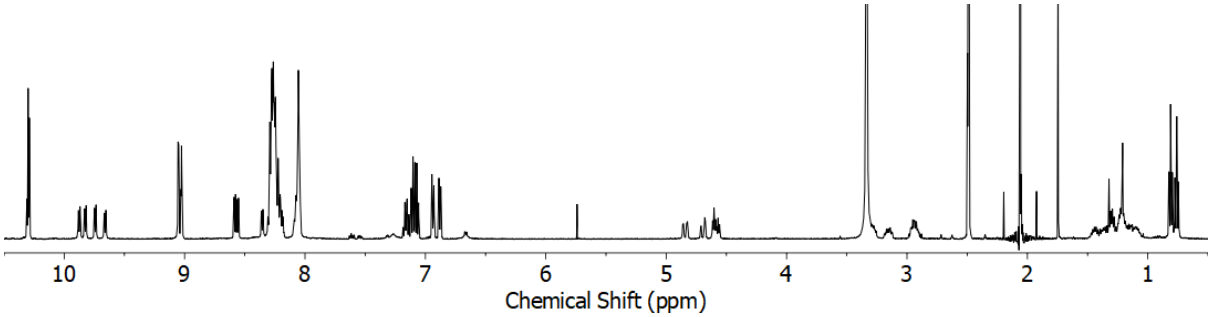

Figure S115 ^{1}H NMR spectrum (500 MHz, d_6-DMSO) of $[Pd(\mathbf{L^{Bu}})_x(\mathbf{L^{Bn}})_{(4-x)}](BF_4)_4$.

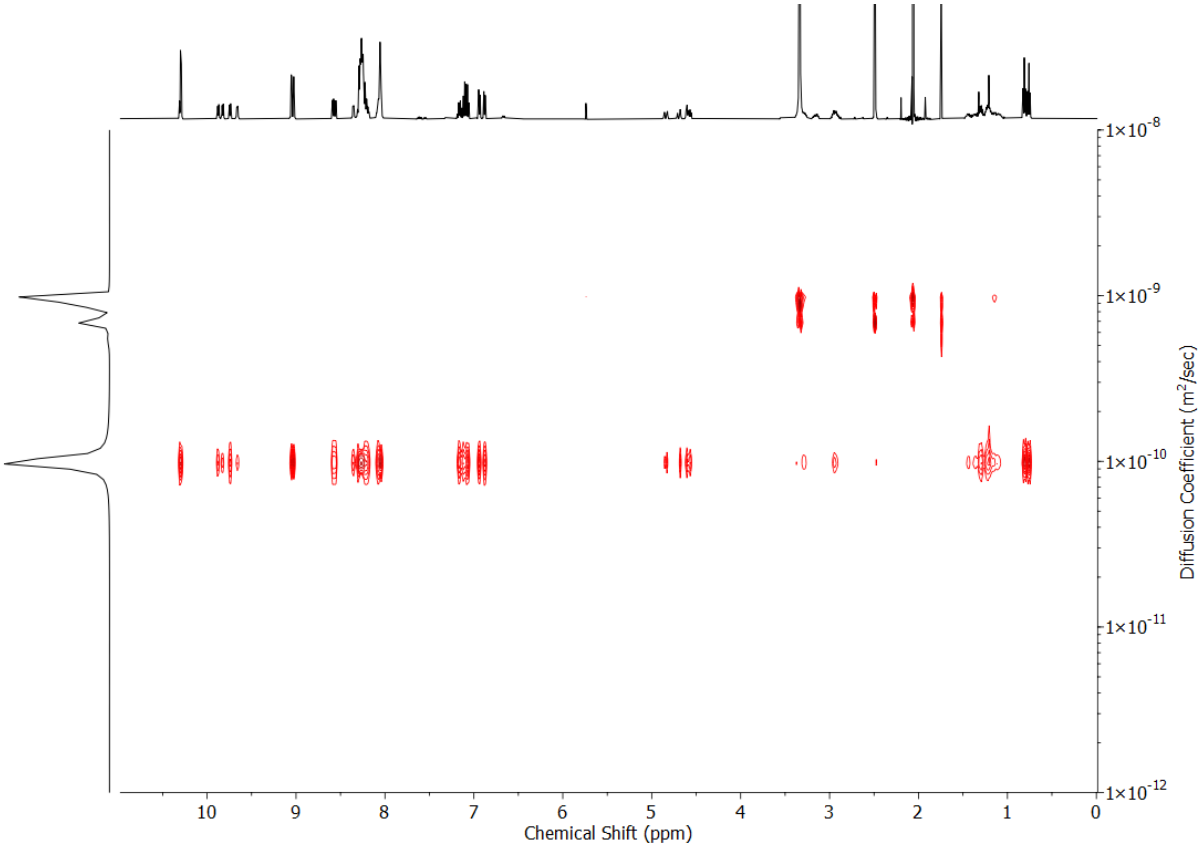

Figure S116 DOSY NMR (d_6-DMSO, 500 MHz) of $[Pd_2(\mathbf{L^{Bu}})_x(\mathbf{L^{Bn}})_{(4-x)}](BF_4)_4$.

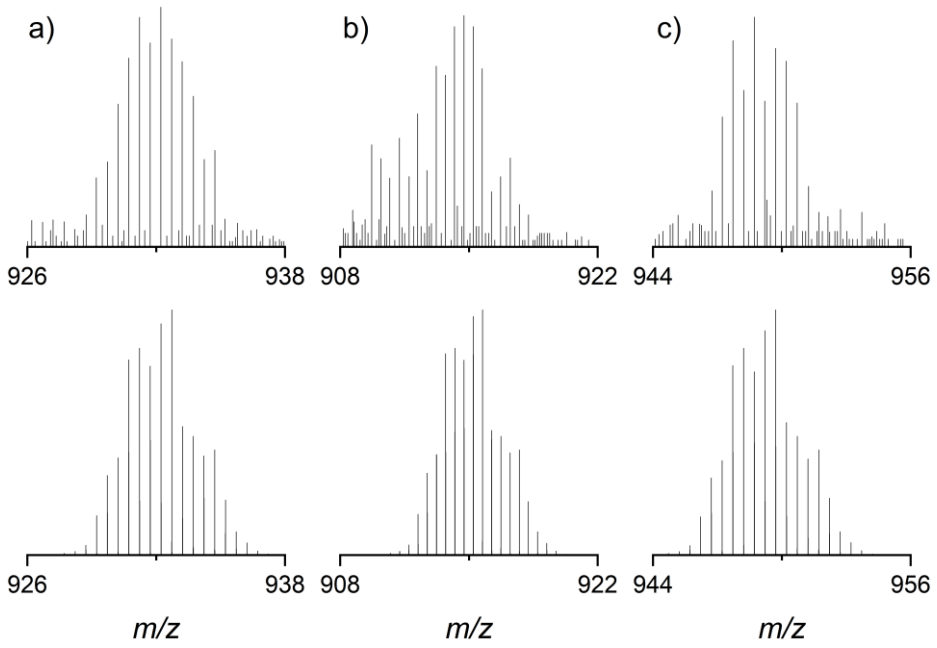

Figure S117 Observed (top) and calculated (bottom) isotopic patterns for a) $\{[Pd_2(\mathbf{L^{Bu}})_3(\mathbf{L^{Bn}})](BF_4)_2\}^{2+}$; b) $\{[Pd_2(\mathbf{L^{Bu}})_2(\mathbf{L^{Bn}})_2](BF_4)_2\}^{2+}$; c) $\{[Pd_2(\mathbf{L^{Bu}})(\mathbf{L^{Bn}})_3](BF_4)_2\}^{2+}$.

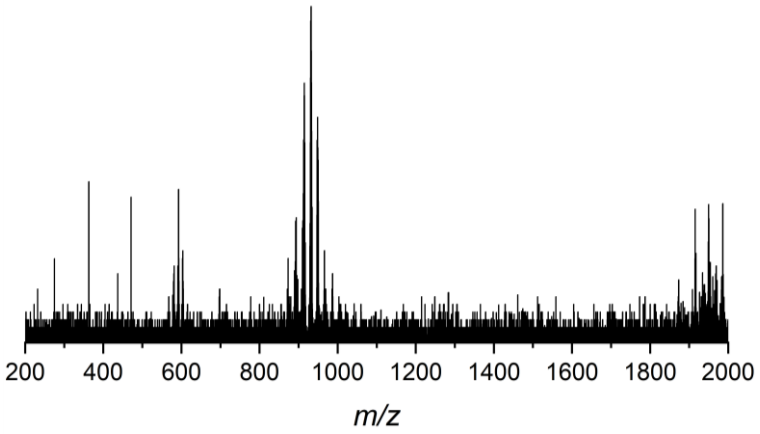

Figure S118 ESI-MS of combinatorial library $[Pd_2(\mathbf{L^{Bu}})_x(\mathbf{L^{Bn}})_{(4-x)}](BF_4)_4$.

$[Pd_2(\mathbf{L}^{Bu})_x(\mathbf{L}^{Phth})_{(4-x)}](BF_4)_4$

$\mathbf{L}^{Bu}$ (10.6 mg, 0.030 mmol, 1 eq.), $\mathbf{L}^{Phth}$ (13.7 mg, 0.030 mmol) and $[Pd(CH_3CN)_4](BF_4)_2$ (13.3 mg, 0.030 mmol, 1 eq.) were sonicated in d_6-DMSO (0.75 mL) until a homogenous solution was obtained.

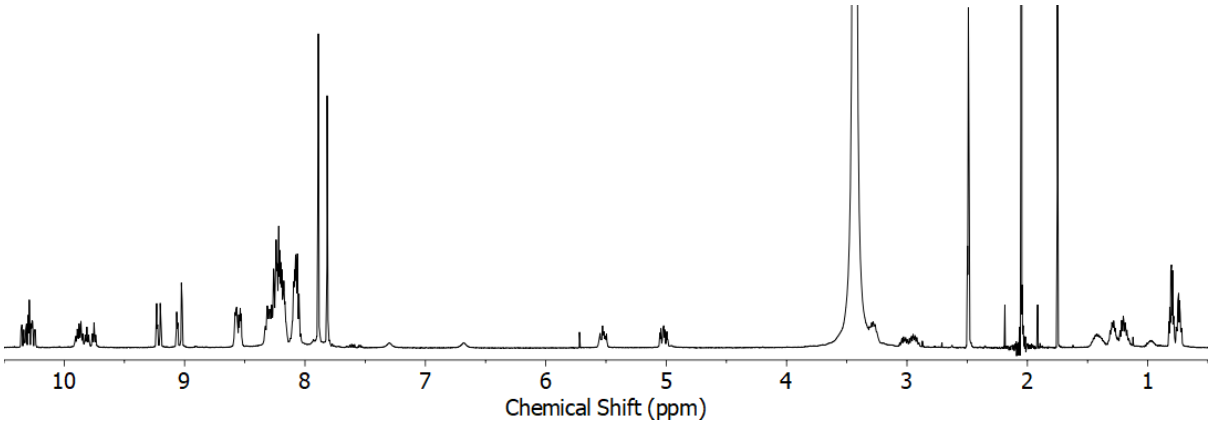

Figure S119 ^{1}H NMR spectrum (500 MHz, d_6-DMSO) of $[Pd(\mathbf{L}^{Bu})_x(\mathbf{L}^{Phth})_{(4-x)}](BF_4)_4$.

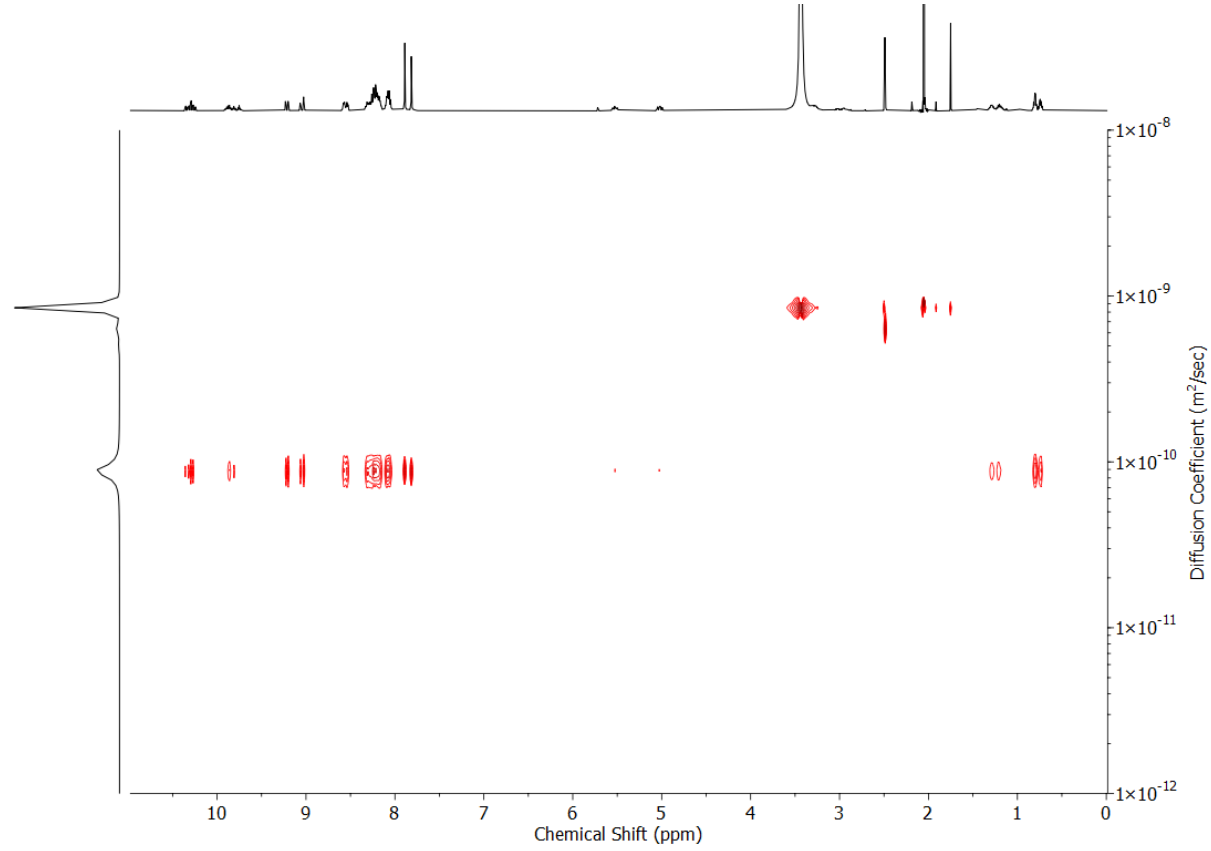

Figure S120 DOSY NMR (d_6-DMSO, 500 MHz) of $[Pd_2(\mathbf{L}^{Bu})_x(\mathbf{L}^{Phth})_{(4-x)}](BF_4)_4$.

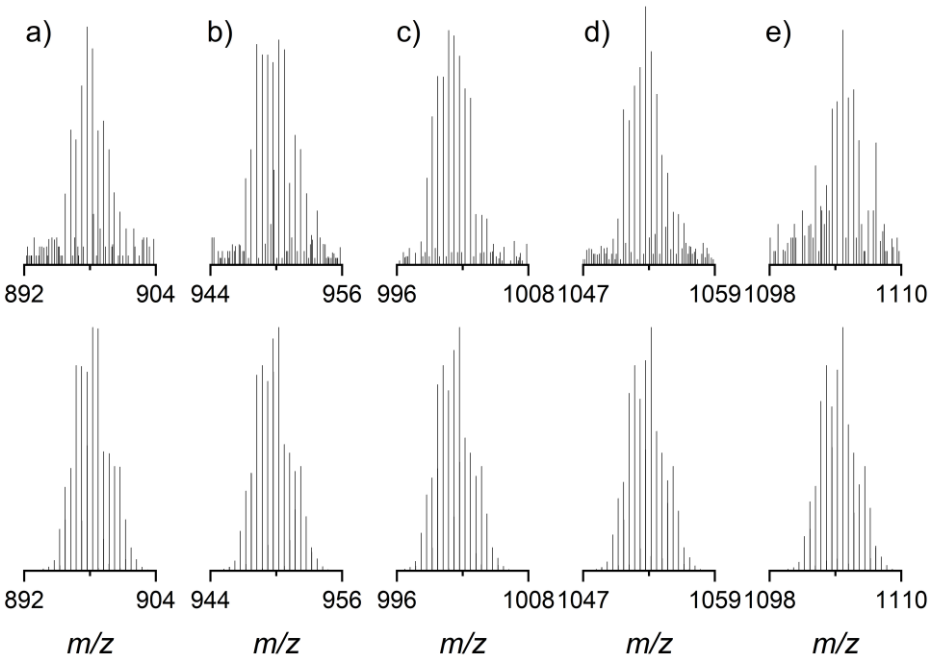

Figure S121 Observed (top) and calculated (bottom) isotopic patterns for a) $\{[Pd_2(\mathbf{L}^{\mathbf{Bu}})_4](BF_4)_2\}^{2+}$; b) $\{[Pd_2(\mathbf{L}^{\mathbf{Bu}})_3(\mathbf{L}^{\mathbf{Phth}})](BF_4)_2\}^{2+}$; c) $\{[Pd_2(\mathbf{L}^{\mathbf{Bu}})_2(\mathbf{L}^{\mathbf{Phth}})_2](BF_4)_2\}^{2+}$; d) $\{[Pd_2(\mathbf{L}^{\mathbf{Bu}})(\mathbf{L}^{\mathbf{Phth}})_3](BF_4)_2\}^{2+}$; e) $\{[Pd_2(\mathbf{L}^{\mathbf{Bu}})(\mathbf{L}^{\mathbf{Phth}})_4](BF_4)_2\}^{2+}$.

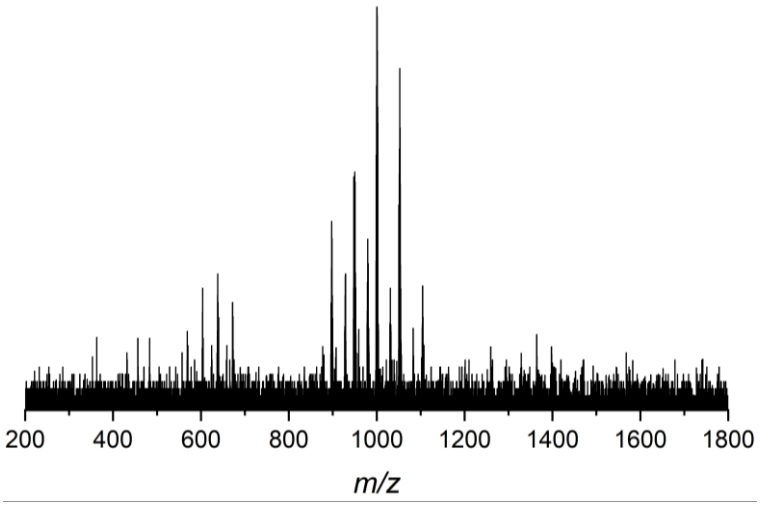

Figure S122 ESI-MS of combinatorial library $[Pd_2(\mathbf{L}^{\mathbf{Bu}})_x(\mathbf{L}^{\mathbf{Phth}})_{(4-x)}](BF_4)_4$.

$[Pd_2(\mathbf{L}^{OH})_x(\mathbf{L}^{Ene})_y(\mathbf{L}^{Anth})_z](BF_4)_4$

$\mathbf{L}^{OH}$ (7.4 mg, 0.020 mmol, 1 eq.), $\mathbf{L}^{Phth}$ (9.1 mg, 0.020 mmol, 1 eq.), $\mathbf{L}^{Anth}$ (10.3 mg, 0.020 mmol, 1 eq.) and $[Pd(CH_3CN)_4](BF_4)_2$ (13.3 mg, 0.030 mmol, 1.5 eq.) were sonicated in d_6-DMSO (1.5 mL) until a homogenous solution was obtained.

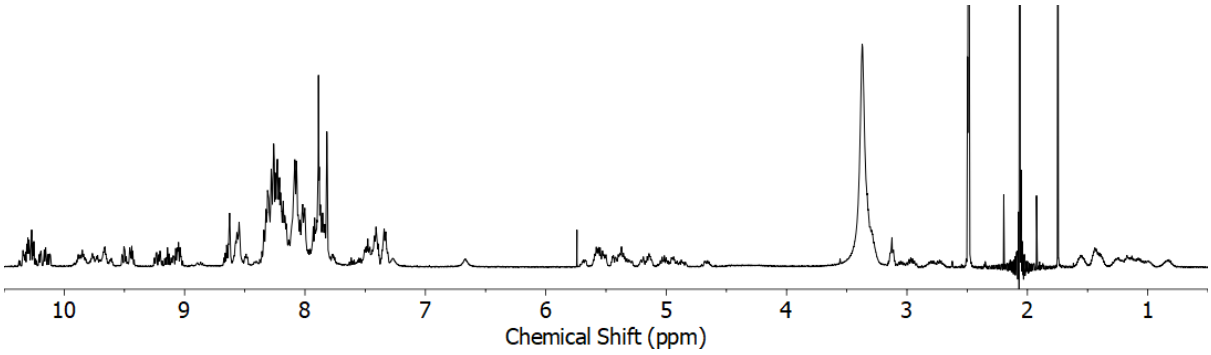

Figure S123 ^{1}H NMR spectrum (500 MHz, d_6-DMSO) of $[Pd(\mathbf{L}^{OH})_x(\mathbf{L}^{Ene})_y(\mathbf{L}^{Anth})_z](BF_4)_4$.

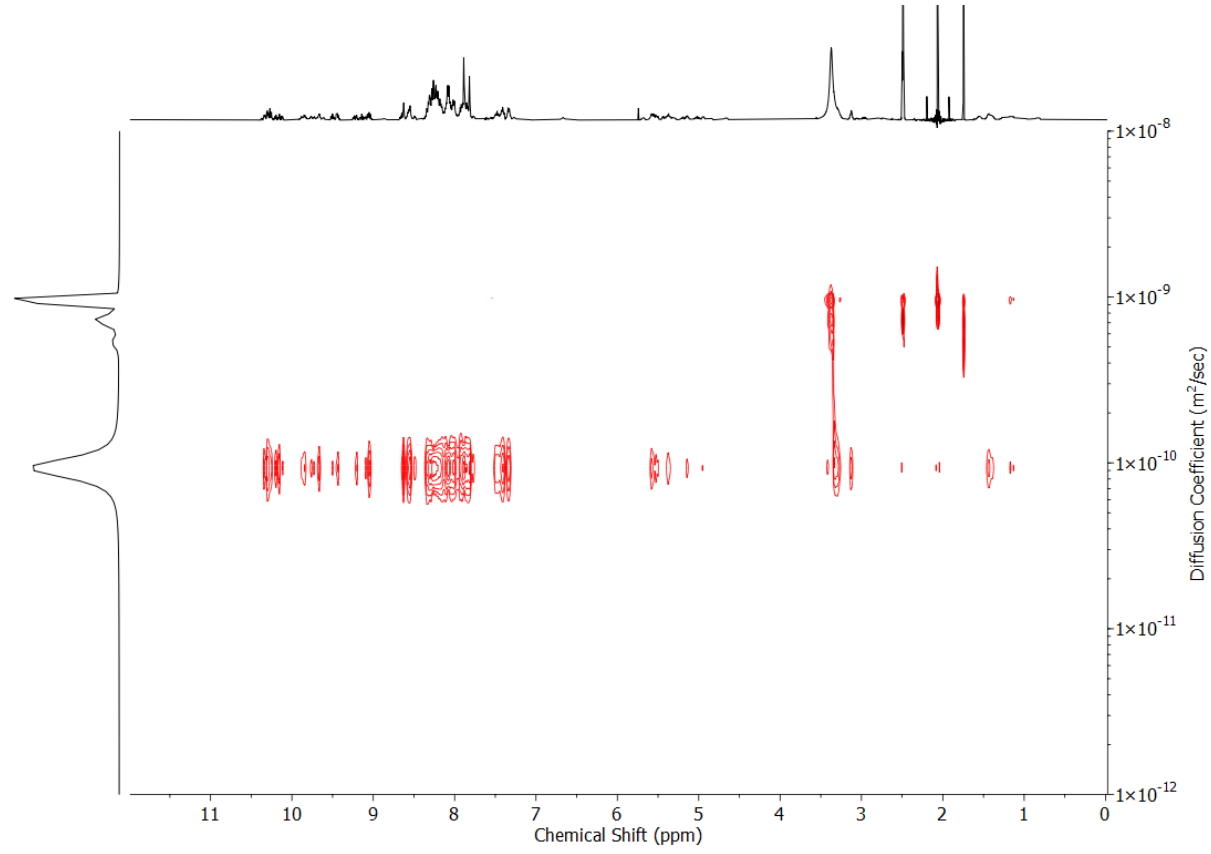

Figure S124 DOSY NMR (d_6-DMSO, 500 MHz) of $[Pd_2(\mathbf{L}^{OH})_x(\mathbf{L}^{Ene})_y(\mathbf{L}^{Anth})_z](BF_4)_4$.

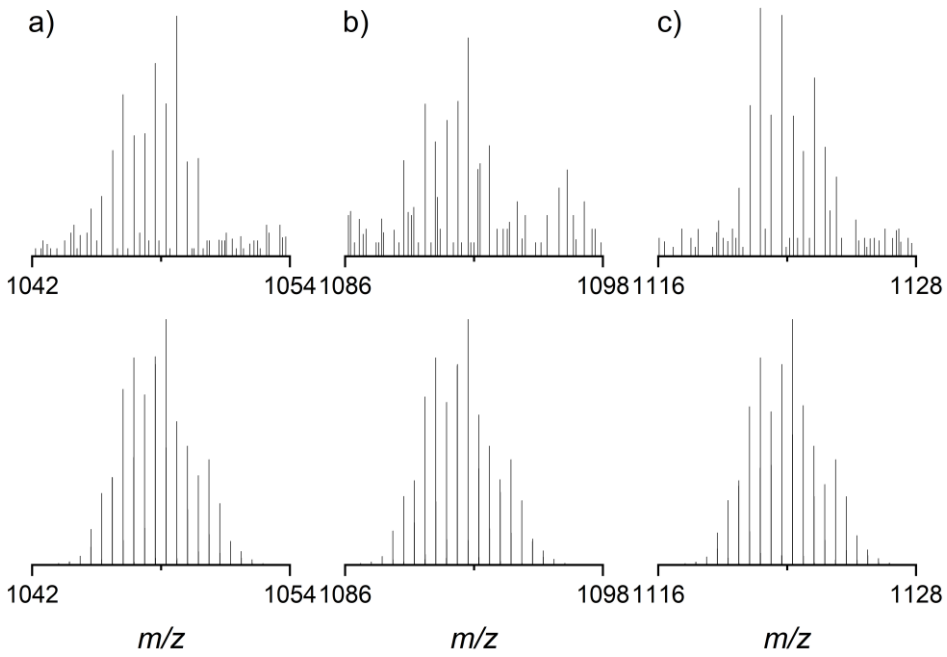

Figure S125 Observed (top) and calculated (bottom) isotopic patterns for a) $\{[Pd_2(\mathbf{L}^{OH})_2(\mathbf{L}^{Phth})(\mathbf{L}^{Anth})](BF_4)_2\}^{2+}$; b) $\{[Pd_2(\mathbf{L}^{OH})(\mathbf{L}^{Phth})_2(\mathbf{L}^{Anth})](BF_4)_2\}^{2+}$; c) $\{[Pd_2(\mathbf{L}^{OH})(\mathbf{L}^{Phth})(\mathbf{L}^{Anth})_2](BF_4)_2\}^{2+}$.

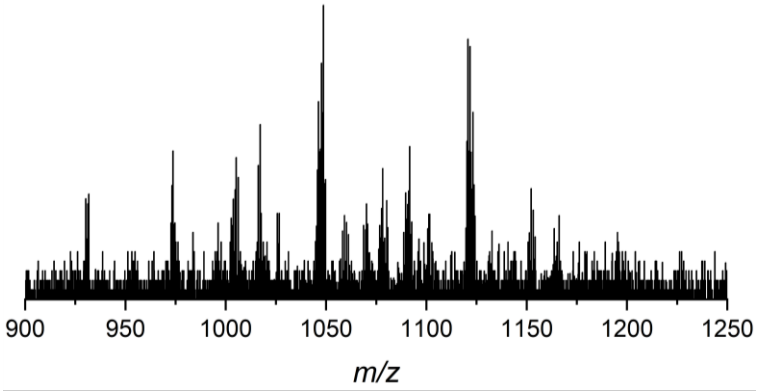

Figure S126 Partial ESI-MS of combinatorial library $[Pd_2(\mathbf{L}^{OH})_x(\mathbf{L}^{Phth})_y(\mathbf{L}^{Anth})_z](BF_4)_4$.

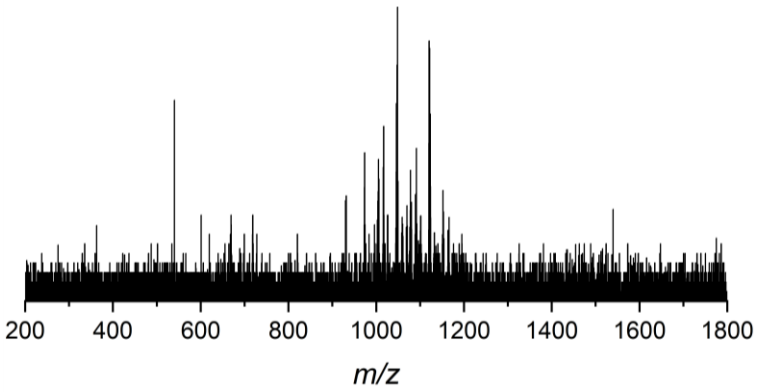

Figure S127 ESI-MS of combinatorial library $[Pd_2(\mathbf{L}^{OH})_x(\mathbf{L}^{Phth})_y(\mathbf{L}^{Anth})_z](BF_4)_4$.

Table S1 List of number of possible isomers for homoleptic, and binary and ternary heteroleptic *cis*-Pd_2L_4 cages.

Cage	L^1	L^2	L^3	Number of diastereomers	Total number of isomers
1	4	0	0	1	1
2	0	4	0	1	1
3	0	0	4	1	1
4	3	1	0	1	2
5	3	0	1	1	2
6	1	3	0	1	2
7	0	3	1	1	2
8	1	0	3	1	2
9	0	1	3	1	2
10	2	2	0	3	4
11	2	0	2	3	4
12	0	2	2	3	4
13	2	1	1	3	6
14	1	2	1	3	6
15	1	1	2	3	6
				Total	47

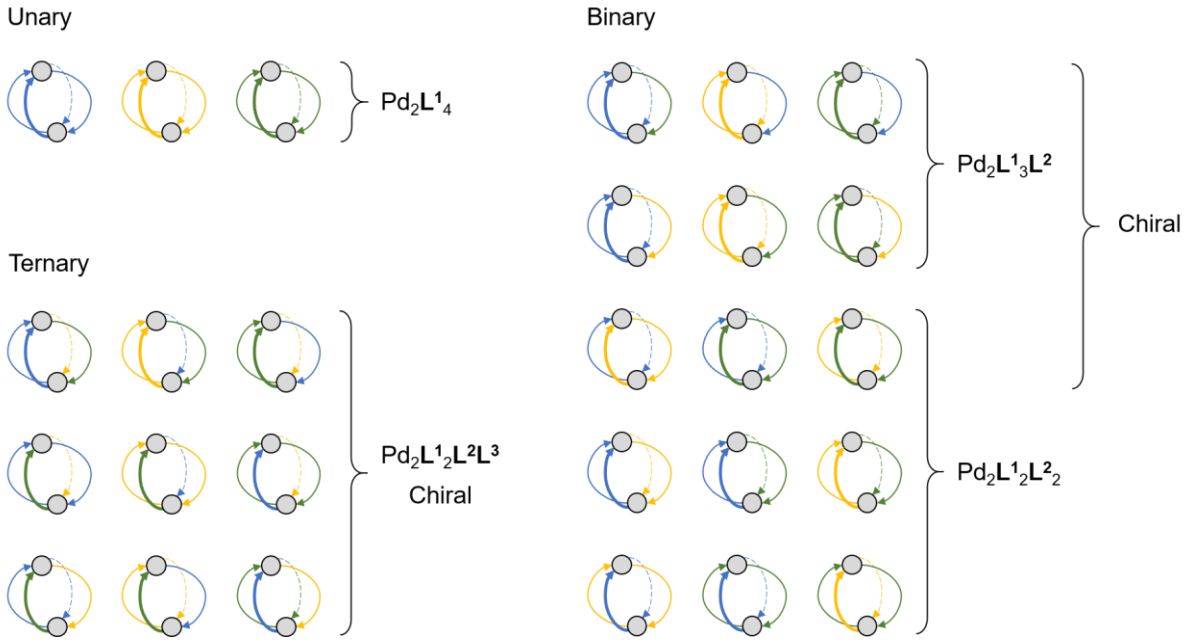

Figure 128 Cartoon representation of possible isomers for homoleptic, and binary and ternary heteroleptic *cis*-Pd_2L_4 cages

Geometry Optimised Structures

Molecular mechanics models were constructed using Avogadro[2] and energy-minimised using UFF.[3] Geometry optimisations were subsequently performed using the semi-empirical method PM6[4] in Gaussian 16.[5]

Table S2 Results summary for structure optimisation of "All up" $[Pd_2(\mathbf{L^{Me}})]^{4+}$

Calculation Type = FOPT
Calculation Method = RPM6
Formula = $C_{80}H_{56}N_{16}Pd_2$
Basis Set = ZDO
Charge = 4
Spin = Singlet
Solvation = None
E(RPM6) = 2.3382136 Hartree
RMS Gradient Norm = 2.9e-08 Hartree/Bohr
Imaginary Freq =
Dipole Moment = 0.4512 Debye
Point Group = C1
Molecular Mass = 1452.2943 amu

Maximum force = 0 Converged
RMS force = 0 Converged
Maximum displacement = 4.1e-05 Converged
RMS displacement = 7e-06 Converged
Predicted energy change = -4.950729e-12 Hartree

Table S3 Results summary for structure optimisation of "Three-up-one-down" $[Pd_2(\mathbf{L^{Me}})]^{4+}$

Calculation Type = FOPT
Calculation Method = RPM6
Formula = $C_{80}H_{56}N_{16}Pd_2$
Basis Set = ZDO
Charge = 4
Spin = Singlet
Solvation = None
E(RPM6) = 2.2786545 Hartree
RMS Gradient Norm = 4.6e-08 Hartree/Bohr
Imaginary Freq =
Dipole Moment = 1.4818913 Debye
Point Group = C1
Molecular Mass = 1452.2943 amu

Maximum force = 2e-06 Converged
RMS force = 0 Converged
Maximum displacement = 5.7e-05 Converged
RMS displacement = 9e-06 Converged
Predicted energy change = -4.734033e-12 Hartree

Table S4 Results summary for structure optimisation of *trans*-$[Pd_2(\mathbf{L^{Me}})]^{4+}$

Calculation Type = FOPT
Calculation Method = RPM6
Formula = $C_{80}H_{56}N_{16}Pd_2$
Basis Set = ZDO
Charge = 4
Spin = Singlet
Solvation = None
E(RPM6) = 2.2642098 Hartree
RMS Gradient Norm = 4.3e-08 Hartree/Bohr
Imaginary Freq =
Dipole Moment = 0.0006 Debye
Point Group = C1
Molecular Mass = 1452.2943 amu

Maximum force = 2e-06 Converged
RMS force = 0 Converged
Maximum displacement = 4.9e-05 Converged
RMS displacement = 6e-06 Converged
Predicted energy change = -4.097872e-12 Hartree

Table S5 Results summary for structure optimisation of *cis*-$[Pd_2(\mathbf{L^{Me}})]^{4+}$

Calculation Type = FOPT
Calculation Method = RPM6
Formula = $C_{80}H_{56}N_{16}Pd_2$
Basis Set = ZDO
Charge = 4
Spin = Singlet
Solvation = None
E(RPM6) = 2.2273589 Hartree
RMS Gradient Norm = 1.24e-07 Hartree/Bohr
Imaginary Freq =
Dipole Moment = 0.0002 Debye
Point Group = C1
Molecular Mass = 1452.2943 amu

Maximum force = 4e-06 Converged
RMS force = 0 Converged
Maximum displacement = 6e-05 Converged
RMS displacement = 8e-06 Converged
Predicted energy change = -1.36126e-11 Hartree

Solvodynamic Radii Calculations

Solvodynamic radii were calculated using a variation of the Stokes-Einstein equation:

$$R_S = \frac{k_B T}{6\pi\eta D}$$

Where R_S is the solvodynamic radius (m)

k_B is the Boltzmann constant (1.38×10^{-23} J K^{-1})

T is the temperature (K)

η is the solvent viscosity (2.180×10^{-3} kg $s^{-1}m^{-1}$ for d_6-DMSO)[6]

D is the diffusion coefficient (m^2s^{-1})

Table S6 Calculated solvodynamic radii

Cage	D (m^2s^{-1})	R_S (Å)
$[Pd_2(\mathbf{L}^{\mathbf{Bu}})_4](BF_4)_4$	1.03×10^{-10}	9.7
$[Pd_2(\mathbf{L}^{\mathbf{Bn}})_4](BF_4)_4$	9.53×10^{-11}	10.5
$[Pd_2(\mathbf{L}^{\mathbf{OH}})_4](BF_4)_4$	9.64×10^{-11}	10.4
$[Pd_2(\mathbf{L}^{\mathbf{Ene}})_4](BF_4)_4$	9.89×10^{-11}	10.1
$[Pd_2(\mathbf{L}^{\mathbf{Phth}})_4](BF_4)_4$	8.89×10^{-11}	11.3
$[Pd_2(\mathbf{L}^{\mathbf{Anth}})_4](BF_4)_4$	9.07×10^{-11}	11.0
$[Pd_2(\mathbf{L}^{\mathbf{Bu}})_x(\mathbf{L}^{\mathbf{Bn}})_{(4-x)}](BF_4)_4$	9.98×10^{-11}	10.0
$[Pd_2(\mathbf{L}^{\mathbf{Bu}})_x(\mathbf{L}^{\mathbf{Phth}})_{(4-x)}](BF_4)_4$	8.90×10^{-11}	11.3
$[Pd_2(\mathbf{L}^{\mathbf{OH}})_x(\mathbf{L}^{\mathbf{Phth}})_y(\mathbf{L}^{\mathbf{Anth}})_z](BF_4)_4$	9.20×10^{-11}	10.9

Proton Affinity Calculations

$$PA = -\Delta H = -((\varepsilon_0 + H_{corr})_{BH+} - (\varepsilon_0 + H_{corr})_B)$$

	$\varepsilon_0 + H_{corr}$	PA (kJ mol^{-1})
$\mathbf{L^{Bu}}$	-1107.0432	1118
$\mathbf{L^{Bu}H^+}$	-1107.4689	
$\mathbf{L^{Phth}}$	-1500.9847	1102
$\mathbf{L^{Phth}H^+}$	-1501.4043	

Table S7 Results summary for structure optimisation and frequency calculation of $\mathbf{L^{Bu}}$

Calculation Type = FREQ
Calculation Method = RB3LYP
Formula = $C_{23}H_{20}N_4$
Basis Set = 6-31G(d)
Charge = 0
Spin = Singlet
Solvation = scrf=solvent=dmso
E(RB3LYP) = -1107.447 Hartree
RMS Gradient Norm = 1.73e-07 Hartree/Bohr
Imaginary Freq = 0
Dipole Moment = 4.1639731 Debye
Polarizability (?) = 414.172 a.u.
Point Group = C1
Molecular Mass = 352.1688 amu

Maximum force = 0 Converged
RMS force = 0 Converged
Maximum displacement = 5e-05 Converged
RMS displacement = 1.1e-05 Converged
Predicted energy change = -8.511519e-13 Hartree

Imaginary Freq = 0
Temperature = 298.15 Kelvin
Pressure = 1 atm
Frequencies scaled by = 1
Electronic Energy (EE) = -1107.447 Hartree
Zero-point Energy Correction = 0.37977 Hartree
Thermal Correction to Energy = 0.402865 Hartree
Thermal Correction to Enthalpy = 0.40381 Hartree
Thermal Correction to Free Energy = 0.321838 Hartree
EE + Zero-point Energy = -1107.0672 Hartree
EE + Thermal Energy Correction = -1107.0441 Hartree
EE + Thermal Enthalpy Correction = -1107.0432 Hartree
EE + Thermal Free Energy Correction = -1107.1252 Hartree
E (Thermal) = 252.802 kcal/mol
Heat Capacity (Cv) = 88.537 cal/mol-kelvin
Entropy (S) = 172.523 cal/mol-kelvin

Table S8 Results summary for structure optimisation and frequency calculation of $\mathbf{L^{Bu}H^+}$

Calculation Type = FREQ
Calculation Method = RB3LYP
Formula = $C_{23}H_{21}N_4$
Basis Set = 6-31G(d)
Charge = 1
Spin = Singlet
Solvation = scrf=solvent=dmso
E(RB3LYP) = -1107.8871 Hartree
RMS Gradient Norm = 1.574e-06 Hartree/Bohr
Imaginary Freq = 0
Dipole Moment = 20.039729 Debye
Polarizability (?) = 414.80167 a.u.
Point Group = C1
Molecular Mass = 353.17662 amu

Maximum force = 0 Converged
RMS force = 0 Converged
Maximum displacement = 2e-05 Converged
RMS displacement = 5e-06 Converged
Predicted energy change = -4.137923e-13 Hartree

Imaginary Freq = 0
Temperature = 298.15 Kelvin
Pressure = 1 atm
Frequencies scaled by = 1
Electronic Energy (EE) = -1107.8871 Hartree
Zero-point Energy Correction = 0.394159 Hartree
Thermal Correction to Energy = 0.41721 Hartree
Thermal Correction to Enthalpy = 0.418165 Hartree
Thermal Correction to Free Energy = 0.337583 Hartree
EE + Zero-point Energy = -1107.4929 Hartree
EE + Thermal Energy Correction = -1107.4699 Hartree
EE + Thermal Enthalpy Correction = -1107.4689 Hartree
EE + Thermal Free Energy Correction = -1107.5495 Hartree
E (Thermal) = 261.81 kcal/mol
Heat Capacity (Cv) = 89.126 cal/mol-kelvin
Entropy (S) = 169.599 cal/mol-kelvin

Table S9 Results summary for structure optimisation and frequency calculation of $\mathbf{L^{Phth}}$

Calculation Type = FREQ
Calculation Method = RB3LYP
Formula = $C_{28}H_{17}N_5O_2$
Basis Set = 6-31G(d)
Charge = 0
Spin = Singlet
Solvation = scrf=solvent=dmso
E(RB3LYP) = -1501.4039 Hartree
RMS Gradient Norm = 4.25e-07 Hartree/Bohr
Imaginary Freq = 0
Dipole Moment = 6.5451258 Debye
Polarizability (?) = 490.518 a.u.
Point Group = C1
Molecular Mass = 455.13822 amu

Maximum force = 0 Converged
RMS force = 0 Converged
Maximum displacement = 3.3e-05 Converged
RMS displacement = 8e-06 Converged
Predicted energy change = -2.182248e-12 Hartree

Imaginary Freq = 0
Temperature = 298.15 Kelvin
Pressure = 1 atm
Frequencies scaled by = 1
Electronic Energy (EE) = -1501.4039 Hartree
Zero-point Energy Correction = 0.391245 Hartree
Thermal Correction to Energy = 0.418173 Hartree
Thermal Correction to Enthalpy = 0.419117 Hartree
Thermal Correction to Free Energy = 0.327205 Hartree
EE + Zero-point Energy = -1501.0126 Hartree
EE + Thermal Energy Correction = -1500.9857 Hartree
EE + Thermal Enthalpy Correction = -1500.9847 Hartree
EE + Thermal Free Energy Correction = -1501.0766 Hartree
E (Thermal) = 262.408 kcal/mol
Heat Capacity (Cv) = 105.274 cal/mol-kelvin
Entropy (S) = 193.446 cal/mol-kelvin

Table S10 Results summary for structure optimisation and frequency calculation of $\mathbf{L^{Phth}}H^+$

Calculation Type = FREQ
Calculation Method = RB3LYP
Formula = $C_{28}H_{18}N_5O_2$
Basis Set = 6-31G(d)
Charge = 1
Spin = Singlet
Solvation = scrf=solvent=dmso
E(RB3LYP) = -1501.8375 Hartree
RMS Gradient Norm = 1.829e-06 Hartree/Bohr
Imaginary Freq = 0
Dipole Moment = 13.385819 Debye
Polarizability (?) = 495.71333 a.u.
Point Group = C1
Molecular Mass = 456.14605 amu

Maximum force = 0 Converged
RMS force = 0 Converged
Maximum displacement = 0.000134 Not converged
RMS displacement = 2.5e-05 Converged
Predicted energy change = -5.341069e-12 Hartree

Imaginary Freq = 0
Temperature = 298.15 Kelvin
Pressure = 1 atm
Frequencies scaled by = 1
Electronic Energy (EE) = -1501.8375 Hartree
Zero-point Energy Correction = 0.405281 Hartree
Thermal Correction to Energy = 0.432242 Hartree
Thermal Correction to Enthalpy = 0.433187 Hartree
Thermal Correction to Free Energy = 0.342008 Hartree
EE + Zero-point Energy = -1501.4322 Hartree
EE + Thermal Energy Correction = -1501.4052 Hartree
EE + Thermal Enthalpy Correction = -1501.4043 Hartree
EE + Thermal Free Energy Correction = -1501.4955 Hartree
E (Thermal) = 271.236 kcal/mol
Heat Capacity (Cv) = 105.931 cal/mol-kelvin
Entropy (S) = 191.901 cal/mol-kelvin

X-ray Crystallography

Crystals of $[Pd_2(\mathbf{L}^{\mathbf{Bu}})_4](BF_4)_4$ were grown by vapour diffusion of $^{i}Pr_2O$ into a DMF solution of the compound. Data were collected at 173 K using an Agilent Xcalibur 3 E diffractometer. Cell determination, data collection, data reduction, cell refinement and absorption correction were performed with CrysalisPro.[7] The structure was solved using SHELXT[8] within WINGX and refined against F_2 using anisotropic thermal displacement parameters for all non-hydrogen atoms, except for one DMF and one $^{i}Pr_2O$ molecule, using SHELXL-2017/1[9] within WINGX[10]. Hydrogen atoms were placed in calculated positions and refined using a riding model.

CCDC	2043240	
Empirical formula	$[Pd_2(C_{23}H_{20}N_4)_4](BF_4)_4 \cdot (C_3H_7NO)_4 \cdot (C_6H_{14}O)_2$	
Formula weight	2466.48	
Temperature	173(2) K	
Wavelength	0.71073 Å	
Crystal system	Monoclinic	
Space group	P 2_1/n	
Unit cell dimensions	a = 13.4683(3) Å	a= 90°
	b = 18.1293(4) Å	b= 99.400(2)°
	c = 24.7113(5) Å	g = 90°
Volume	5952.8(2) $Å^3$	
Z	2	
Density (calculated)	1.376 Mg/m^3	
Absorption coefficient	0.389 mm^{-1}	
F(000)	2552	
Crystal size	0.484 × 0.182 × 0.145 mm^3	
Theta range for data collection	2.359 to 28.334°.	
Index ranges	-16≤h≤14, -21≤k≤16, -32≤l≤31	
Reflections collected	33881	
Independent reflections	12454 [R(int) = 0.0322]	
Completeness to theta = 25.242°	99.7%	
Absorption correction	Semi-empirical from equivalents	
Max. and min. transmission	1.000 and 0.94338	
Refinement method	Full-matrix least-squares on F^2	
Data / restraints / parameters	12454 / 0 / 689	
Goodness-of-fit on F^2	1.032	
Final R indices [I>2sigma(I)]	R_1 = 0.0752, wR_2 = 0.2057	
R indices (all data)	R_1 = 0.1046, wR_2 = 0.2361	
Largest diff. peak and hole	1.859 and -0.998 e.$Å^{-3}$	

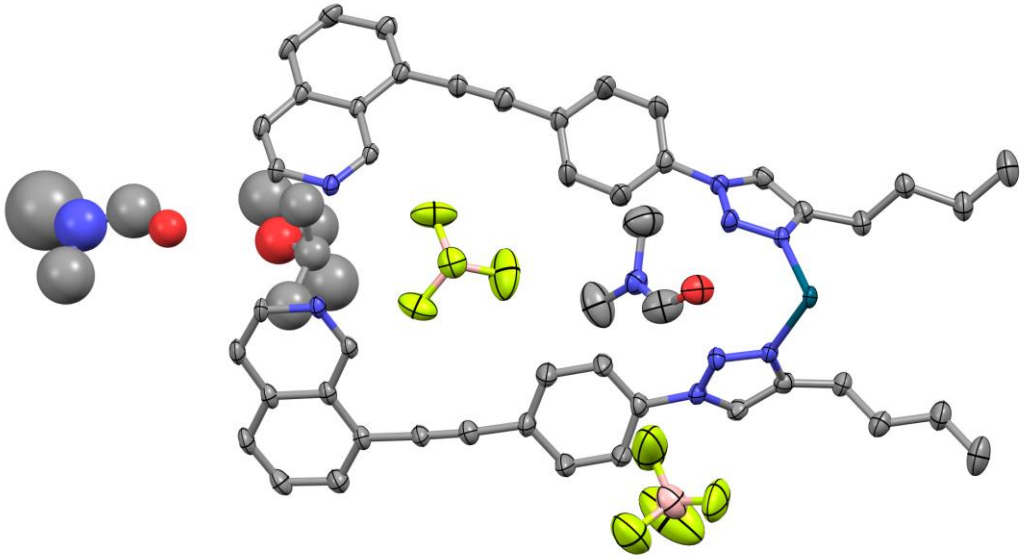

Figure S129 Ellipsoid plot of the asymmetric unit of $[Pd_2(\mathbf{L}^{\mathbf{Bu}})_4](BF_4)_4 \cdot (C_3H_7NO)_4 \cdot (C_6H_{14}O)_2$. Ellipsoids shown at 50% probability. Hydrogen atoms omitted for clarity.

Crystals of [Pd(**1**)$_4$](BF$_4$)$_2$ were grown by vapour diffusion of Et$_2$O into a DMF solution of the compound. Data were collected at 173 K using an Agilent Xcalibur 3 E diffractometer. Cell determination, data collection, data reduction, cell refinement and absorption correction were performed with CrysalisPro.[7] The structure was solved using SHELXT[8] within Olex2[11] and refined against F_2 using anisotropic thermal displacement parameters for all non-hydrogen atoms using SHELXL-2018/3[9] within Olex2. Disordered BF_4 counteranions and solvent molecules could not be appropriately modelled; electron density was accounted for using a mask. Hydrogen atoms were placed in calculated positions and refined using a riding model.

CCDC	2050421	
Empirical formula	$[Pd(C_{17}H_{10}N_4)_4](BF_4)_2 \cdot 4(C_4H_{10}O)$	
Formula weight	1657.66	
Temperature	173.00(14) K	
Wavelength	0.71073 Å	
Crystal system	Tetragonal	
Space group	I 4/m	
Unit cell dimensions	a = 14.1424(3) Å	a= 90°
	b = 14.1424(3) Å	b= 90°
	c = 36.1928(11) Å	g = 90°
Volume	7238.8(4) Å^3	
Z	4	
Density (calculated)	1.521 Mg/m^3	
Absorption coefficient	0.345 mm^{-1}	
F(000)	3424	
Crystal size	0.286 × 0.214 × 0.073 mm^3	
Theta range for data collection	2.251 to 28.223°.	
Index ranges	-13≤h≤15, -10≤k≤18, -45≤l≤47	
Reflections collected	12412	
Independent reflections	3912 [R(int) = 0.0315]	
Completeness to theta = 25.242°	99.6%	
Absorption correction	Semi-empirical from equivalents	
Max. and min. transmission	1.000 and 0.79900	
Refinement method	Full-matrix least-squares on F^2	
Data / restraints / parameters	3912 / 0 / 193	
Goodness-of-fit on F^2	1.077	
Final R indices [I>2sigma(I)]	R_1 = 0.0469, wR_2 = 0.1270	
R indices (all data)	R_1 = 0.0655, wR_2 = 0.1424	
Largest diff. peak and hole	0.94 and -0.36 e.Å^{-3}	

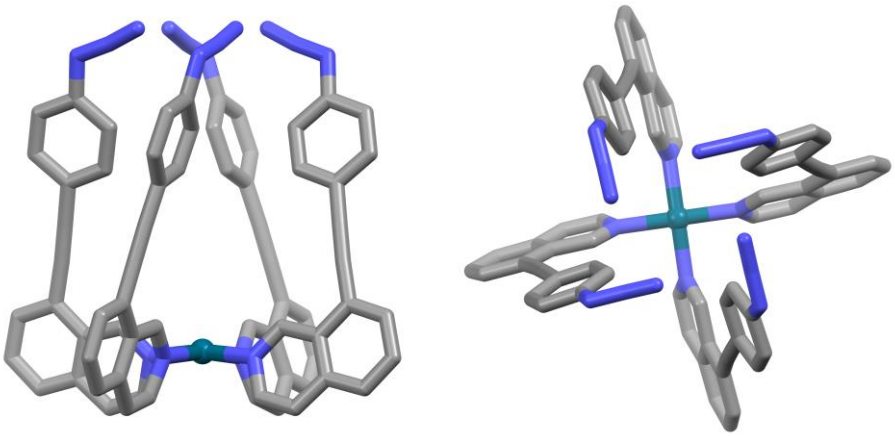

Figure S130 Stick representation of the SCXRD structure of [Pd(**1**)$_4$](BF$_4$)$_2$ shown from the side (left) and the top (right).

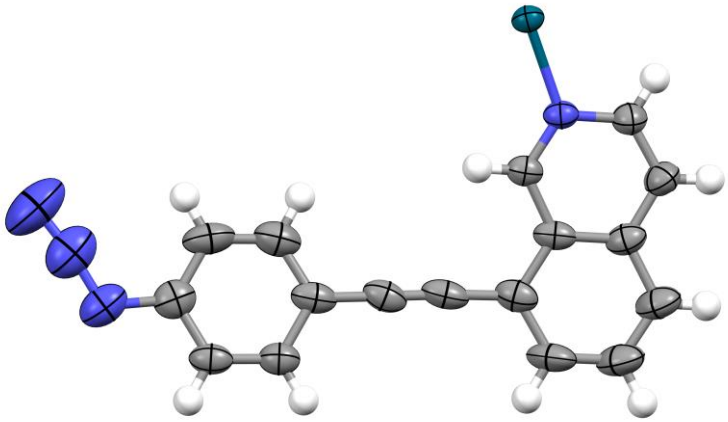

Figure S131 Ellipsoid plot of the asymmetric unit of [Pd(**1**)$_4$](BF$_4$)$_2$·4(C$_4$H$_{10}$O). Ellipsoids shown at 50% probability.

References

[1] N. Guven and P. Camurlu, *Polymer*, 2015, **73**, 122-130.

[2] M. D. Hanwell, D. E. Curtis, D. C. Lonie, T. Vandermeersch, E. Zurek and G. R. Hutchinson, *J. Cheminform.*, 2012, **4**, 17.

[3] A. K. Rappé, C. J. Casewit, K. S. Colwell, W. A. Goddard III and W. M. Skiff, *J. Am. Chem. Soc.*, 1992, **114**, 10024-10035.

[4] J. J. P. Stewart, *J. Mol. Model.*, 2007, **13**, 1173-1213.

[5] Gaussian 16, Revision C.01, M. J. Frisch, G. W. Trucks, H. B. Schlegel, G. E. Scuseria, M. A. Robb, J. R. Cheeseman, G. Scalmani, V. Barone, G. A. Petersson, H. Nakatsuji, X. Li, M. Caricato, A. V. Marenich, J. Bloino, B. G. Janesko, R. Gomperts, B. Mennucci, H. P. Hratchian, J. V. Ortiz, A. F. Izmaylov, J. L. Sonnenberg, D. Williams-Young, F. Ding, F. Lipparini, F. Egidi, J. Goings, B. Peng, A. Petrone, T. Henderson, D. Ranasinghe, V. G. Zakrzewski, J. Gao, N. Rega, G. Zheng, W. Liang, M. Hada, M. Ehara, K. Toyota, R. Fukuda, J. Hasegawa, M. Ishida, T. Nakajima, Y. Honda, O. Kitao, H. Nakai, T. Vreven, K. Throssell, J. A. Montgomery, Jr., J. E. Peralta, F. Ogliaro, M. J. Bearpark, J. J. Heyd, E. N. Brothers, K. N. Kudin, V. N. Staroverov, T. A. Keith, R. Kobayashi, J. Normand, K. Raghavachari, A. P. Rendell, J. C. Burant, S. S. Iyengar, J. Tomasi, M. Cossi, J. M. Millam, M. Klene, C. Adamo, R. Cammi, J. W. Ochterski, R. L. Martin, K. Morokuma, O. Farkas, J. B. Foresman, and D. J. Fox, Gaussian, Inc., Wallingford CT, 2016.

[6] M. Holz, X. Mao, D. Seiferling and A. Sacco, *J. Chem. Phys.*, 1996, **104**, 669-679.

[7] *CrysAlis Pro*, Riagku Oxford Diffraction, Yarnton, Oxfordshire, England, **2015**.

[8] G. M. Sheldrick, *Acta Cryst.*, 2015, A**71**, 3-8.

[9] G. M. Sheldrick, *Acta Cryst.*, 2015, C**71**, 3-8.

[10] L. J. Farrugia, *J. Appl. Crystallogr.*, 2012, **45**, 849-854.

[11] O. V. Dolomanov, L. J. Bourhis, R. J. Gildea, J. A. Howard and H. Puschmann, *J. Appl. Crystallogr.*, 2009, **42**, 339-341.